

**ADVANCED CHARACTERIZATION STUDIES OF THE  
LOCAL STRUCTURE OF DIAMOND-LIKE CARBON  
FILMS**



**A Thesis Submitted in Partial Fulfillment of the Requirements for the  
Degree of Doctor of Philosophy in Physics  
Suranaree University of Technology  
Academic Year 2020**

การใช้เทคนิควิเคราะห์ขั้นสูงเพื่อศึกษาโครงสร้างพื้นฐานของฟิล์มคาร์บอน  
ที่มีลักษณะคล้ายเพชร



นายฐานันต์ จันทร์แจ่มศรี

วิทยานิพนธ์นี้เป็นส่วนหนึ่งของการศึกษาตามหลักสูตรปริญญาวิทยาศาสตรดุษฎีบัณฑิต

สาขาวิชาฟิสิกส์

มหาวิทยาลัยเทคโนโลยีสุรนารี

ปีการศึกษา 2563

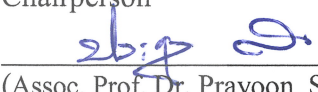
**ADVANCED CHARACTERIZATION STUDIES OF THE LOCAL  
STRUCTURE OF DIAMOND-LIKE CARBON FILMS**

Suranaree University of technology has approved this thesis submitted in partial fulfillment of the requirement for the Degree of Doctor of Philosophy.

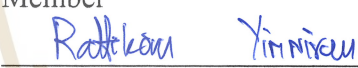
Thesis Examining Committee

  
\_\_\_\_\_  
(Assoc. Prof. Dr. Panomsak Meemon)

Chairperson

  
\_\_\_\_\_  
(Assoc. Prof. Dr. Prayoon Songsirithigul)

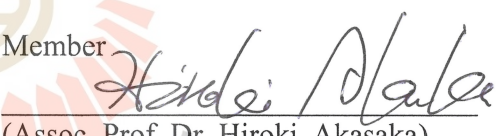
Member

  
\_\_\_\_\_  
(Prof. Dr. Rattikorn Yimnirun)

Member

  
\_\_\_\_\_  
(Assoc. Prof. Dr. Saroj Rujirawat)

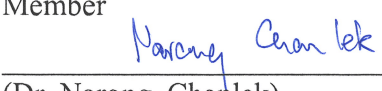
Member

  
\_\_\_\_\_  
(Assoc. Prof. Dr. Hiroki Akasaka)

Member

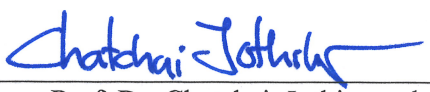
  
\_\_\_\_\_  
(Dr. Pinit Kidkhunthod)

Member

  
\_\_\_\_\_  
(Dr. Narong Chanlek)

Member

  
\_\_\_\_\_  
(Prof. Dr. Santi Maensiri)

  
\_\_\_\_\_  
(Assoc. Prof. Dr. Chatchai Jothityangkoon)

Vice Rector for Academic Affairs  
and Quality Assurance

Dean of Institute of Science

ฐานันต์ จันทร์แจ่มศรี : การใช้เทคนิควิเคราะห์ขั้นสูงเพื่อศึกษาโครงสร้างพื้นฐานของฟิล์มคาร์บอนที่มีลักษณะคล้ายเพชร (ADVANCED CHARACTERIZATION STUDIES OF THE LOCAL STRUCTURE OF DIAMOND-LIKE CARBON FILMS) อาจารย์ที่ปรึกษา : รองศาสตราจารย์ ดร.ประยูร ส่งสิริฤทธิกุล, 130 หน้า

วิทยานิพนธ์ฉบับนี้ มีวัตถุประสงค์เพื่อศึกษาคุณสมบัติของวัสดุคาร์บอนที่เหมาะสมสำหรับนำมาประยุกต์ใช้เพื่อการปลูกฟิล์ม โดยคาร์บอนมีคุณสมบัติตามโครงสร้างที่แตกต่างกัน ซึ่งคาร์บอนที่มีโครงสร้างแบบเพชร หรือ  $sp^3$  จะให้คุณสมบัติด้านความแข็งแรงกับวัสดุที่ถูกเคลือบ และมีความเป็นฉนวนไฟฟ้า ในขณะที่คาร์บอนมีโครงสร้างแบบกราฟไฟต์ หรือ  $sp^2$  จะทำให้ผิววัสดุมีความลื่น ความวาว และการนำไฟฟ้าที่ดี เป็นต้น หากนำคาร์บอนทั้งสองชนิดมารวมกันเราจะเรียกวัสดุนี้ว่าคาร์บอนที่มีโครงสร้างคล้ายเพชร โดยคุณสมบัติของวัสดุดังกล่าวขึ้นอยู่กับสัดส่วนโครงสร้างของคาร์บอนแต่ละชนิด หากมีปริมาณ  $sp^3$  ที่มาก ตัวคาร์บอนฟิล์มจะมีความแข็งแรงเป็นคุณสมบัติที่โดดเด่น ในทางกลับกัน หากโครงสร้างของคาร์บอนมีปริมาณ  $sp^2$  ที่มากกว่า  $sp^3$  ก็ส่งผลให้มีคุณสมบัติของความลื่น ความวาว ที่ผิววัสดุ และการนำไฟฟ้าอย่างเห็นได้ชัด อย่างไรก็ตาม คุณสมบัติที่เกี่ยวข้องกับสัดส่วนของโครงสร้างที่เป็นผลมาจากปริมาณของ  $sp^2$  และ  $sp^3$  จึงขึ้นอยู่กับวัตถุประสงค์ในการประยุกต์ใช้เพื่อก่อให้เกิดประโยชน์ในภาคอุตสาหกรรม ด้วยเหตุที่กล่าวไปข้างต้นผู้จัดทำจึงได้ศึกษาคุณสมบัติของฟิล์มจากชิ้นงานตัวอย่าง โดยใช้เทคนิคการดูดกลืนของรังสีเอกซ์ในย่านพลังงานต่ำ (NEXAFS) เพื่อศึกษาคุณสมบัติทางไฟฟ้าในโครงสร้างคาร์บอน รวมถึงศึกษาความไม่เป็นระเบียบของโครงสร้างด้วยเทคนิครามาน (Raman spectroscopy) อีกทั้งปริมาณของ  $sp^2$  และ  $sp^3$  ในโครงสร้างของคาร์บอนยังถูกจำแนกด้วยวิธีสเปกโตรสโคปีของอนุภาคอิเล็กตรอนที่ถูกปลดปล่อยด้วยรังสีเอกซ์ (XPS)

ด้วยเหตุนี้ กระบวนการเตรียมฟิล์มจึงเป็นหนึ่งในปัจจัยที่จะได้มาซึ่งคุณสมบัติของฟิล์มตามที่ต้องการ ผู้จัดทำยังได้มุ่งเน้นไปที่การปลูกฟิล์มด้วยเทคนิคทางเคมีด้วยพลาสมา (PECVD) โดยศึกษาเงื่อนไขต่าง ๆ ของระบบ PECVD ที่ใช้ในการปลูกฟิล์ม ได้แก่ กำลังไฟฟ้าที่ใช้ในระบบ เวลาในการปลูกฟิล์ม ความดันในห้องทดลอง เป็นต้น โดยฟิล์มที่ได้จะถูกนำมาวิเคราะห์โครงสร้างของคาร์บอนด้วยเทคนิคตามที่กล่าวมาข้างต้น โดยผลการทดลองแสดงให้เห็นว่า โครงสร้างของคาร์บอนฟิล์มเปลี่ยนแปลงไปตามตัวแปรต่าง ๆ อย่างเห็นได้ชัด อันได้แก่ความไม่เป็นระเบียบของโครงสร้างเพิ่มขึ้นเมื่อให้กำลังไฟฟ้าที่ใช้ในการปลูกที่มากขึ้น พร้อมทั้งส่งผลให้มีสัดส่วนของคาร์บอนแบบ  $sp^2$  ที่มากขึ้นด้วย

ให้คุณสมบัติใหม่ที่น่าสนใจไปใช้ประโยชน์ได้อย่างแพร่หลาย เช่น การเติมโลหะเงิน (Ag) เข้าไปในโครงสร้างของคาร์บอนฟิล์มจะสามารถลดการก่อตัวของแบคทีเรียได้ จึงถูกนำไปประยุกต์ใช้กับผ้าพันแผล หรือการเติมไทเทเนียม (Ti) เพื่อลดแรงเสียดทานบนผิวชิ้นงาน เป็นต้น ในงานนี้ ผู้จัดทำได้เล็งเห็นถึงความสำคัญของการเติมโลหะสังกะสี (Zn) ซึ่งมีคุณสมบัติในการยับยั้งการก่อตัวของโรคกระดูกพรุนได้ โดยมักจะพบได้ในผู้สูงอายุ เพื่อที่จะให้ได้มาซึ่งฟิล์มที่น่าสนใจ คาร์บอนจะถูกเตรียมด้วยระบบ CVD พร้อม ๆ กับการเติม Zn ลงไปในโครงสร้างด้วยระบบสปัตเตอร์ (sputtering system) ผู้จัดทำมุ่งหวังเป็นอย่างยิ่งที่จะทราบถึงพฤติกรรมของ Zn ที่ได้ไปอยู่ในโครงสร้างของคาร์บอน โดยปริมาณ Zn ที่มากขึ้นในเนื้อฟิล์มถูกยืนยันด้วยเทคนิค XPS และเมื่อนำมาวิเคราะห์ด้วยเทคนิครามานสเปกโทรสโกปี พบว่าเมื่อมีปริมาณ Zn ที่มากขึ้น คาร์บอนฟิล์มจะมีความไม่เป็นระเบียบมากขึ้นตามไปด้วย ยังส่งผลไปถึงความเป็นรูพรุนของฟิล์มที่มากขึ้นตามผลการทดสอบด้วยเครื่องวิเคราะห์ความแข็งแรงของวัสดุ (Indentation Hardness Test) และเมื่อนำมาวิเคราะห์ด้วยเทคนิคการดูดกลืนของรังสีเอกซ์ (XAS) พบว่า Zn มีเลขออกซิเดชันเป็นศูนย์ และไม่ได้สร้างพันธะกับคาร์บอนในโครงสร้าง

มหาวิทยาลัยเทคโนโลยีสุรนารี

สาขาวิชาฟิสิกส์

ปีการศึกษา 2563

ลายมือชื่อนักศึกษา



ลายมือชื่ออาจารย์ที่ปรึกษา



ลายมือชื่ออาจารย์ที่ปรึกษาร่วม



ลายมือชื่ออาจารย์ที่ปรึกษาร่วม



ลายมือชื่ออาจารย์ที่ปรึกษาร่วม



THANUN CHUNJAMESRI : ADVANCED CHARACTERIZATION  
STUDIES OF THE LOCAL STRUCTURE OF DIAMOND-LIKE  
CARBON FILMS) THISIS ADVISOR : ASSOC. PROF. PRAYOON  
SONGSIRIRITTHIGU, Ph.D. 130 PP.

This thesis was made for studying the properties of carbon which is appropriate for films deposition. Generally, carbon has 2 mains hybridization structure. Diamond structure C-sp<sup>3</sup> qualify the strength properties. While, the graphite structure C-sp<sup>2</sup> qualify silky, low friction and high electric conductivity etc. The combination of these structures was widely called diamond-like carbon (DLC). DLC properties depend on ratio of C-sp<sup>2</sup> and C-sp<sup>3</sup>. If the fraction C-sp<sup>3</sup> is high, it's will show majority in strength and high hardness properties. In the other hand, If the fractions C-sp<sup>2</sup> is high, it qualifies silky, low friction and high electric conductivity as major properties. However, properties which is related to its structure ratio depend on selection for the advantage in Industrial. From above reason, the commercial sample was studied as one part in this work. Its electronic structure was studies by near edge X-ray absorption fine structure (NEXAFS), synchrotron techniques. Carbon film were also studied disordering properties by Raman spectroscopy techniques. And the fraction of carbon sp<sup>2</sup> and sp<sup>3</sup> was classified by using X-ray photoelectron spectroscopy techniques (XPS).

According to DLC structure, films preparation process is also important factor for requesting the films properties. We focus on films preparations by using plasm enhance chemical vapor deposition techniques (PECVD). The condition of PECVD system was studied such as influence of power, time dependence, and working

pressure etc. Prepared films were characterized by above techniques. In detail of results, carbon structure was obviously related with deposited conditions. For example, higher generating power affect to increasing in films disordering which is measured by Raman spectroscopy. And it also related to increasing in C-sp<sup>2</sup> fractions explained by XPS results etc.

Nowadays, there are more research studying doping metal to DLC structure for solving its properties and export to new applications. We focus studying behavior of zinc in diamond-like carbon structure which deposited by combination of chemical vapor deposition (CVD) and sputtering technique. Variation of Zn concentrations were studied. Zn-DLC were characterized based-on synchrotron techniques. In details, increasing in Zn concentration were performed by XPS. Also, its affect to disordering of DLC structure which is confirmed by Raman spectroscopy. Film's thickness was investigated by laser microscopy techniques as in order 1 micron. Zn content also related to highly films porosity which confirmed by indentation hardness test. From X-ray absorption spectroscopy technique (XAS) results, Zn behave majority metallic state in oxygen and carbon environment as neighboring atoms. It indicates non-bonding of zinc core-shell atom. It also shows a good agreement with electronic structure in Carbon K-edge spectra by NEXAFS results.

School of Physics

Academic Year 2020

Student's signature 

Advisor's signature 

Co-advisor's signature 

Co-advisor's signature Pinit N.

Co-advisor's signature 

## ACKNOWLEDGEMENTS

The following are people, to whom I would like to express my sincere words of kindly acknowledge for thesis

Firstly, I would like to express my thesis sincere gratitude Prof. Dr. Rattikorn Yimmirun who is my supervisor. He is a greatly advisory for all step in Ph.D. life, give powerful inspiration, kind patience, give the concept, new idea. Not only academic knowledge, but he also shares the extremely experience in his live which made optimization for me. I also would like to thank Assoc. Prof. Dr. Saroj Rujirawat who is my co-advisor. Whenever, I have a problem during doing experiments, he often suggests me the good idea for solutions. He also kindly introduces about synchrotron techniques which is more advantage in my thesis. Moreover, I would like to thank my advisor, Assoc. Prof. Dr. Prayoon Songsiriritthigul who give a direction for Ph.D. program. He gave a concept about the process for working in my topic, he also teaches me how to successfully in philosophy program. I would like to thank Dr. Pinit Kidkhunthod who is my co-advisor, he is a good exemplum for high earnestness person which give greatly impression for working. He teaches me about XAS techniques. He taught me how to write manuscript. Moreover, I kindly thank a good chance for a student trainee in BL-5.2, SLRI, he gave me very specifical experience for XAS operation and setup experiment system. I would like to thank, Dr. Narong Chanlek who teach me XPS technique and vacuum process. He always gives me a good chance for working with other people which made great participations. Whenever I feel confused, he guides a good one detection for solving the problem. He also read a draft of manuscript. The most important, he has a greatly living philosophy which was taken

as a model in my life. I would like to thank Assoc. Prof. Dr. Hiroki Akasaka who give me a good chance for worldwide experience in Japan. He is very strong man. When I went to Tokyo, he gave me new technique, new ideas, and new friends in Tokyo. He also took me to interesting place for giving a good motivation. I would like to thank you for all staff members in school of Physics for teaching me about lecture, doing documents process, exchange idea by seminar. And I also thank you all students in institute of science who always kindly good friendship. I would like to thank all scientist in SLRI who support me for using beamline experiment, exchange idea and give me a knowledge. I would like to thank you all staff member in beamline-5.2 who worked together. Moreover, I deeply grateful for my DPST scholarship who support the budget since 2012-2021. The authors would like to acknowledges the NANOTEC, NSTDA, Ministry of Science and Technology, Thailand, through its program of Research Network NANOTEC for partial financial support and the Synchrotron Light Research Institute (Public Organization), Thailand for XPS and NEXAFS experiments from scientists at BL-5.2, BL-5.3 and BL-3.2Ua. Moreover, the authors would like to acknowledges VISTEC and Tokyo Institute of Technology cooperation. In the end, I would like to kindly thanks my parents who always in the background for all step. When I was young, my father (Tavatchai Chunjaemsri) always made motivation about science knowledge such as planet, space, world map, science experiments for kids etc. He gave to me about worldwide the experience. Learning by doing is a code of conduct in his live which I always bring to apply in my life. Also, my mother (Kanittha Chunjaemsri) always gives me the good encouragement and the positive thinking when I feel disheartened. Thank you again for their kindly supporting

Thanun Chunjaemsri

# CONTENTS

	<b>Page</b>
ABSTRACT IN THAI.....	I
ABSTRACT IN ENGLISH .....	III
ACKNOWLEDGEMENTS.....	V
CONTENTS.....	VII
LIST OF TABLES .....	XI
LIST OF FIGURES .....	XII
LIST OF ABBREVIATIONS.....	XVII
<b>CHAPTER</b>	
<b>I INTRODUCTION .....</b>	<b>1</b>
1.1 Introduction of DLC and Advance Characterization .....	1
<b>II PREVIOUS WORK AND BACKGROUND OF DLC .....</b>	<b>6</b>
2.1 Carbon electron configuration and hybridization.....	6
2.2 Diamond-Like Carbons: DLC.....	10
2.2.1 Amorphous Carbon (a-C).....	13
2.2.2 Hydrogenated amorphous carbons (a-C:H) .....	13
2.2.3 Tetrahedral amorphous carbon (ta-C) .....	14
2.2.4 Hydrogenated tetrahedral amorphous carbon (ta-C:H).....	14
2.3 DLC applications and metal doped .....	14
2.3.1 Ag-DLC.....	15
2.3.2 Ti-DLC .....	16

## CONTENTS (Continued)

	<b>Page</b>
2.3.3 Zn-DLC .....	18
2.4 Preparations of diamond-like carbon films .....	20
2.5 Deposition techniques for growing DLC films .....	21
2.5.1 Sputtering techniques .....	21
2.5.2 Plasma enhances chemical vapor deposition (PECVD).....	22
2.5.3 Filtered cathodic vacuum arc (FCVA).....	23
2.6 Technique for characterizations .....	25
2.6.1 Raman Spectroscopy .....	25
2.6.2 X-rays Photoelectron Spectroscopy (XPS) .....	28
2.6.3 Indentation hardness.....	32
2.6.4 Glow discharge optical emission spectroscopy (GD-OES) .....	33
2.6.5 Laser microscopy .....	34
2.6.6 Atomic Force Microscope (AFM).....	35
2.7 Advance characterization .....	36
2.7.1 X-ray Absorptions Spectroscopy (XAS).....	36
2.7.2 Near-edge X-ray Absorptions Fine Structure (NEXAFS) .....	41
<b>III DLC AND THERMAL TREATED PROPERTIES .....</b>	<b>46</b>
3.1 Concept of DLC and Thermal-treated properties .....	46
3.2 Experiment and Characterizations.....	47
3.2.1 DLC films preparation: Heat treatment.....	47
3.2.2 Measurements of XPS .....	47

## CONTENTS (Continued)

	<b>Page</b>
3.2.3 Measurements of NEXAFS.....	48
3.2.4 Measurements of Raman.....	48
3.3 Results and Discussion.....	49
3.3.1 XPS Result.....	49
3.3.2 NEXAFS Result.....	51
3.3.3 Raman Result.....	52
3.4 Summarize of Thermal-treated DLC and characterized.....	55
<b>IV INFLUENCE OF POWER DEPENDENCE BY PECVD.....</b>	<b>56</b>
4.1 Concept of power dependence by PECVD.....	56
4.2 Experimental setup.....	57
4.3 Deposition Conditions.....	58
4.4 Film characterizations.....	59
4.4.1 XPS analysis.....	59
4.4.2 Raman spectroscopy analysis.....	59
4.4.3 NEXAFS analysis.....	60
4.5 Results and Discussion.....	60
4.6 Summarize of RF power and gas flow rate with films properties.....	70
4.7 Primary results of other interesting condition for PECVD.....	71
<b>V EFFECT OF ZN DOPED AND LOCAL STRUCTURE.....</b>	<b>76</b>
5.1 Zn-doped and introduction.....	76
5.2 Zn-doped DLC Experiment.....	78

## CONTENTS (Continued)

	<b>Page</b>
5.2.1 Zn-DLC film preparations.....	78
5.2.2 Zn-doped Deposition Conditions .....	79
5.3 Zn-DLC films characterizations.....	80
5.3.1 Raman spectroscopy analysist.....	80
5.3.2 Indentation hardness analysist.....	80
5.3.3 Laser microscopy .....	81
5.3.4 X-ray Absorptions spectroscopy analysists.....	81
5.3.5 Results and Discussion.....	81
5.4 Summarize of Zn-doped DLC.....	94
5.5 Introduce of Ti-doped DLC and interesting.....	95
<b>VI CONCLUSION.....</b>	<b>99</b>
APPENDIX.....	101
REFERENCES.....	114
CURRICULUM VITAE.....	130

## LIST OF TABLES

Table	Page
1 Comparison properties of carbon materials.....	13
2 Characterized Results of Thermal-treat of DLC Films. ....	55
3 The PECVD deposition parameters of DLC films .....	59
4 Numerical characterized XPS and Raman results of DLC films for all preparation conditions .....	69
5 Characterized of DLC films prepared with different time and substrate-polished .....	73
6 The system deposition parameters of DLC films .....	80
7 Deconvoluted peaks of DLC filing in NEAXFS spectra.....	91
8 Summarized of the chemical characterization data of Zn-DLC films.....	92
9 Summarized of the physical characterization data of Zn-DLC films.....	92

## LIST OF FIGURES

Figure	Page
1 Summarized of the physical characterization data of Zn-DLC films.....	7
2 Carbon atom geometry of hybridized orbitals in $sp$ , $sp^2$ , $sp^3$ .....	8
3 Single, Double and Triple bond for carbon hybridization.....	9
4 Fundamental of Diamond-like carbon (DLC) structure .....	11
5 Ternary phase diagram of amorphous carbons. The three corners represent to diamond, graphite, and hydrocarbons, respectively. (Ferrari and Robertson., 2000) .....	12
6 The antibacterial effect from Ag-DLC layer after 3h (a) and 24h (Písařík et al., 2017).....	16
7 (a) Raman spectra and (b) the corresponding G-peak position and $I_D / I_G$ ratio of the Ti-DLC films deposited at different Ar/CH <sub>4</sub> flow ratio.....	17
8 (a) The XPS C 1S peak (b) the relations of $sp^2/sp^3$ ratio.....	17
9 Friction coefficient of Ti-DLC film and pure DLC film.....	18
10 Raman spectra (a) XPS spectra (b) for Zn-DLC (Wong et al., 2011).....	19
11 Overall thin films depositions process diagram .....	20
12 Diagram of sputtering system.....	21
13 Schematic diagram of PECVD system.....	22
14 (a) PECVD system in SLRI and (b) generated plasma in chamber .....	23
15 The antibacterial effect from Ag-DLC layer after 3h (a) and 24h (Písařík et al., 2017).....	24

## LIST OF FIGURES (Continued)

<b>Figure</b>	<b>Page</b>
16 Basics principle of atomic vibration with interaction wavelength (a), and state diagram of scattering pattern (b) .....	26
17 Raman principle and typical of Raman system (WITec Pte. Ltd.) .....	27
18 Photoelectric effect and typical of XPS system (BL-5.3 SLRI).....	28
19 wide scan of XPS spectra of DLC films.....	30
20 Diagram of fitting XPS area for DLC films .....	31
21 Operation of Indentations Hardness for DLC Measuring .....	32
22 Theoretical of elements investigation by GDOS techniques.....	33
23 The principle of laser microscopy technique.....	34
24 The principle of AFM technique .....	35
25 Theoretical and algorithm of XAS (BL-5.2 SLRI) .....	36
26 The fundamental processes which contribute to XANES spectra of photo absorption (a), fluorescent photon (b) and Auger electron (c).....	38
27 Theoretical and algorithm for XANES and EXAFS spectra (BL-5.2 SLRI)....	39
28 Energy range of XANES and EXAFS spectra(a) / K-space spectra(b) / R-space spectra(c) (BL-5.2 SLRI).....	40
29 Investigating for NEXAFS spectra from C K-edge (BL-3.2Ua SLRI) .....	42
30 Theoretical and algorithm for NEXAFS spectra .....	42
31 Fill and unfilled orbital of electron hybridization .....	44
32 Theoretical of electron excitation explaining NEXAFS spectra (Hähner, 2006).....	45

## LIST OF FIGURES (Continued)

<b>Figure</b>	<b>Page</b>
33 experimental setup of ex-situ thermal-treated system .....	47
34 High resolution XPS spectra of C 1s(a), O 1s(b), Si 2p(c) peaks, XPS survey spectra of the DLC film at RT(d), graph fitting of C 1s(e), O 1s(f), Si 2p(g).....	50
35 All deconvolutions from spectra XPS of Thermal-treated DLC films.....	51
36 Raman spectrum fitting of DLC film at RT(a) and, DLC films heated to difference five temperature(b) .....	53
37 NEXAFS carbon <i>K</i> -edge spectra of the DLC films and HOPG.....	54
38 Schematic diagram of PECVD system.....	58
39 High resolution XPS C 1s peaks of the DLC films prepared with different RF powers using CH <sub>4</sub> flow rates of (a) 10 cm <sup>3</sup> /min and (b) 5 cm <sup>3</sup> /min.....	62
40 <i>sp</i> <sup>3</sup> / <i>sp</i> <sup>2</sup> ratio of DLC films as a function of RF power using CH <sub>4</sub> flow rate 10 (blue), and 5 cm <sup>3</sup> /min (red) .....	63
41 Raman spectra of the DLC films prepared with different RF power using flow rates (a) 10 cm <sup>3</sup> /min and (b) 5 cm <sup>3</sup> /min.....	65
42 (a) Raman peaks position and (b) I <sub>D</sub> /I <sub>G</sub> at 10 cm <sup>3</sup> /min, (c) Raman peaks position and (d) I <sub>D</sub> /I <sub>G</sub> at 5 cm <sup>3</sup> /min, with difference RF power .....	66
43 Carbon <i>K</i> -edge NEXAFS spectra of the DLC films prepared with a different RF power using CH <sub>4</sub> flow rates of 5 cm <sup>3</sup> /min and 10 cm <sup>3</sup> /min, respectively .....	68

## LIST OF FIGURES (Continued)

<b>Figure</b>	<b>Page</b>
44 SEM imaging diagram.....	70
45 SEM images of the DLC films deposited by PECVD at different RF powers using CH <sub>4</sub> flow rates of (a-e) 10, and (f-h) 5 cm <sup>3</sup> /min.....	70
46 Raman spectra of the DLC films prepared with different time and substrate-polished .....	72
47 XPS spectra of DLC films prepared with different time and substrate-polished .....	74
48 NEXAFS spectra of DLC films prepared with different time and substrate-polished .....	75
49 Schematic diagram of CVD and sputtering system.....	79
50 Raman spectra of DLC films and Zn-DLC .....	82
51 G-positions of Raman spectra of DLC films and Zn-DLC .....	83
52 $I_D/I_G$ ratio of Raman spectra of DLC films and Zn-DLC .....	84
53 Loading-unloading feature indentation hardness test of a) DLC, b) 0.05Zn-DLC, c) 0.1Zn-DLC and d) 0.2Zn-DLC.....	85
54 Indentation hardness profile of DLC and Zn-DLC films .....	85
55 Zn <i>K</i> -edge spectra of Zn doped DLC films .....	86
56 Fourier transformation of $k^2$ -weighted spectra of EXAFS Zn <i>K</i> -edge.....	88
57 Aser microscopy measuring by using step profiler for studying thickness.....	89
58 Carbon <i>K</i> -edge of DLC and Zn-DLC spectra.....	90
59 Roughness profile of DLC and Zn-DLC films by Laser microscopy .....	93

## LIST OF FIGURES (Continued)

<b>Figure</b>	<b>Page</b>
60 Roughness profile of DLC and Zn-DLC films by AFM .....	93
61 2D roughness profiles by Laser microscopy of DLC and Zn-DLC .....	94
62 Raman spectroscopy and fitting of Ti-DLC films .....	95
63 G-positions of Raman spectroscopy of Ti-DLC films .....	96
64 $I_D/I_G$ of Raman spectroscopy of Ti-DLC films .....	96
65 Morphology profiles measured by Laser microscopy techniques of Ti-DLC .....	97
66 2D roughness profiles by Laser microscopy of Ti-DLC .....	98

## LIST OF ABBREVIATIONS

A	Current Ampere
Å	Angstrom
<i>a</i> -C	Amorphous carbon
AFM	Atomic Force Laser Microscopy
Ag	Silver
Ag-DLC	Si doped Diamond-like Carbon
AgNP	Silver Nanoparticle
amp	Amplitude
Ar	Argon
C	Carbon
C <sub>2</sub> H <sub>2</sub>	Acetylene
C <sub>2</sub> H <sub>2</sub>	Ethyl
C <sub>2</sub> H <sub>4</sub>	Ethene
C <sub>2</sub> H <sub>6</sub>	Ethane
CH <sub>4</sub>	Methane
cm	Centimeter
CO <sub>2</sub>	Carbon Dioxide
C-sp <sup>2</sup>	Carbon sp <sup>3</sup> Hybridization
C-sp <sup>3</sup>	Carbon sp <sup>3</sup> Hybridization
CVD	Chemical Vapor Deposition
DC	Direct current

## LIST OF ABBREVIATIONS (Continued)

DLC	Diamond-like carbon
EXAFS	Extended X-ray Absorption Fine Structure
FCA	Filtered Cathodic Vacuum Arc
FTIR	Fourier transform infrared spectroscopy
GDOS	Glow discharge optical spectroscopy
H	Hydrogen
$\hbar$	Planck's Constant
HOPG	Highly Oriented Pyrolytic Graphite
$h\nu$	Photon Source Energy.
$I_D$	Disordering intensity
$I_G$	Graphite intensity
$I_s$	sputtering current
M-DLC	Metal doped Diamond-like carbon
min	Minute
mW	milli Watts
NEXAFS	Near-edge X-ray Absorptions Find Structure
nm	nanometers
Pa	Passcal
PECVD	Plasma enhance chemical vapor deposition
PEY	Partial Electron Yield Mode
$P_s$	Sputtering Pules
PVD	physical vapor deposition

**LIST OF ABBREVIATIONS (Continued)**

RF	Radio Frequency
sccm	Standard Cubic Centimeters per Minute
SEM	Scanning Electron Microscopy
Si-DLC	Si doped Diamond-like carbon
SLRI	Synchrotron Light Research Institute
$sp^2$	$sp^2$ Hybridization
$sp^3$	$sp^3$ Hybridization
ta-C	Tetrahedral Amorphous
ta-C:H	Tetrahedral Amorphous with Hydrogenated
TEY	Total Electron Yield Mode
Ti	Titanium
Ti-DLC	Titanium doped Diamond-like Carbon
Vc	Pulsed bias voltage
W	Watt
XANES	X-ray Absorption Near Edge Structure
XAS	X-ray Absorptions Spectroscopy
XPS	Photoelectron Spectroscopy
Zn	Zinc
Zn-DLC	Zinc doped Diamond-like carbon
$E_0$	Ejected electron energy at interesting shell
$E_B$	Binding Energy
$E_{kin}$	Kinetic Energy of Electron.

**LIST OF ABBREVIATIONS (Continued)**

$I_0$	Incident light Intensity
$I_1$	Transmitted Light Intensity
$\phi$	Work Functions
$\rightarrow$	Arrow (electron transition)
$\mu\text{m}$	micron
$\pi$	Pi State
$\sigma$	Sigma State
$E$	probing X-ray energy
$k$	Wave Number
$x$	Thickness of Sample
$\mu$	Transmission Coefficient

# CHAPTER I

## INTRODUCTION

### 1.1 Introduction of DLC and Advance Characterization

In nature, compositions based on carbon structure are popular. Organic carbon, such as charcoal carbon from burning, carbon form in tissue, and essential nutrient for humans; and inorganic carbon, such as CO<sub>2</sub> from breathing, benzene ring (C<sub>6</sub>), carbonic acid, and so on, are all present in everyday life (Allison et al., 1960; Graham et al., 2017). Graphite, diamond, and many polymer chains are examples of well-known allotropes (Popov et al., 2019). Carbon's properties have led to a variety of applications, including pencils, anode electrodes in batteries, synthesis carbon nanotubes for chemical sensors, and fullerene for material transport (Khademhosseini et al., 2018; Schroeder et al., 2018; Blackburn et al., 2018). Surprisingly, carbon is a well-known chemical that is applied to the surface of materials (as known as carbon film). For example, graphene (a carbon film) is a very thin, ultra-high conductivity material (Ma et al., 2017). However, the carbon structure fraction in the above materials is dependent on carbon hybridization. In addition, the amount of hydrogen in the film was taken into account. Carbon films come in a variety of structures, from amorphous to nanocrystalline, and they're categorized in triagonal phase diagrams (Ferrari and Robertson., 2000). The diagram's interested areas gain as widely understood in coating material science; it was called Diamond-like carbon (DLC).

DLC has two major carbon structures: The C- $sp^3$  fraction is known for its hardness, while the C- $sp^2$  fraction is known for its silky and conductivity properties. As a consequence, the properties of DLC films are primarily determined by their carbon structure, especially the ratio of  $sp^3$  to  $sp^2$  carbon bond hybridizations (Li et al., 2002). These reasons lead to research of many deposition techniques which give various of DLC structure such as physical vapor deposition (PVD), chemical vapor deposition (CVD) and filtered cathodic vacuum arc (FCA), (Guo et al., 2017; Nakao et al., 2017; Lin et al., 2017; Lu et al., 2018). However, one of them is plasma enhanced chemical vapor deposition (PECVD) which is highly attractive for DLC film preparation, it was extensively discussed in chapter IV.

DLC was seriously studied the physical properties. It was coated for protecting materials such as damaged from drill bit spinning, frictions on watch surface, knife, coating on table surface for increasing life time etc. (Strmčnik et al., 2019). From previously article, they presented advantage of high C- $sp^3$  which was coated on knife surface for improving its property (Pancielejko et al., 2012). Additionally, DLC with high C- $sp^2$  coatings can improve tribological properties of the product such as hardness and friction as well as electrical resistivity. Recently, DLC has attracted great attention owing to its outstanding properties suitable for many industrial productions such as hard disk protective film, wear protection, and food processing etc. (Mikamoto et al., 2020; Maeda et al., 2015; Rohrbeck et al., 2014).

Nowadays, the amorphous carbon has been deeply studied and applied in many applications fields (Paul, 2017). The DLC structure was developed with doped-metal (M-DLC) and non-metal for improving its properties. For example, Si doped DLC (Si: DLC) causes low friction coefficient and high wear resistance against sliding

(Liang et al., 2017). Silver nanoparticle (AgNP) doped DLC coated synthetic silk tissue is used as antibacterial bandage, it is more effective for regeneration the human would (Schwarz et al., 2011; Juknius et al., 2016). Moreover, zinc was chosen for studying in this work which is well known for osteoporosis preventing as the following reported (Yonezawa et al., 2020; Yamaguchi, 2010). Additionally, carbon also is a material which is appropriate for bio-compatibility (Thomson et al., 1991). However, the previous researches hadn't been deeply studied in detail of characterization.

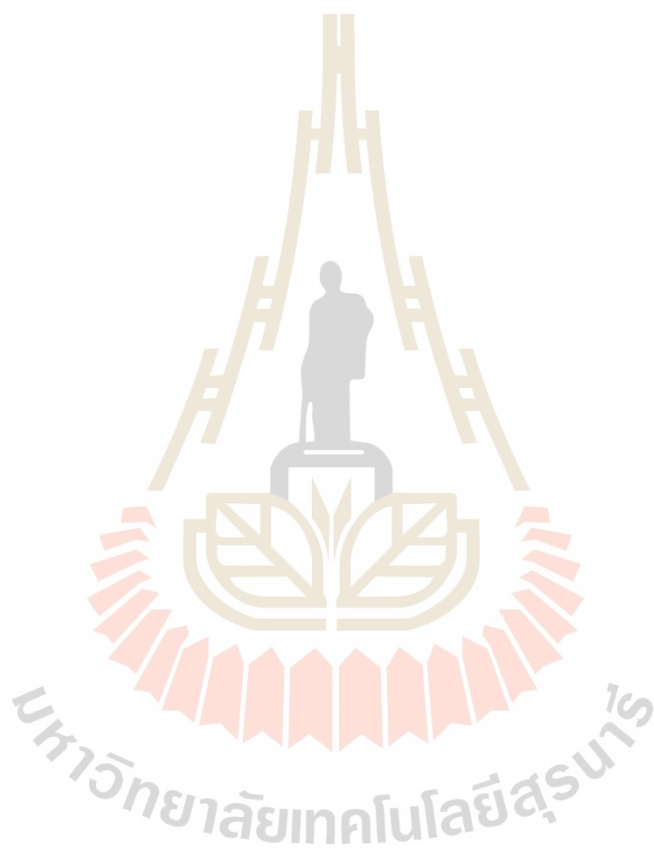
Many spectroscopic techniques were used to investigate the properties of DLC. For instance, X-ray photoelectron spectroscopy (XPS) is a high-performance technique for investigating surface properties and probing interesting elements; however, it cannot describe the high-depth structure of carbon films in details (Rittihong et al., 2020). It also can't distinguish between C-C and C-H  $sp^3$  bonding at carbon legion (Siow et al., 2018;). Raman spectroscopy is a well-known technique for fingerprinting vibration patterns related to carbon structure; however, this technique does not reflect the behavior of the  $sp^3$  fraction; instead, it only represents graphitic vibration and disordering of carbon structure (He and Yeo., 2018). Fourier transform infrared spectroscopy (FTIR) is another good fingerprint technique that only shows atomic bonding information; but we can't use this technique to learn about the surrounding structures. Nuclear magnetic resonance (NMR) is a powerful tool for investigating carbon chemical states. It can be used to determine the carbon  $sp^3:sp^2$  ratio in a sample, but it is not surface sensitive and only looks at the bulk of the material (Bryce et al., 2018). Glow discharge optical spectroscopy (GDOS) is a high-throughput technique for probing hydrogen contents in carbon films, which is linked

to their properties. And indentation hardness, were also utilized to characterize the physical properties of DLC films (Zhou et al., 2017). However, both of these techniques have a history of causing DLC film damaging.

From above reasons lead to deeply studying in this research based on synchrotron characterization techniques which use near-edge X-ray absorptions fine structure (NEXAFS). It is a powerful technique for investigating the electronic structure of DLC films at the carbon *K*-edge (Kikuma et al., 1998). This technique can be measure as high depth profiles which truly provide carbon film structure (Rittihong et al., 2020). The electronic structure from this technique relates not only hydrogen content but also represents to  $sp^2$  and  $sp^3$  fraction which are important factor to classify DLC film properties. The most importance is less deeply studies behavior of interested atom in amorphous carbon structure (Wong et al., 2011). Consequently, the X-ray Absorptions Spectroscopy (XAS) is also powerful techniques can provide the local coordination information such as surrounding atoms, oxidation state, or metal forming etc. (Tasdemir et al., 2014). This technique does not damage the sample, it cannot choose interested area; but it provides bulk properties information which represent to beam size.

In this research, advanced characterization based on synchrotron techniques was mainly considered for characterization DLC structure, along with various spectroscopy techniques. Thermally treated DLC was also considered for commercial samples, and it was discussed extensively in Chapter III. Furthermore, DLC was prepared under different conditions using the PECVD method, as shown in Chapter IV. Finally, we are interested in focusing metal doped DLC by integrating sputtering

and CVD processes. zinc was introduced in DLC films and its behavior was deeply analyzed in Chapter V.



## CHAPTER II

### PREVIOUS WORK AND BACKGROUND OF DLC

#### 2.1 Carbon electron configuration and hybridization

Carbon is generally material which widely found for everywhere in the world. Carbon occurs in every life and it is a basis of organic chemistry such as issue, organism, polymers chain, DNA, protein, CO<sub>2</sub> etc. (Graham et al., 2017). Its atomic number is 6 and the symbol is C. Natural isotropy of carbon occurs in three forms: <sup>12</sup>C for natural founding, <sup>13</sup>C for stability, and <sup>14</sup>C for radiating. The electronic structure of carbon is 1s<sup>2</sup> 2s<sup>2</sup> 2p<sup>2</sup>. Whenever it has interaction with other elements, it will promote electron to higher state which electronic exiation to the empty 2p<sub>z</sub>. Then, it will hybrid itself for requesting unpair electron from 2s. Carbon hybridization is dependent on the formation of environments linked to its resources, it can be classified into three types: *sp*, *sp*<sup>2</sup>, and *sp*<sup>3</sup>. The behavior of carbon hybridization was shown in the following Figure 1 (socratic.org).

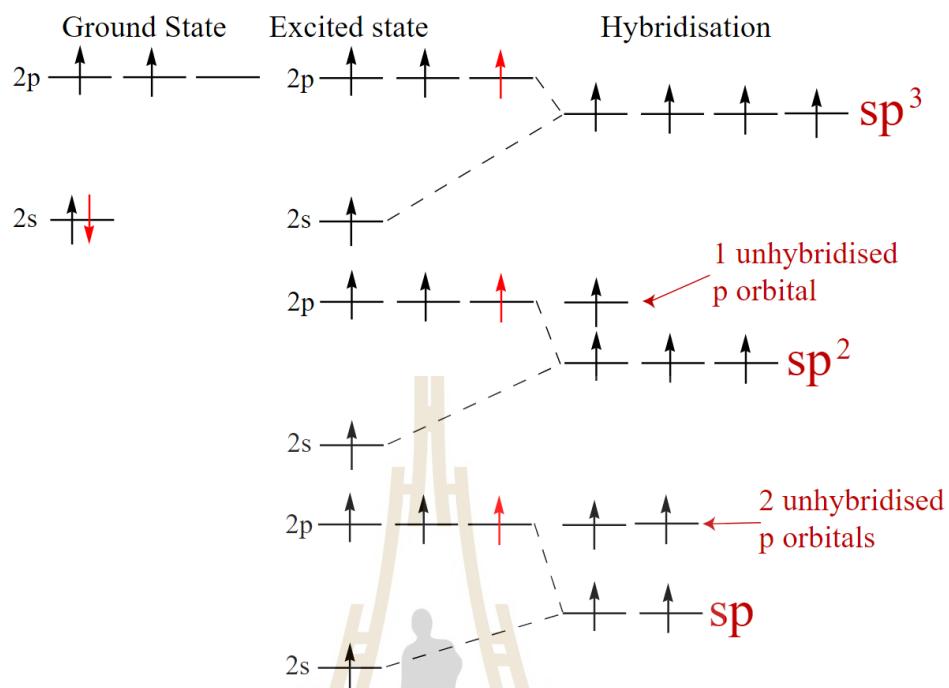


**Figure 1** Ground state, Excited state and Hybridization of electron configuration of carbon.

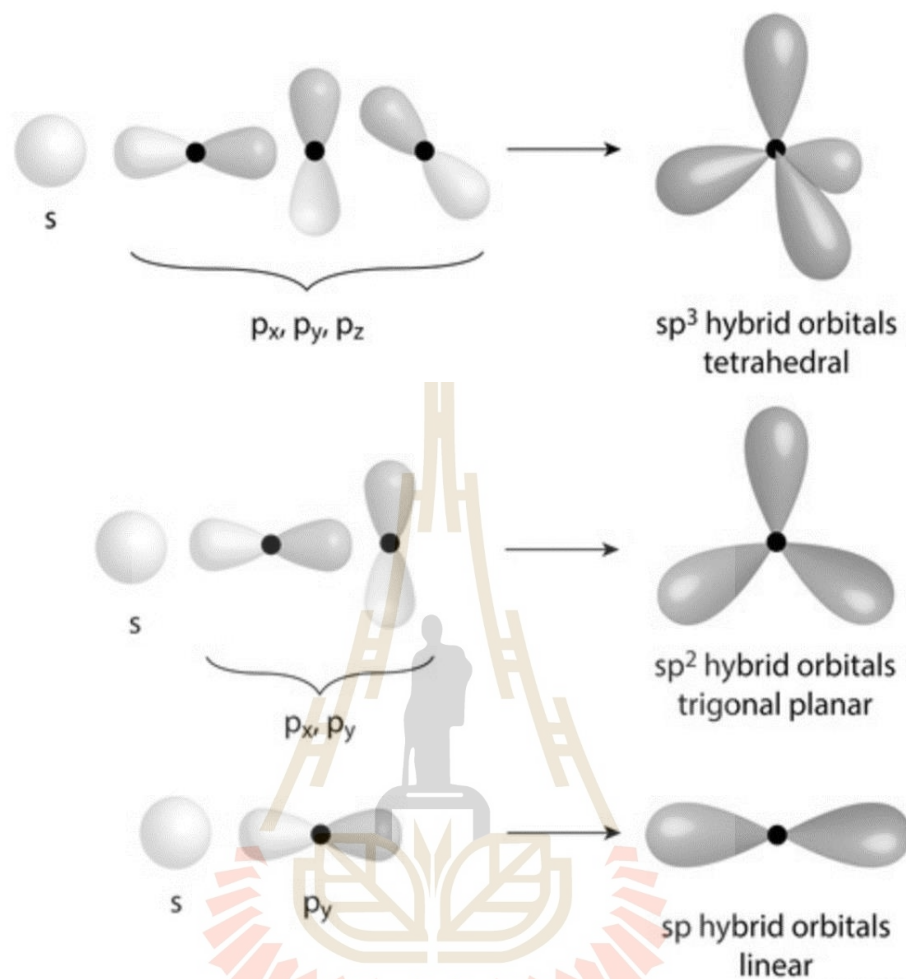


**Figure 2** Carbon atom geometry of hybridized orbitals in  $sp$ ,  $sp^2$ ,  $sp^3$ .

The fundamental of carbon bonding can be natural found in 3 main formulars. Each hybridization of carbon structure exhibit 2 type bonding which are  $\sigma$  and  $\pi$  bond. Sigma-bond is head-to-head interaction, it can be free rotation. This bonding occurs in every carbon hybridization. The pi-bond is generated when two unhybridized  $p$  orbitals in two carbon atoms overlap side by side. In other words, rotation around the internuclear axis does not change the extent to which the  $\sigma$  bonding orbitals overlap because the bonding electron density is symmetric about the axis; it was found in  $sp$  and

$sp^2$  hybridization (forbidden in  $sp^3$ ). To make it simple to comprehend, Figure 3 depicts the three basic forms of carbon hybridization: single, double, and triple.

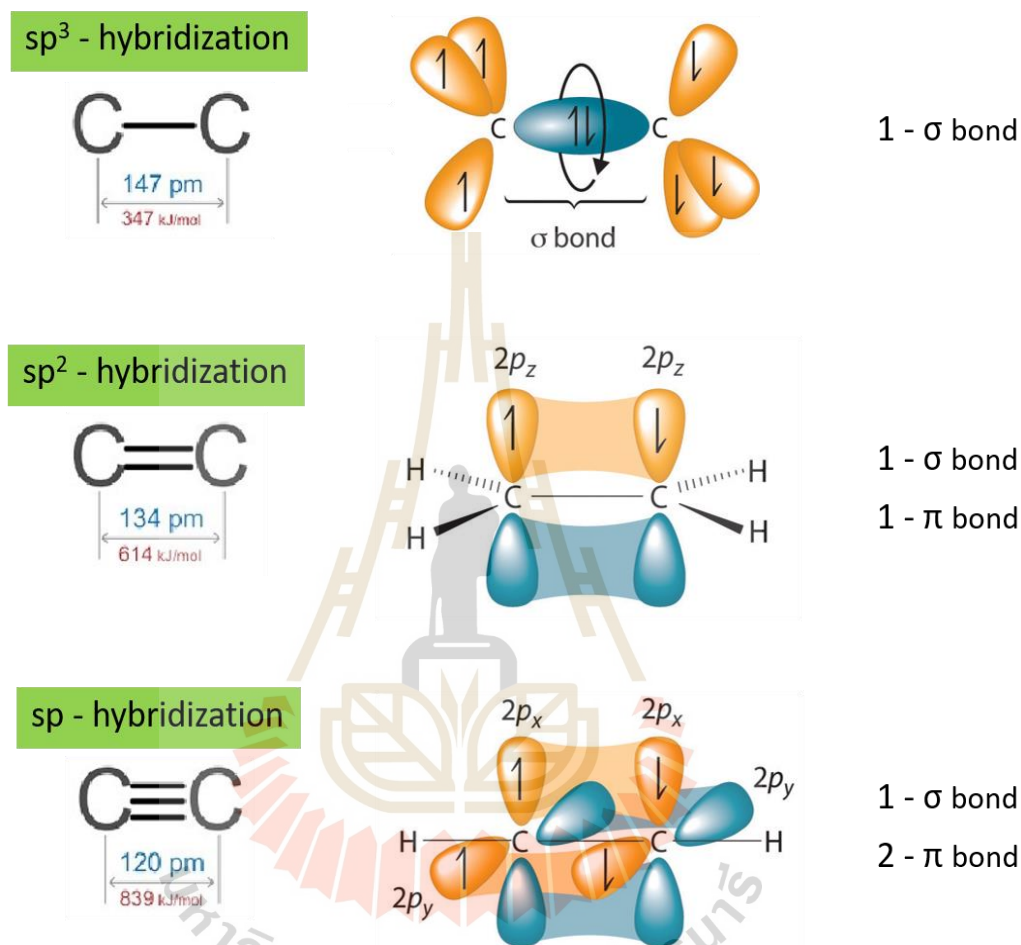


**Figure 3** Single, Double and Triple bond for carbon hybridization.

From 3 type of hybridizations (Figure 2),  $sp$  forming is oriented with bond angle of 180 degrees which s orbital mixed with one p orbital, in a linear geometry, it widely found in polymer chain and organic such as ethyl ( $C_2H_2$ ). Its properties are high strength when it created a bonding. While,  $sp^2$  hybridization are oriented with angle of 120 degree in triangular plane which s orbital mixed with two p orbitals. Whenever, there are many  $sp^2$  forming in a plane, this cluster was called “graphene”, it has very good

electronic properties which was popularly applied in electronic device, transporting material and “thin films coating which reported in this work”. And carbon  $sp^3$  exhibit tetrahedral forming which is oriented with angle of 109.5 degree in three dimensions. An example of hybridization can be seen in carbon such as ethane ( $C_2H_6$ ). Its cluster without hydrogenate was called diamond which is well-known for highest hardness and high price materials in the world. Higher bond energy is related with increasing in bonding in structure; while, bond length decreases with number of  $\pi$  bond for symmetry.

Diamond, on the other hand, cannot be synthesized in a laboratory and does not have a pure structure, the results also gave the carbon in  $sp^2$ -fraction (Aisenberg et al., 1971). Coincidence from synthesist this material brought to discovered in mixing of  $sp^3$  from diamond and  $sp^2$ . Then, this material was well-known called as Diamond-Like Carbons (DLC).

## 2.2 Diamond-Like Carbons: DLC

DLC was firstly reported in 1971. It was accidentally found by Aisenberg et al. who mainly study hard films based on carbon composition. During, they studied high pressure synthesis crystalline diamonds, it was not purity phase, they also found another carbon structure which include in this synthesis carbon compositions which later was called Diamond-like carbon or DLC (Aisenberg et al., 1971). Since 1971, it was deeply studies structure which including 2 mains carbon structure C-  $sp^2$  and C-  $sp^3$  hybridizations which is composition of graphite and diamond structure. They found C-  $sp^2$  fraction exhibits the silky properties while C-  $sp^3$  fraction also exhibits the strength, hardness, and shiny properties (Dwivedi et al., 2011). Moreover, other elements in the structure such as hydrogen and oxygen also considered for film properties and film

qualitative (Kim et al., 2016). During that time, DLC was highly interested for thin films science which was new major for driving worldwide films applications. The question is how can we apply this property in materials application for daily life.

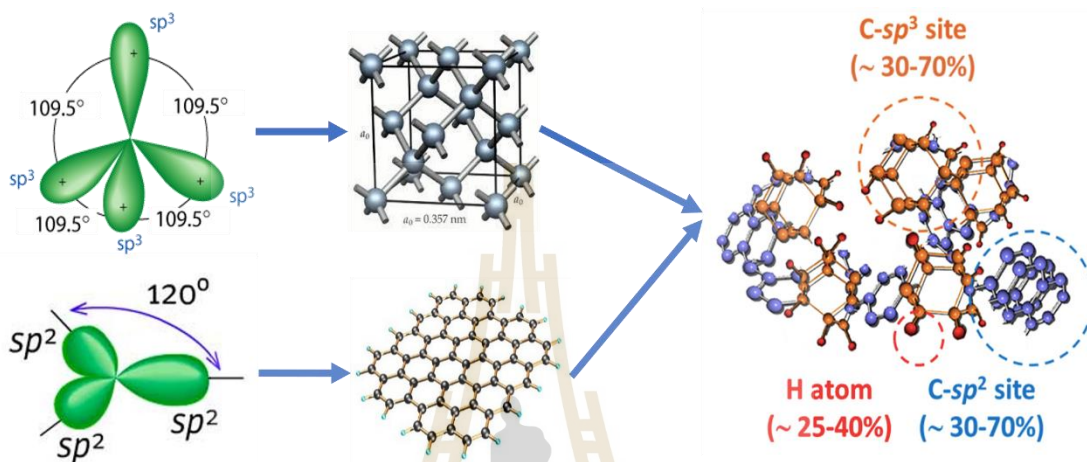


**Figure 4** Fundamental of Diamond-like carbon (DLC) structure.

Carbon materials' adaptability stems from the fact that their physical properties are highly dependent on the ratio of  $sp^2$  graphite-like to  $sp^3$  diamond-like links (Li et al., 2002). From microcrystalline graphite to glassy carbon, there are different types of  $sp^2$  bonded carbons with varying degrees of graphitic ordering. In general, an amorphous carbon can have any combination of  $sp^3$  and  $sp^2$  sites, as well as up to 60% hydrogen (Ferrari and Robertson., 2000).

DLC was simply divided into four primary forms based on many previous reports. To begin with, amorphous Carbon ( $a$ -C) with a high proportion of  $sp^3$  bonds. The C-C  $sp^3$  content of hydrogenated amorphous carbons ( $a$ -C:H) is quite low. Tetrahedral amorphous carbon ( $ta$ -C) is a type of DLC with a higher  $sp^3$  content, and it is hydrogenated ( $ta$ -C:H). Another element is the degree of clustering in the  $sp^2$  phase, which gives DLC films their unique features.

The properties of DLC films are strongly related to its structure, especially the ratio of  $sp^3$  to  $sp^2$  hybridizations of carbon bonds. Most hydrogen-free coatings are applied using a method of physical vapor deposition (PVD) by arc evaporation, which produces tetrahedral amorphous carbon such as sputtering technique. While, DLC with hydrogen content are applied using a method of chemical vapor deposition (CVD) which used hydrocarbon gas for depositions such as  $CH_4$ ,  $C_2H_2$  etc. The compositions are conveniently shown on the ternary phase diagram in Figure 5. And type of DLC was deeply explained as the following.

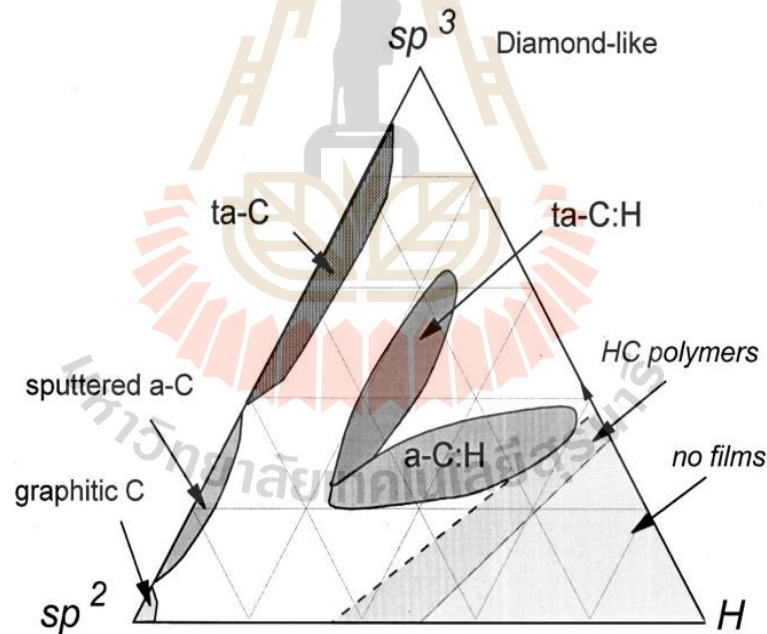


**Figure 5** Ternary phase diagram of amorphous carbons. The three corners represent to diamond, graphite, and hydrocarbons, respectively. (Ferrari and Robertson, 2000).

**Table 1** Comparison properties of carbon materials.

properties	Graphite	Diamond	DLC
Specific gravity	2.25	3.52	1.0-3.0
Specific electric resistance ( $\Omega \cdot \text{cm}$ )	$10^{-3}$	$10^{12}$ - $10^{16}$	$10^{9-14}$
Thermal conductivity (W/cm/K)	0.4-2.1	1000-2000	0.2-30
Young's modulus (GPa) Hardness numb	....	1000-2000	100-800
Hardness number (Hv)	....	10000- 12000	1000- 8000
Oxidation start temperature (K)	400-450	600	300-500
Lattice constant (nm)	a=0.2456 c=0.6708	a=0.3567 ....	.... ....

### 2.2.1 Amorphous Carbon (a-C)

The majority of amorphous carbon films were discovered as a result of the sputtering method (Fiaschi et al., 2019). In structure, the proportion of  $sp^3$  varied between 20 and 60%. It has an excellent characteristic that prevents hydrogen contamination. This structure had a lot of shiny and silky properties. Black is major of film character. This mixture was discovered in thick films. It was mostly coated for material foundation prior to the application layer, such as alloy compound or metal layer, being deposited (Ning et al., 2020; Dhandapani et al., 2019).

### 2.2.2 Hydrogenated amorphous carbons (a-C:H)

This hydrogenated DLC include C- $sp^3$  fraction 20-50% and hydrogen content 0-40%, approximately. This structure was commonly found by chemical vapor deposition techniques; because, initial gas flow include hydrogen which is mainly composition such as methane ( $\text{CH}_4$ ), acetylene ( $\text{C}_2\text{H}_2$ ), benzene ( $\text{C}_6\text{H}_6$ ), etc. The researcher reported, the hydrogen component in DLC lead to color change of carbon film's structure

(Shimada et al., 2015; Zhou et al., 2020). However, a-C:H was applied as one of multilayer film by previously report (Kot et al., 2013; Catena et al., 2017).

### **2.2.3 Tetrahedral amorphous carbon (ta-C)**

Tetrahedral amorphous carbon is the most powerful DLC, according to the trigonal phase diagram. It was a common occurrence due to the filter cathodic vacuum arc (FCVA) deposition procedure. The structure of high  $sp^3$  content was variable in range from 40 to 60%. Hardness is a quality that can be exceedingly hard, exceeding 90 GPa; as a result, this feature has been used in numerous protection coatings in tooling components such as watches, spinning, endmills, and drill bits (Mikamoto et al., 2020; Strmnik et al., 2019; Rohrbeck et al., 2014).

### **2.2.4 Hydrogenated tetrahedral amorphous carbon (ta-C:H)**

This carbon film likewise uses hydrocarbon gas as a deposition starting source, which was decomposed using the CVD procedure. High producing plasma, on the other hand, is an important factor in boosting C- $sp^3$  fraction (increase in tetrahedral carbon). It has excellent corrosion and wear resistance properties. Nowadays, this structure makes it easy to modify surface thin films for applications like UV- C radiation treatment, flexible intermediates of multilayer, and so on. (Lackner et al., 2015; Milenov et al., 2021).

## **2.3 DLC applications and metal doped**

Diamond-like carbon (DLC) films have been largely studied for their excellent mechanical properties and their high potential in many industrial applications. Recently, several attempts have been made to improve the properties of DLC films such as gas flow rate dependence of films preparations, roughness properties improving, techniques

for growing etc. Moreover, metal-doped in DLC is one interesting parameter for improving structure and leading newly applications. Due to promising features such as high hardness, low friction coefficient and residual stress, and high wear-resistance, metal-doped diamond-like carbon (M-DLC) films have gotten a lot of attention in the scientific community as the following.

### **2.3.1 Ag-DLC**

DLC doped with silver nanoparticles is effective as an antibacterial coating (Schwarz et al., 2011). Cell division processes are disrupted, resulting to cell death, due to morphological abnormalities in the bacteria cell membrane and probable DNA damage caused by the Ag-DLC interaction. When Ag NPs interact with water molecules, they are known to oxidize to Ag<sup>+</sup> ions. The antibacterial activity of Ag NP based nanocomposites is widely acknowledged. Because of the aforementioned reasons, Ag-DLC was employed in medical applications such as leading around a bandage to solve a lesion. The body's healing rate will be accelerated as a result of the ag response. Because fast regeneration reduces the number of people infected with bacteria. The properties of Ag reactions are presented in the Ag-DLC report utilizing characterisation techniques. There are two types of bacteria that are commonly present in life (*S. aureus* and *P. Aeruginosa*). After growing on Ag-DLC, the bacteria were destroyed after 3 hours and definitely after 24 hours, as shown in Figure 6. When more silver was added, the antibacterial effect was increased.

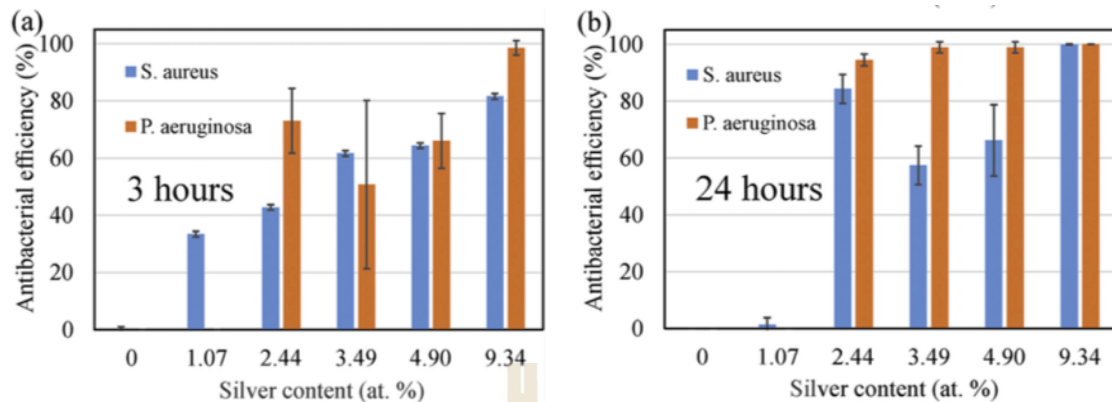


**Figure 6** The antibacterial effect from Ag-DLC layer after 3h (a) and 24h (Písařík et al., 2017).

### 2.3.2 Ti-DLC

Ti-doped is important factor in the mechanical applications. It was widely used to decrease the friction properties of the films. The interesting reported presents the variations Ar/CH<sub>4</sub> flow rate by using sputtering technique for growing Ti-DLC films. At relatively high Ar/CH<sub>4</sub> flow ratio, the ionization rate of CH<sub>4</sub> gas increases because of the collision of large amount of Ar<sup>+</sup> ion and CH<sub>4</sub> gas, which causes of increasing in the growth rate during deposition. Moreover, the target surface was collided with Ar<sup>+</sup> ions which is large amount of titanium atoms can be sputtered out, easier. Raman spectroscopy was used to obtain the detailed disorder structure of the DLC films. Feature of Raman spectra in Figure 7(a) was changed at D-band after variations of Ti-doped. Increasing of I<sub>D</sub>/I<sub>G</sub> ratio relate with Ar flow rate and Ti concentrations shown in Figure 7(b). Moreover, the bonding natures of Ti-DLC were studied using XPS analysis presented in Figure 8(a-b). The spectra show increasing of *sp*<sup>2</sup>-fractions when increasing volume of Ar/CH<sub>4</sub> flow rate (Cui et al., 2012).

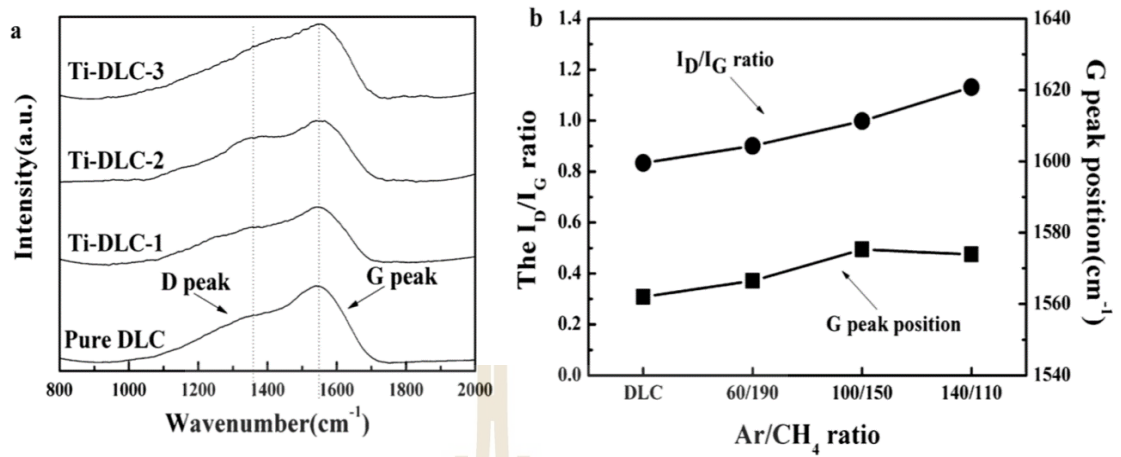


**Figure 7** (a) Raman spectra and (b) the corresponding G-peak position and  $I_D/I_G$  ratio of the Ti-DLC films deposited at different Ar/CH<sub>4</sub> flow ratio.

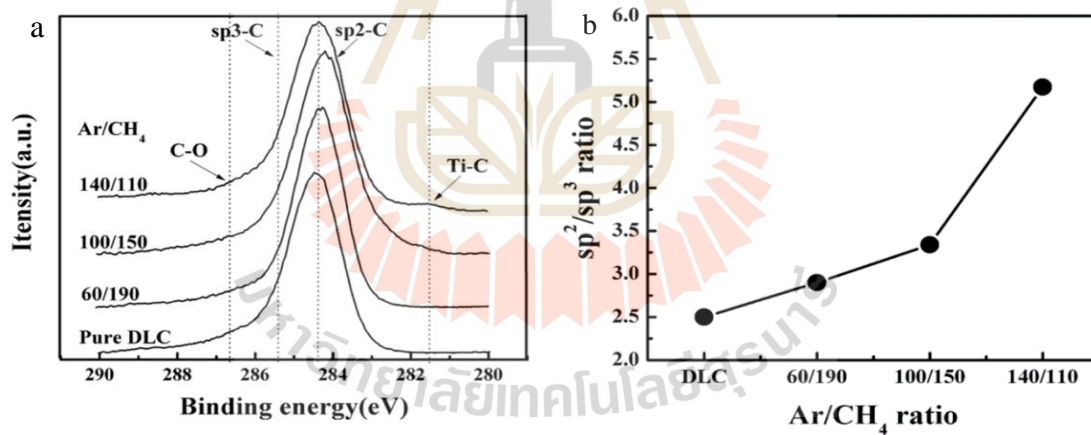


**Figure 8** (a) The XPS C 1S peak (b) the relations of  $sp^2/sp^3$  ratio.

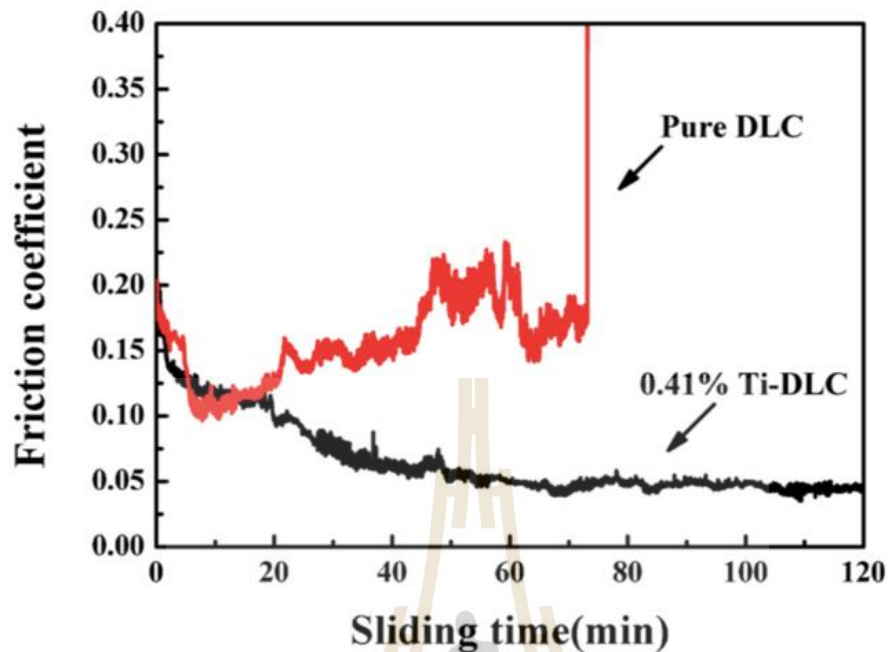


**Figure 9** Friction coefficient of Ti-DLC film and pure DLC film.

The friction coefficient was evaluated using the following conditions: load, 10N; counterparts: sliding velocity, 10 cm/s. The 0.41 percent Ti-DLC films have a lower friction coefficient than Pure-DLC based on spectra. The films deposited at various Ar/CH<sub>4</sub> flow ratios have an XPS C 1S peak. Low Ti doping has a low effect on internal stress while maintaining hardness. In addition, Ti was added to the DLC film to give it a reduced friction coefficient and better wear resistance (Caschera et al., 2007).

### 2.3.3 Zn-DLC

Zn-doped is one interesting metal for medical application. This metal was widely used for Decrease the frictions properties. Moreover, Zn can solve osteoporosis problem which is mostly found in old human. Most case of problems was happened at the bones-joint positions such as knee, elbow, hip bones or ankle etc. All of these, lead to the bedridden of patient that cannot do anything by themselves. From above reason, the Zn-

doped on DLC very important for solving elderly people. AFM of Zn-DLC films give low roughness when compared with pure-DLC (Wong et al., 2011), which was performed for decreasing frictions at bone-joint. Moreover, the reported present the higher  $I_D/I_G$  ratio of Raman spectroscopy after Zn-doped. And the XPS spectra present decreasing of  $sp^3$  content when increasing Zinc concentrations.

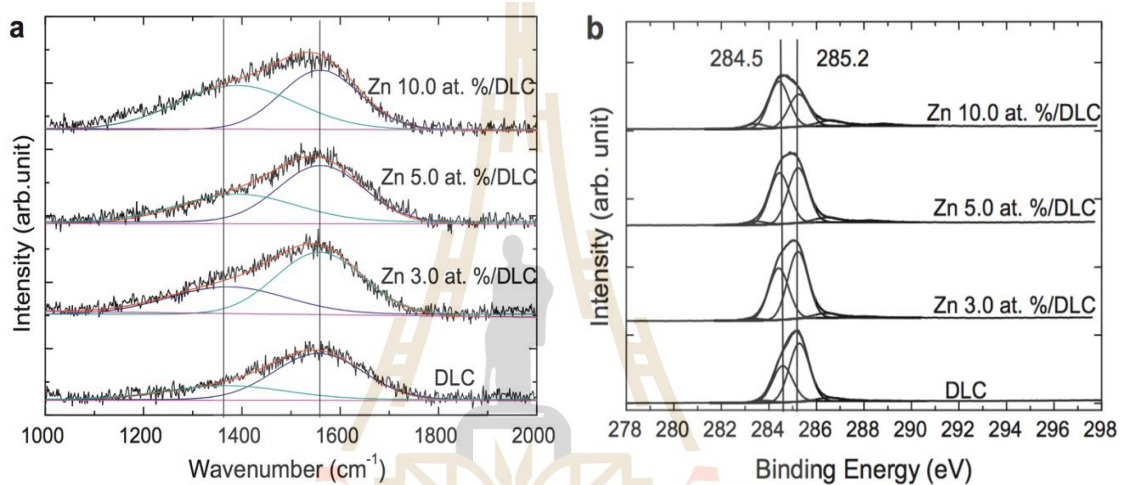


**Figure 10** Raman spectra (a) XPS spectra (b) for Zn-DLC (Wong et al., 2011).

## 2.4 Preparations of diamond-like carbon films

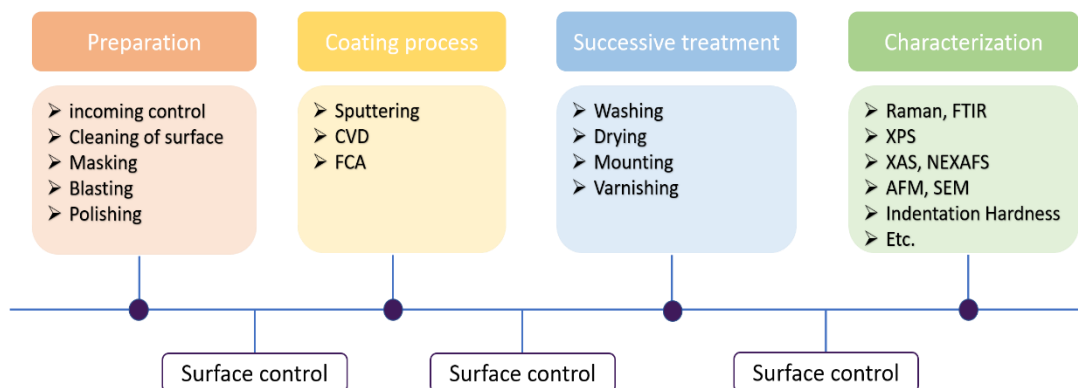


**Figure 11** Overall thin films depositions process diagram.

The Figure 11 show over all of thin films depositions process, it was carefully made step by step. In the solution, depositions process begins with surface preparations, the substrate was prepared as the following; cleaning by acetone or ethanal, masking, polishing and etc. Then, the substrate was put on prepared chamber which was controlled at ultra-vacuum for background pressure. The second is coating process which relate to opportunely of required DLC fraction. In this work, sputtering, and CVD techniques are interested. The third is films surface treatments, this part is very necessary in industrials for i films quality before exported to next process. Its surface was improved by physical and chemical techniques such as washing, drying, mounting and varnishing etc. In the last, the successfully prepared films were study film's structure, mechanical and chemical properties by films characterizing such as disordering structure by Raman, chemical bonding by FTIR, surface properties by XPS and local structure by XAS etc. Before going on to characterization, we'll go over the deposition procedure for several types of DLC films.

## **2.5 Deposition techniques for growing DLC films**

### **2.5.1 Sputtering techniques**

In principle detail, sputtering is plasma-based technique which was generated by controlling voltage or power. Typical, a sputtering chamber is effectively evacuated to high vacuum to minimize background pressures and removing contaminations gases. After background pressure has been reached, sputtering gas which includes the plasma such as Argon and Helium are slowly flowed into the chamber. The total pressure is regulated in the  $10^{-2}$  milli-bar range using as pressure control system. Then, the target

surface is eroded by high-energy ions from the generated plasma. And the removed atoms travel through the vacuum environment and deposit onto a substrate to form a thin film.

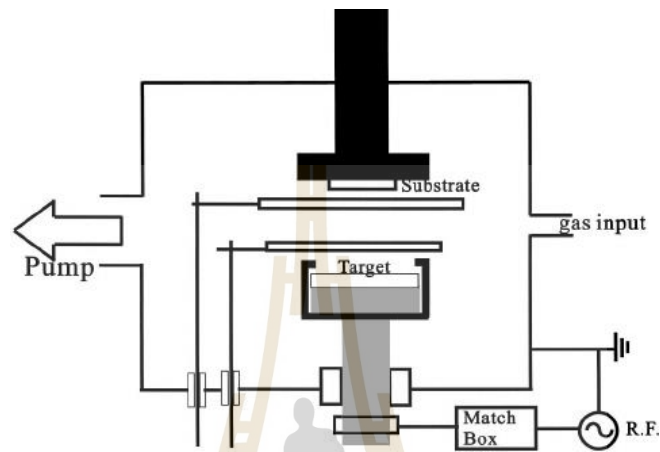


**Figure 12** Diagram of sputtering system.

The sputtering technique was well known for conducting material, typically a metal, such as a Copper (Cu) and Nickel (Ni). It was mostly found in high quality optical coating such as Silicon (Si) and Titanium (Ti). This technique does not require melting or evaporation of the target materials which lead to many advantages over others PVD technologies. However, carbon material also is widely used for deposition thick DLC films. Typically, graphite target was used which proper for giving high content of carbon  $sp^2$ . The sputtering diagram was show in the Figure 12.

### 2.5.2 Plasma enhances chemical vapor deposition (PECVD)

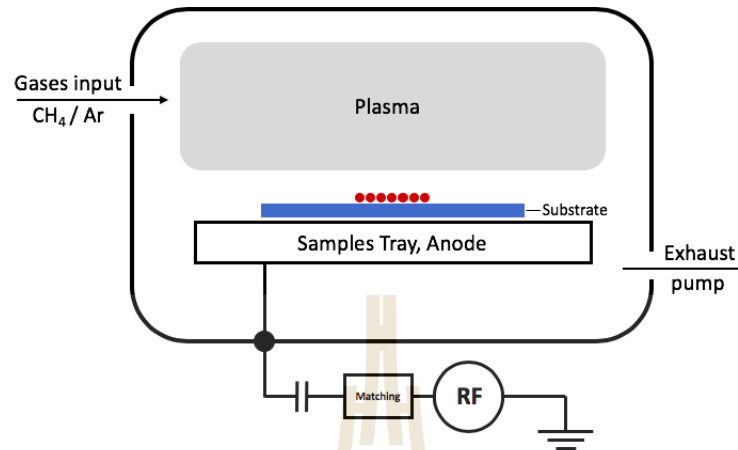


**Figure 13** Schematic diagram of PECVD system.

Chemical vapor deposition (CVD) is a deposition method for producing high-performance, high-quality, solid materials etc. This technique is the process relating chemical reactions between an organic compound and the other gases. The mixing gases have been deposited nonvolatile solid thin films on substrates. This technique is employed in a wide range of industry applications, such as the deposition of refractory materials, semiconductors, optical fibers, powder production and photo chemical vapor deposition (PCVD) for catalysts etc. However, the prominence of this technique is Plasma enhance chemical vapor deposition (PECVD). It was effetely used for producing amorphous carbon films. In detail, base pressure was controlled, typically under vacuum in range  $5 \times 10^{-2}$  Pa before deposition. The processing temperatures range is between RT-400°C. The substrate has been generated negative please in chamber source. And then, the carbon will diffuse toward the generated substrate, which typically - methane (CH<sub>4</sub>) acetylene (C<sub>2</sub>H<sub>2</sub>) and ethene (C<sub>2</sub>H<sub>4</sub>) were used for source gases deposition.

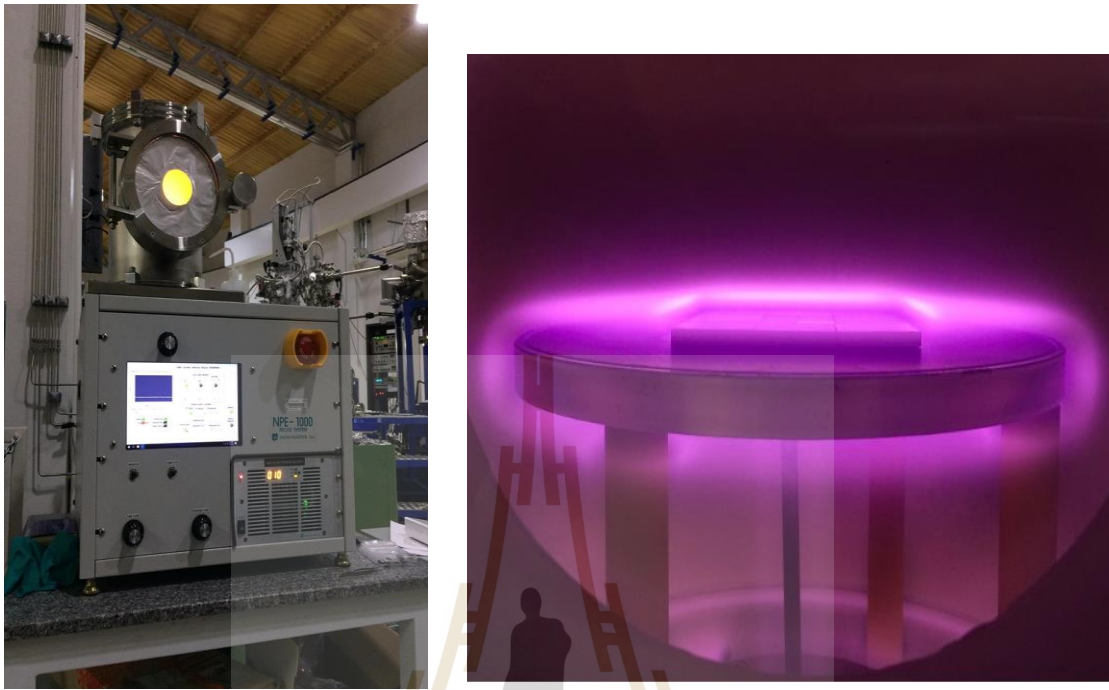


**Figure 14** (a) PECVD system in SLRI and (b) generated plasma in chamber.

### 2.5.3 Filtered cathodic vacuum arc (FCVA)

Filtered cathodic vacuum arc (FCA) or (FCVA) is one of most interesting technique with very complicated process for DLC films depositions. It gives high fraction ratio of  $sp^3$  and low hydrogen content in carbon structure. Deposition's rate is very low for films forming which lead to very high ultra-thin films product and high quality of interested films condition. However, this technique related more process during deposition such as operation, very clearly contamination, high ultra- background pressure etc. As a result, the cost of a depositions machine using this technology is extremely high. It's typically used in industrial systems to make one component of a material. The following figure show deposition process of FCVA techniques.

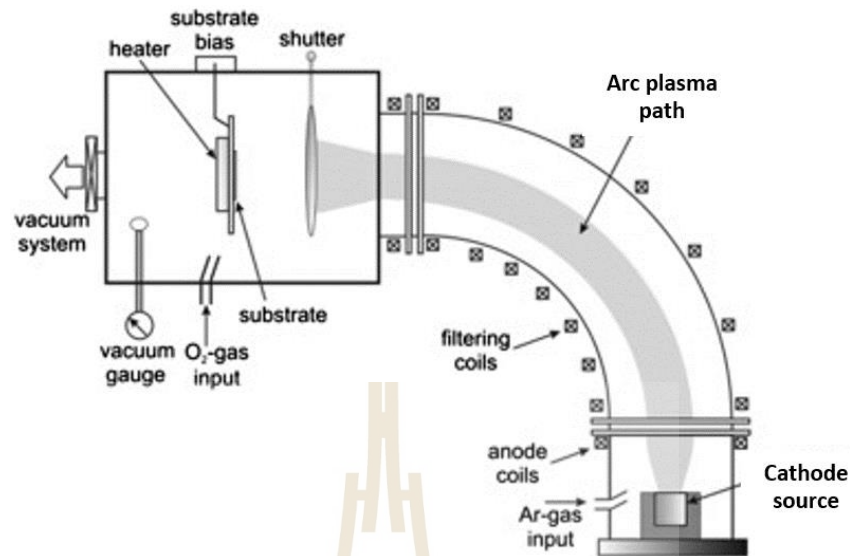


**Figure 15** Schematic of the Filtered Cathodic Vacuum Arc process (Elzwawi et al., 2012).

In detail of deposition, Cathode processes are known of cathodic arc plasma deposition. The process has features that is surprising or strange. the process begins with the outstanding of a highly generated current, low voltage arc on cathode surface which is known as the target. It usually gives a small particle. as the arc is generally a current carrying conductor, it can be influenced by applying of an electromagnetic field, which in practice is used for rapidly moving the arc over the interacted of target surface, so that the total surface is eroded over time. The arc has an extremely high-power density resulting in a high level of ionization, neutral, charged ions, macro-particles and clusters. In case of reactive gas is introduced during the evaporation process, the excitation and ionization can occur during interaction with the ion flux and a compound film will be deposited.

## 2.6 Technique for characterizations

For classification several type of DLC, many characterization techniques are interested to study behavior of carbon films, such as electronic structure, films hardness, disordering of carbon structure, surface properties and deeply studying local structure of DLC films. In this thesis, several techniques were chosen as the following.

### 2.6.1 Raman Spectroscopy

Raman spectroscopy is a scattering and interfering spectroscopic technique for observing low-frequency rotational, vibrational, and other modes in a system. It is extensively used in chemistry to generate a fingerprint spectrum that may be used to identify compounds. It works by scattering monochromatic light inelastically, or Raman scattering, commonly from a laser in the near infrared, visible, or near ultraviolet range. As the laser light interacts with molecular vibrations, phonons, or other excitations in the system, the energy of the laser photons is pushed up or down. The vibrational modes of the system are revealed by the energy shift.

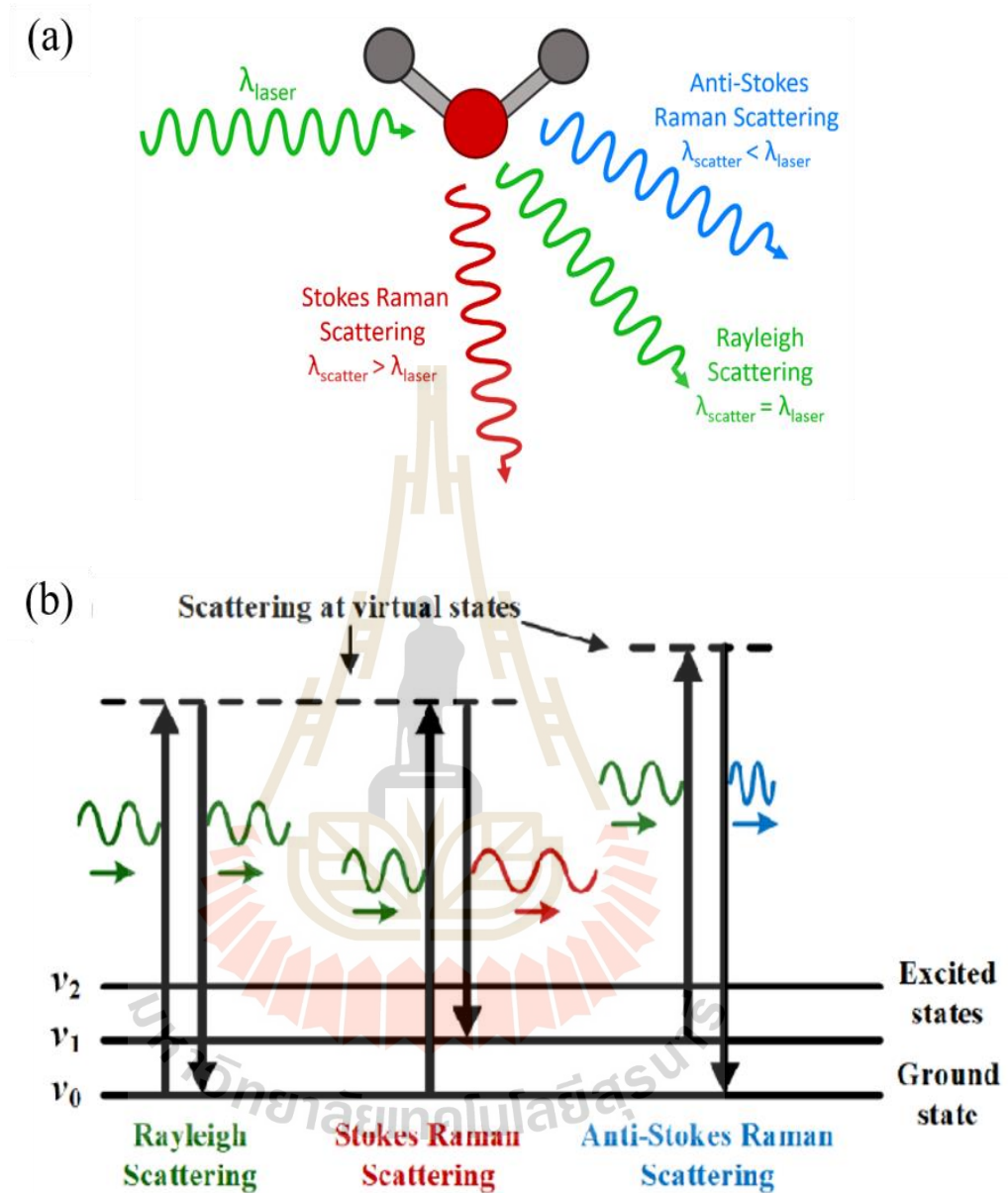


**Figure 16** Basics principle of atomic vibration with interaction wavelength (a), and state diagram of scattering pattern (b).

Typically, the raman system is primarily separated into two sections: input and output. The excitation laser source is the major component of the input ( $h\nu_s$ ), and output system consists of scattered radiations ( $h\nu_l$ ). Figure 16 represent the principle of

atomic vibration by transition state. The major elastic scattering is represented by the Rayleigh pattern. While scattering can occur from atoms or molecules, scattering between molecules can be inelastic due to a change in the molecule's rotational energy which was called Raman scattering. This inelastic pattern can arise for 2 main types which are Stokes Raman scattering (higher own state) and anti-Stokes Raman scattering (lower own state). The interaction can be explained by using the following equations which are typically reported in wavenumbers:

$$\frac{1}{\lambda_{Raman}} = \frac{1}{\lambda_{incident}} - \Delta\bar{\nu}$$

$$\bar{\nu}_s = \bar{\nu}_I - |\Delta\bar{\nu}| \quad \text{Stokes Raman scattering}$$

$$\bar{\nu}_s = \bar{\nu}_I + |\Delta\bar{\nu}| \quad \text{anti-Stokes Raman scattering}$$

Where:  $\bar{\nu}_s$  Frequency of scattered photon ( $\text{cm}^{-1}$ )

$\bar{\nu}_I$  Frequency of incident photon ( $\text{cm}^{-1}$ )

$\Delta\bar{\nu}$  Frequency of Raman shift ( $\text{cm}^{-1}$ )

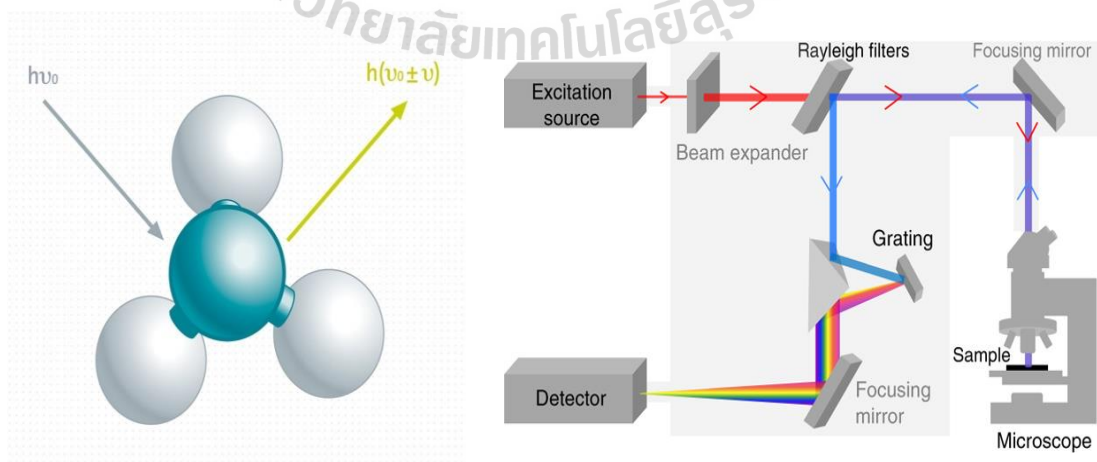


**Figure 17** Raman principle and typical of Raman system (WITec Pte. Ltd.).

In this work, dispersive raman (Sentara, Bruker) was used to identify the feature of carbon composition such as amorphous and graphite properties of the DLC films. The main peak positions include peaks of G-band (as main spectral feature of graphite that indicated the number of its cluster) and D-band (as disorder band) of lattice motion away from carbon bonding. The ratio of D-band and G-band intensities,  $I_D/I_G$ , is correlated to the  $sp^3/sp^2$  ratio (Ferrari and Robertson., 2000). These intensities are the main regions for interpreting DLC films structure in this thesis.

### 2.6.2 X-rays Photoelectron Spectroscopy (XPS)

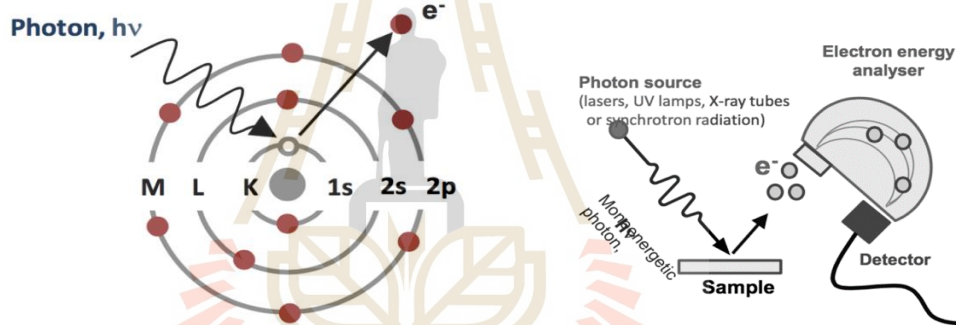


**Figure 18** Photoelectric effect and typical of XPS system (BL-5.3 SLRI).

From the photoelectric principle, core electrons are ejected from the surface irradiated with the X-ray beam source. These exiting have a characteristic kinetic energy depending on the element, orbital and chemical state of the atom. The photoelectric effect can be explaining by following equations:

$$E_{kin} = h\nu - E_E - \emptyset \quad (1)$$

Where:  $E_{kin}$  is kinetic energy of electron.

$h\nu$  is photon source energy.

$E_E$  is binding energy of probing element

$\emptyset$  is work functions of probing element.

XPS is a powerful technique used to study the elemental composition of sample. This technique is very surface sensitive for sample that measure during 1-10 nm of depth. Thicker layers can be analyzed by ion beam depth profiling. The XPS spectra were measured at BL5.3 of Synchrotron Light Research Institute (SLRI) Thailand. XPS measurements were performed using a PHI5000 Versa probe II (ULVAC-PHI, Japan) equipped with a hemispherical electron energy analyzer at the SUT-NANOTEC-SLRI joint research facility, Synchrotron Light Research Institute (SLRI). A monochromatic Al K $\alpha$  X-ray gun (1486.6 eV) was used as the excitation source.

The XPS survey scans were taken from 0-1400 eV using a pass energy of 117.40 eV and an energy step of 1.0 eV to probe diamond-like carbon. For probing elements of interest, high resolution XPS spectra were acquired with a pass energy of 46.95 eV and an energy step of 0.05 eV. PHI Multipack XPS software was used to analyze the XPS spectra. The C1s peak at 284.8 eV was used to calibrate the binding energy of all XPS spectra. Peak deconvolution was achieved via Sherly background removal and Gaussian-Lorentzian line shape combinations. Furthermore, the intensity from XPS was calculated using the following formula:

$$I = \frac{\text{Peak area}}{\text{sensitivity factor}} \quad (2)$$

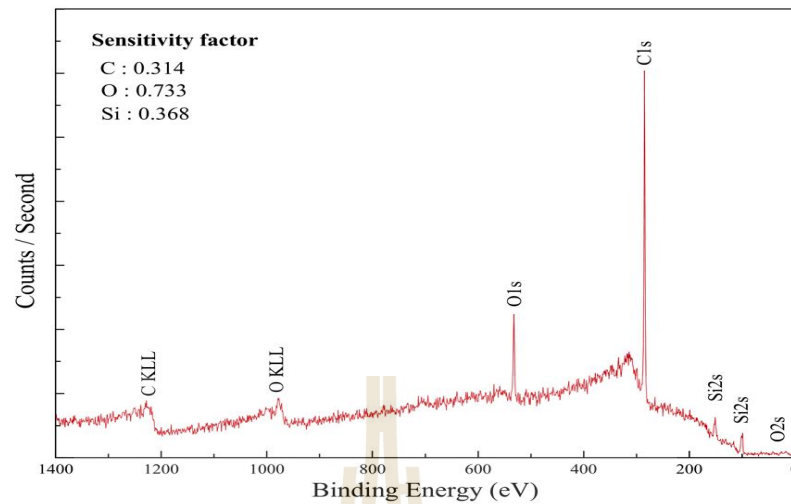


**Figure 19** wide scan of XPS spectra of DLC films.

However, utilizing merely carbon area intensity to corroborate the Correctness from XPS data is not possible. The other compositions were considered by opportunity comparing with equilibrium binding intensity., the intensity of the deconvoluted peak from C-O at the Carbon area should be equal to the intensity of the deconvoluted peak from O-C at the oxygen zone by using the equation (2). The following diagram in Figure 20 depicts the summary XPS fitting method in this study.

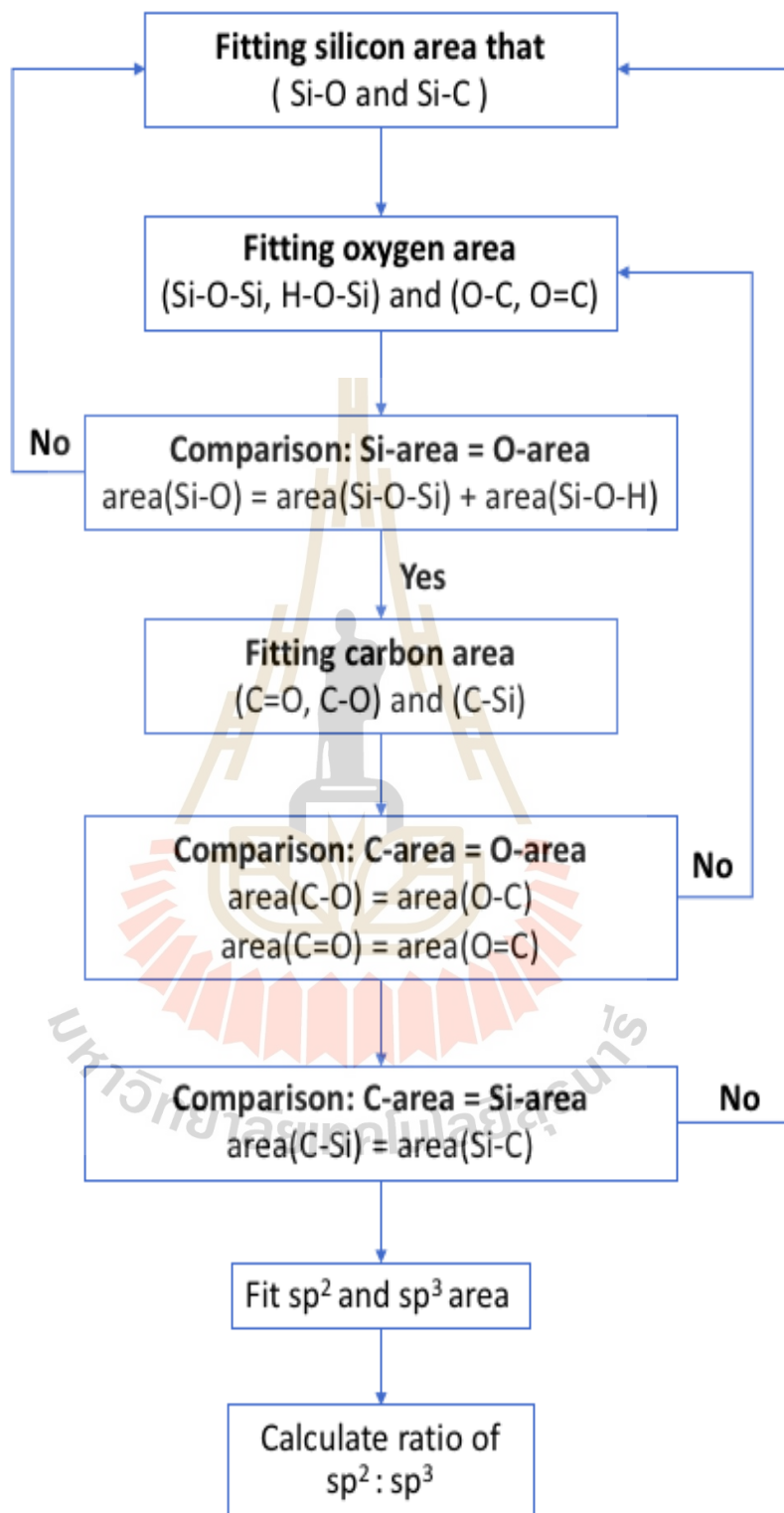


**Figure 20** Diagram of fitting XPS area for DLC films.

### 2.6.3 Indentation hardness

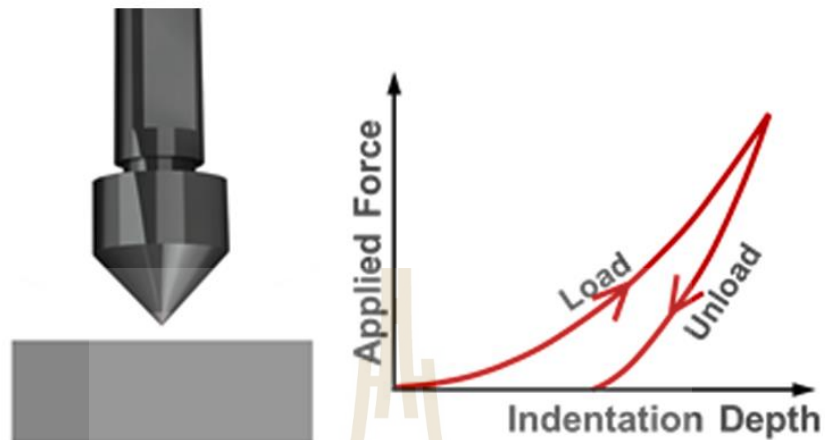


**Figure 21** Operation of Indentations Hardness for DLC Measuring.

This technique is widely used in mechanical engineering for studying the hardness and deformation of materials. According to the Figure 21, the tip was slowly applied to surface of samples as perpendicular direction. It was show load-unload force which related to depth positions of thin films. Normally, depth profile was measured in range 10 percent of the films thickness for eliminate the influence on the substrate. Hardness tests are characterized by the shape and substance of the indenter as well as the magnitude of the load applied. Brinell and Rockwell for microhardness, Knoop for microhardness, and Vickers for both macro- and microhardness are some of the more usual tests. The following formulae were used to estimate the indentation hardness value in this study.

$$\text{Hardness} = \frac{\text{Peak Force (N)}}{\text{Contact Area (cm}^2\text{)}} \quad (3)$$

Testing by indenting materials make a small impression on materials with low applied loads, typically have force 3mN.

#### 2.6.4 Glow discharge optical emission spectroscopy (GD-OES)

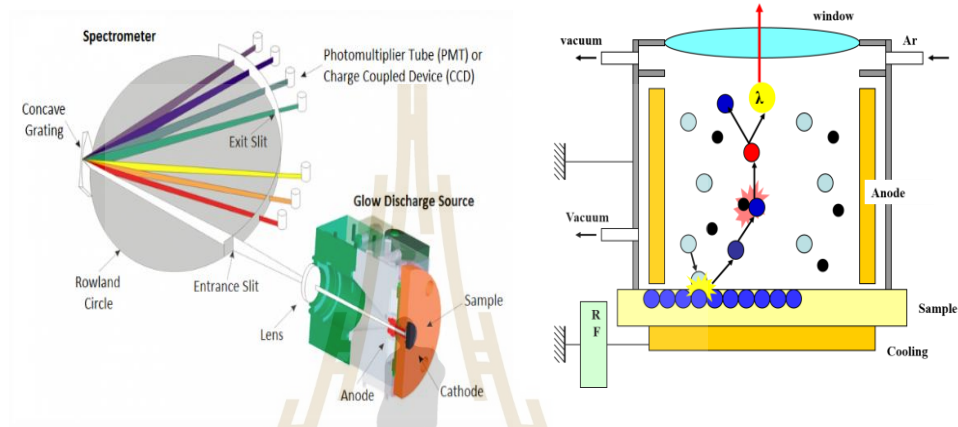


**Figure 22** Theoretical of elements investigation by GDOS techniques.

Glow-discharge optical emission spectrometry (GD-OES) has proved to be an effective method for analyzing elements on solid surfaces (Maruno and Nishimoto, 2018; Nishimoto et al., 2020). GD-OES can be used to calculate the bulk concentration of elements in a sample easily and quantitatively with the right calibration. It excels at detecting low elements in complex structures (Weiss et al., 2017). The calibration of sputter rate is now possible thanks to recent technological advancements. Once the sputter rate has been calibrated, elemental concentrations can be determined not only in the whole sample, but also as a function of depth into the sample.

In theoretical, the knocked-out sample atoms diffuse into the plasma where they collide with high-energy electrons. During these collisions, energy is transferred to the sample atoms promoting them to excited energy states. Returning to the ground state,

the atoms emit light with a characteristic wavelength spectrum. In this case, it was applied for detect outgoing of hydrogen exportation from DLC films which can explained the Hydrogen contamination. Additionally, the interesting doped material was investigated relating to atomic concentration.

### 2.6.5 Laser microscopy

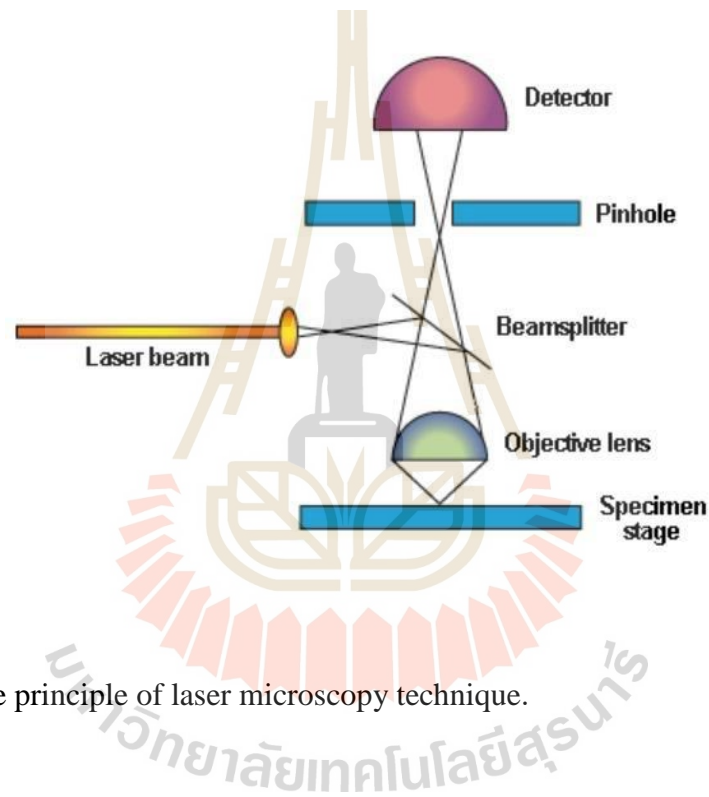


**Figure 23** The principle of laser microscopy technique.

Laser microscopy was used for investing the morphology profiles on interesting surface. This technique was widely used for measuring roughness profile, deep profiles and films homogenies. In principle detail, the incident laser beam, will be spited at correcting mirror. One part of spirited laser was corrected again by objective lens and incident to the sample. The sample scanning method will be performed by aligning the interesting XY positions state and the corrected focus scanning was adjusted by Z position. Therefore, while the sample scan method is appropriate for capture the interesting area. Then, the Laser will travel back to collecting mirror and interfere with

initial source. The final, the laser intensity will be transferred to detector and it was calculated again as morphology data. This technique non requested preparations process. The measuring has no damage to the surface of films.

### 2.6.6 Atomic Force Microscope (AFM)

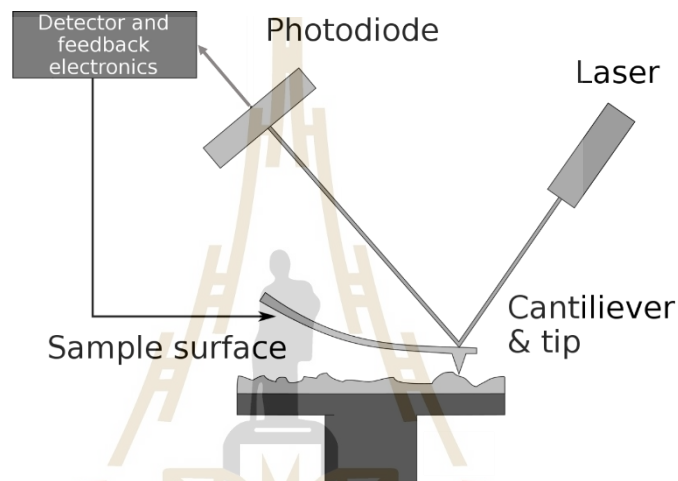


**Figure 24** The principle of AFM technique.

For study carbon films morphology, Atomic force microscopy techniques was widely chosen for study films roughness. It is a very high-resolution type of scanning probe microscopy. The sample is interacted with tip which normally are perpendicular with films surface. The laser source was directly incident on cantilever. Then, reflected beam move to photodiode and detector for analysis data and convert to relative height of films. The mapping of this process is roughness data with related to the oscillations of tip on films surface. The measuring was separated for 2 main type: contact mode/non-contact mode. For contact mode was apply for high roughness sample. In return, non-contact mode was efficiency measure for flat films. Where the amplitude of oscillation

is typically a few nanometers (<10 nm) which demonstrated to strongly the van der Waals forces. Its affect to the frequency of the cantilever related to the reflected beam. Measuring the tip-to-sample distance at each (X, Y) positions data point allows the scanning software to construct a topographic image of the sample surface.

## 2.7 Advance characterization

The physical and chemical characteristics of DLC were studied using a variety of spectroscopic techniques. However, they had not been used to study the local structure of films. This leads to a more in-depth investigation in this study, which is based on synchrotron characterization using X-ray absorption techniques.

### 2.7.1 X-ray Absorptions Spectroscopy (XAS)

X-ray absorption spectroscopy, or XAS, is a widely used method for studying atomic local structure and electronic states. In general, an X-ray excites a core electron in an atom, which can either be promoted to an unoccupied level or ejected from the atom. Both of these methods will result in a core hole.

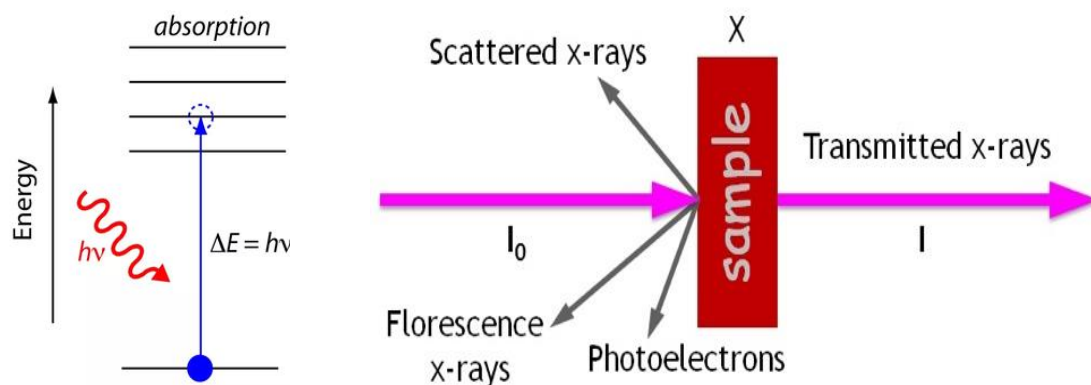


**Figure 25** Theoretical and algorithm of XAS (BL-5.2 SLRI).

From XAS principle, electron was ejected by x-ray source which enough energy for exciting. A typical XAS System is mainly divided into two parts simply input system and output system. Input is electron gas ionized signal at incident chamber ( $I_0$ ). Output is electron ionized signal at transmitted chamber ( $I_1$ ). The electron X-ray absorptions can be explaining by using Beer's law as the following equations:

$$\mu x = \ln(I_0/I_1) \quad (4)$$

Where:  $\mu$  is transmission coefficient  
 $x$  is thickness of sample  
 $I_0$  is incident light intensity  
 $I_1$  is transmitted light intensity

According to Figure 25, XAS spectra can be examined in two regions which are X-ray absorption near edge spectroscopy (XANES) and extended X-ray absorption fine structure spectroscopy (EXAFS). For firstly, XANES is a broad term that refers to the examination of spectra obtained in X-ray absorption spectroscopy operations. The partial density of a molecule's empty states is determined using an element-specific and local bonding-sensitive spectroscopic investigation. The following are the fundamental mechanisms that contribute to the XANES spectra: Photo absorption of an X-ray into a core level, followed by photoelectron emission Figure 26(a), and either Figure 26(b) filling of the core hole by an electron in another level, accompanied by fluorescence; or Figure 26(c) filling of the core hole by an electron in another level, followed by emission

of an Auger electron. Moreover, XANES mostly uses for explaining the oxidations state by edge-shift position.

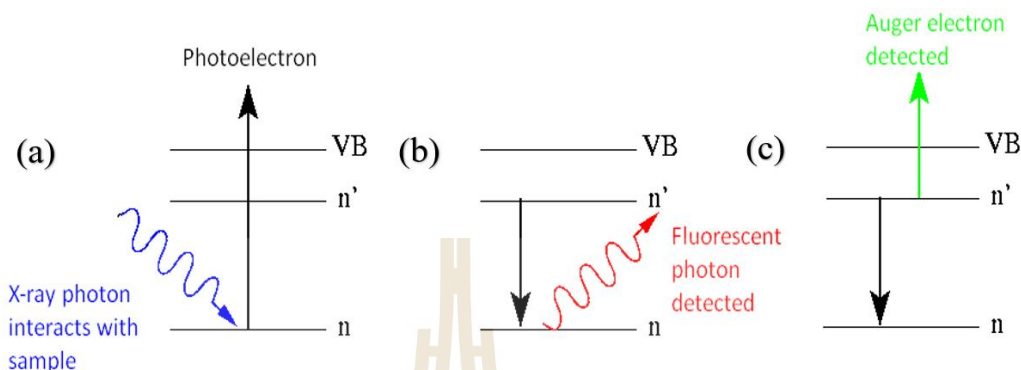


**Figure 26** The fundamental processes which contribute to XANES spectra of photo absorption (a), fluorescent photon (b) and Auger electron (c).

And secondary, EXAFS is a modulation of the final state wavefunction of the absorbing atom induced by the interaction of outgoing photoelectrons released from inner core levels by resonant radiation and backscattered electrons from close neighbor atoms. Sayers (Sayer et al., 1971) properly identified it as a function of the radial distribution function around the center absorbing atom, related to local structure. Plane waves can explain traveling electrons in their most basic form. The oscillatory component of the absorption coefficient is given by in this equation (Azároff, 1963; Newville, 2001).

$$\chi^{(k)} = \sum \frac{(N_i S_0^2) F_i(k)}{k R_i^2} \sin[2k R_i + \delta_i(k)] e^{-2\sigma_i^2 k^2} e^{-\frac{2R_i}{\lambda(k)}}$$

For the interesting point, XAS is used for studying the local structure of atomic material. This technique can be analysis chemical state, structure of considering atom,

bond length, pattern of atom or type of surrounding atoms etc. XAS technique does not destroy the sample and can be applied in many researcher types. For DLC films can be used this technique for study the local structure of M- DLC films by using the Fluorescence-mode. Synchrotron-based for XAS technique will be good information in this work when combine with carbon *K*-edge from NEXAFS.

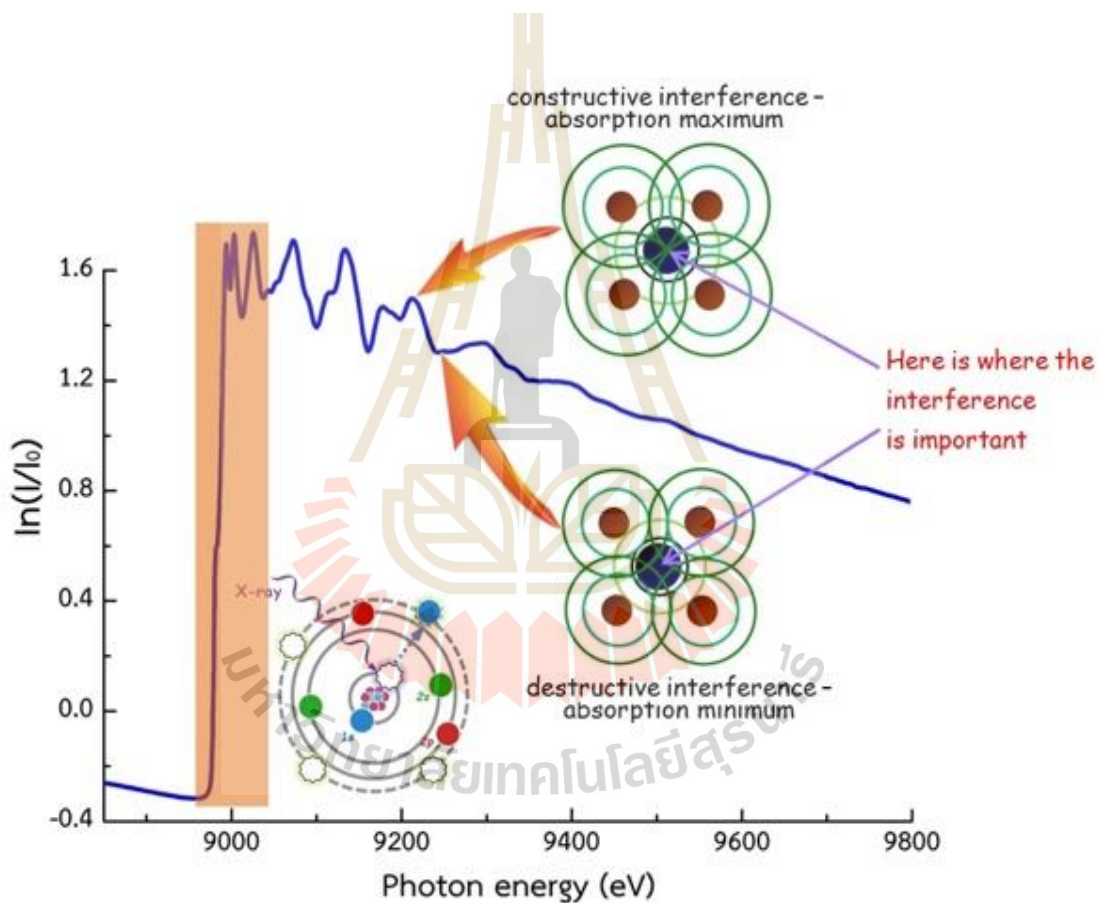


**Figure 27** Theoretical and algorithm for XANES and EXAFS spectra (BL-5.2 SLRI).

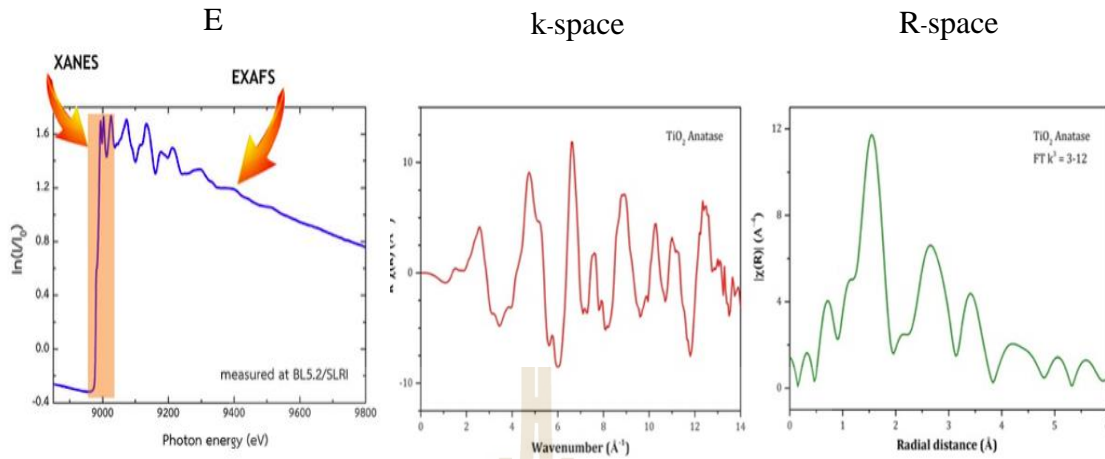


**Figure 28** Energy range of XANES and EXAFS spectra(a) / K-space spectra(b) / R-space spectra(c) (BL-5.2 SLRI).

To study the local structure of probing elements, EXAFS spectrum can be related to wave number (k-space) and Fourier transform for distance of local structure (R-space). Wave number can calculate by following equations:

$$k = \sqrt{\frac{2m(E - E_0)}{h^2}} \quad (5)$$

Where:  $k$  is wave number.

$h$  is planck's constant.

$m$  is electron mass.

$E$  is probing x-ray energy.

$E_0$  is ejected electron energy at interesting shell.

One part of this work, zinc was introduced into DLC structure. Its surrounding environment was studied by using XAS. Electron at  $K$ -edge of Zn atom was ejected at

energy 9659 eV. XANES and EXAFS were measured for study oxidation state and local structure, respectively. It will be deeply discussed again in chapter V.

### 2.7.2 Near-edge X-ray Absorptions Fine Structure (NEXAFS)

NEXAFS has been used for studying the electronic structure of DLC films (Osswald et al., 2006). This powerful technique can investigate specific bonds of carbon (e.g., C=C, C-C, and C-O bonds) and also  $sp^3/sp^2$  ratio of DLC films (Latham et al., 2017; Hemraj-Benny et al., 2006). It can explain details of spectral resonances at the carbon *K*-edge such as partials electron yield patten, functionalized species, chemisorbed impurities and etc. Moreover, it can be used to study the angular dependence of the specific orbitals on thickness of thin films (Latham et al., 2017; Hemraj-Benny et al., 2006). It uses inner-shell excitation processes to investigate a sample's X-ray absorption cross section; when photon energy approaches an atomic absorption edge, inner shell electrons are excited to an unoccupied energy level, resulting in resonance peaks in the absorption spectra (Heymann et al., 2011). Total electron yield (TEY), which can probe sample surfaces in depth 10 nm, and fluorescence yield (FLY), which is bulk sensitive and can probe in depth 100 nm into the sample surface, are two detection methods for these resonances. It has the potential to overcome some of the limitations of previous approaches. It probes the electronic states of a sample using polarized X-ray beams generated by a synchrotron light source (Watts et al., 2006) and is capable of capturing complete sample C. For example, XPS only gave binding energy results which is converted from electron kinetic energy under photoelectric effect and it is surface sensitive technique; while, synchrotron-based NEXAFS can be used for investigating electronic structure under the range of ionization potential (IP) level which was called Rydberg state and it also can investigate the bulk properties. According the Rydberg

region, the spectrum can be classified C-H and C-C bonding which is out of XPS limitation.

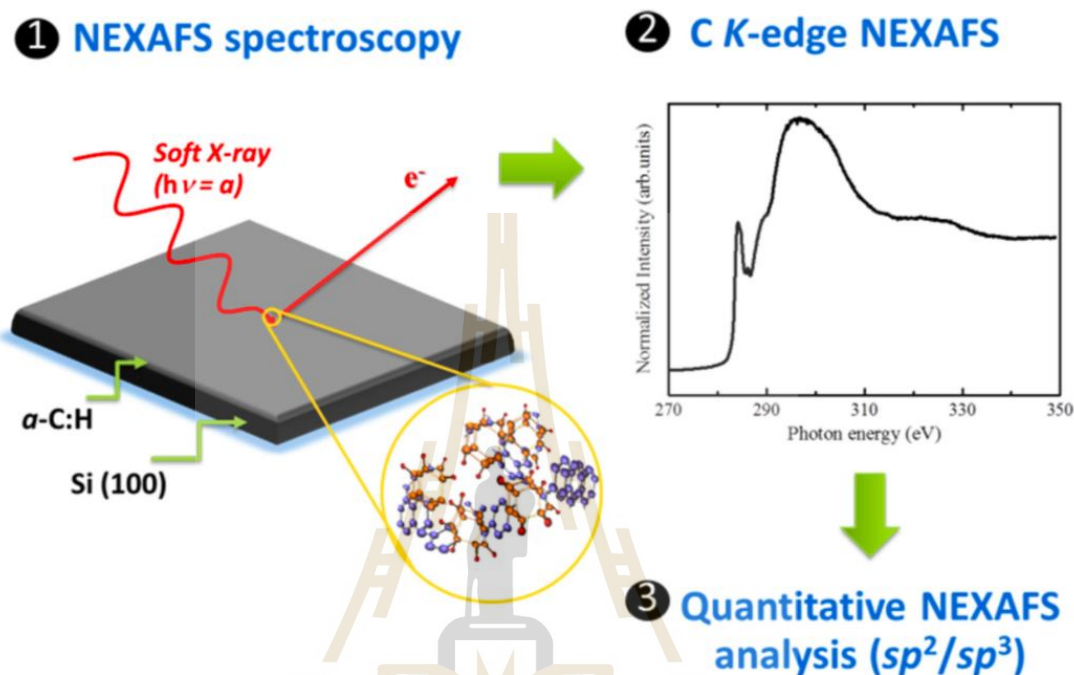


**Figure 29** Investigating for NEXAFS spectra from C K-edge (BL-3.2Ua SLRI).

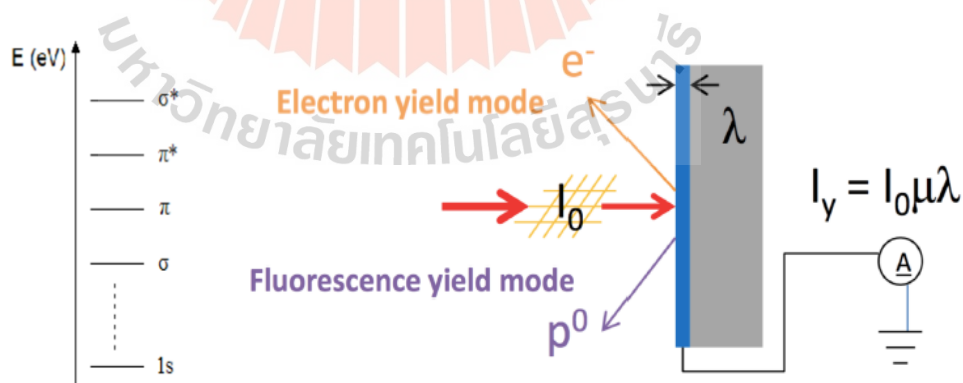


**Figure 30** Theoretical and algorithm for NEXAFS spectra.

The experiment was carried out at Thailand's Synchrotron Light Research Institute (SLRI) on Beamline 3.2Ua. The partial electron yield mode was used for the NEXAFS measurements (PEY). The carbon K-edge spectra of DLC films were a fascinating area

to investigate. Carbon measurements were performed in the energy range of 270-330 eV, with a 0.1 eV energy step. By aligning the  $\pi^*$  resonance peak of highly orientated graphite (HOPG) to 284.8 eV, the position of the carbon K-edge was calibrated. The approach is based on the ratio of the integrated intensity of the C  $1s \rightarrow \pi^*$  and C  $1s \rightarrow \sigma^*$  peaks (hence the name "NEXAFS method"). The  $sp^2$  fractions of DLC films were estimated using the equation below (Jia et al., 2016; Osswald et al., 2006).

$$f_{sp^2(NEXAFS)} = \frac{I_{sam}^{\pi^*}}{I_{sam}(\Delta E)} \frac{I_{ref}(\Delta E)}{I_{ref}^{\pi^*}} \quad (6)$$

where the superscript " $\pi^*$ " denotes the peak C  $1s \rightarrow \pi^*$  bonds, the subscripts "sam" and "ref" represents the DLC films and the reference HOPG (100%  $sp^2$ -bonded carbon), respective. And  $\Delta E$  represent the photon energy range of measuring in NEXAFS spectra (280–320 eV).

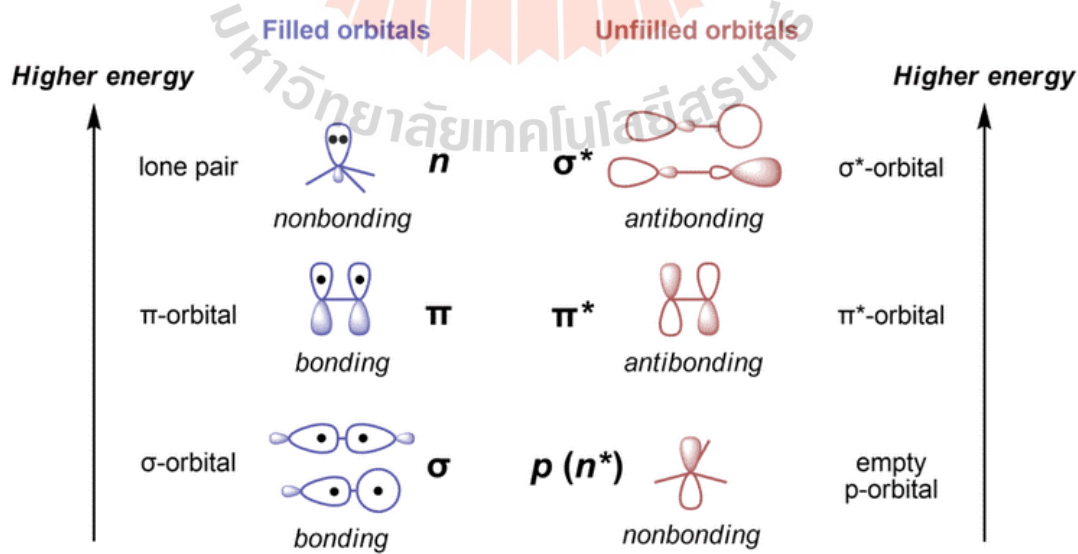


**Figure 31** Fill and unfilled orbital of electron hybridization.

For understanding electron transition state in NEXAFS spectra, the orbital was classified for 2 main types in Figure 31. The first is Filled orbitals; it exhibits after electron hybridization at the ground state. In this case, carbon bonding includes  $\sigma$ -orbital (head-to-head) and  $\pi$ -orbital (side to side). Lone pair electron is forbidden for carbon which not enough electron from its hybridization. While unfilled orbitals related unoccupied electronic state at higher energy level. The electron from ground state can be excited to this state by using photon energy. In theoretical, electron will be excited from  $C\ 1s \rightarrow \pi^*$  (lower state) which is under ionization potential level (IP); and  $C\ 1s \rightarrow \sigma^*$  are represent at the higher state after IP. Both excitations were called antibonding. This phenomenon leads to study electric state of compositions; In this work, carbon was chosen for deeply study. Its electronic structure brings to classify prepared of DLC films. The relation between electron transportation and photon energy, as well as the NEXAFS spectrum, were presented in Figure 32 for easy understanding.

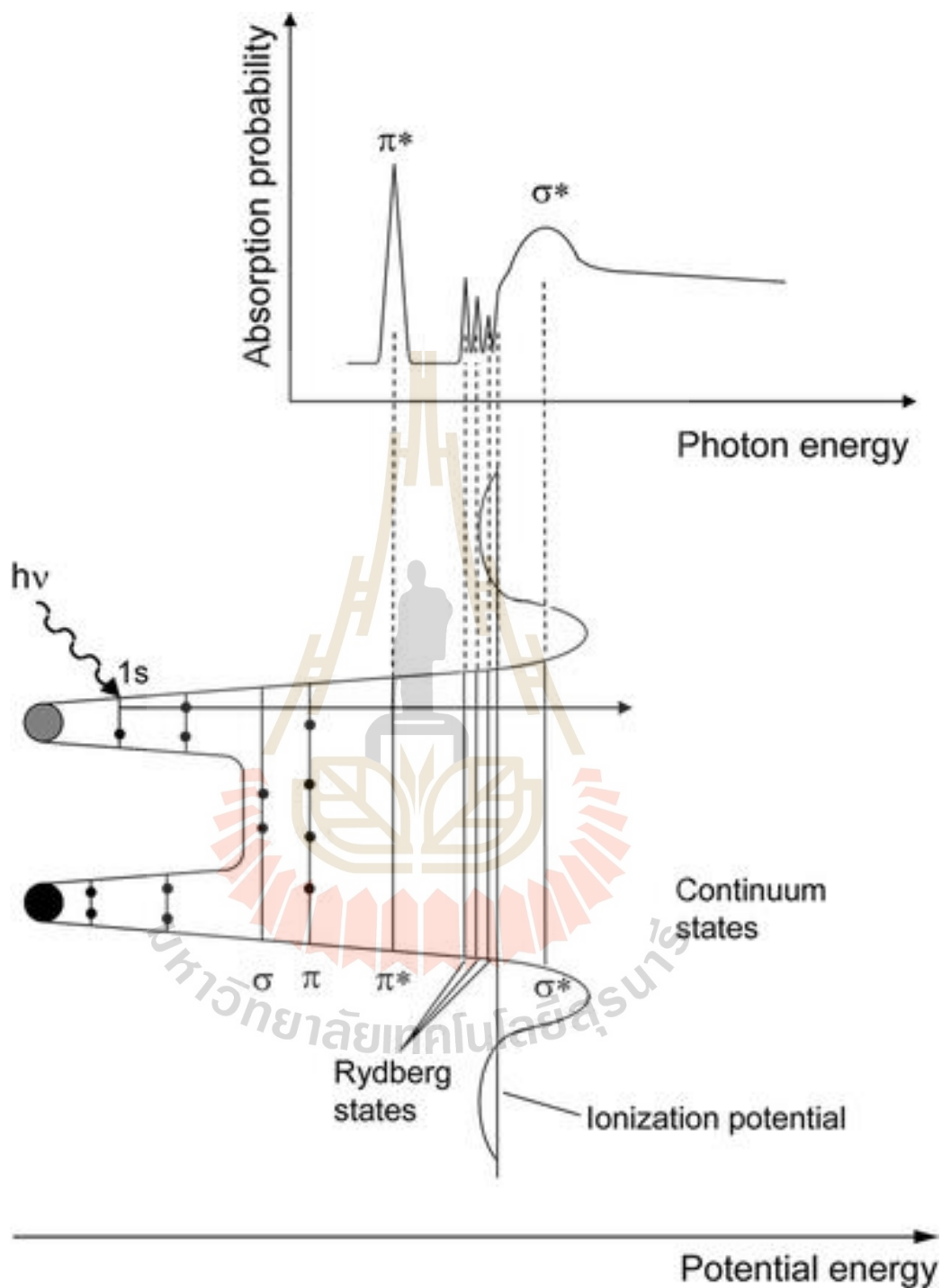


**Figure 32** Theoretical of electron excitation explaining NEXAFS spectra (Hähner, 2006).

## CHAPTER III

### DLC AND THERMAL TREATED PROPERTIES

#### 3.1 Concept of DLC and Thermal-treated properties

When it comes to the preparation of DLC coatings in industry, heat is one of the most significant factors that influence carbon structure, which is linked to the quality of materials such as hard disk drives and drills. As a result, in some industries, the temperature of DLC coated materials was taken into consideration during the manufacturing process. The carbon bonding material in DLC is affected by heat treatment at too high a temperature, resulting in nondurable films. As a result, it would be interesting to learn whether thermal treatment affects the carbon bonding content of DLC films. As a result, it was thoroughly characterized, which is one of the parts of this study.

In this chapter, the details of thermal-treated DLC analysis based on near-edge X-ray absorption fine structure (NEXAFS) of carbon composition structure were reported. Additionally, the Raman spectroscopy was included in this DLC study. The ratio of  $I_D/I_G$  was observed as clearly seen from the D-band and G-band peak positions at  $1350\text{ cm}^{-1}$  and  $1560\text{ cm}^{-1}$ , respectively. Moreover, X-ray photoelectron spectroscopy (XPS) technique confirmed fraction of C- $sp^2$  and C- $sp^3$ . Heat treatment is commonly done to DLC coated materials throughout the production process in several industrial applications. Heat treatment at too high a temperature can change the carbon bonding composition in DLC, making the film nondurable. As a result, it

would be interesting to learn if heat treatment affects the carbon bonding content of DLC films.

## 3.2 Experiment and Characterizations

### 3.2.1 DLC films preparation: Heat treatment

The DLC films were prepared on silicon (100) substrates by the filtered cathodic arc (FCA) preparation. The thickness of films approximately is 30 Å. To study effect of heat treatment, the prepared films were heated from RT to difference five temperature of 50, 100, 150, 200 and 250°C with the heating rate of 10°C/min at normal pressure. The films were hold at those temperature for 1 hour and then cooled down at the rate of 5°C/min.

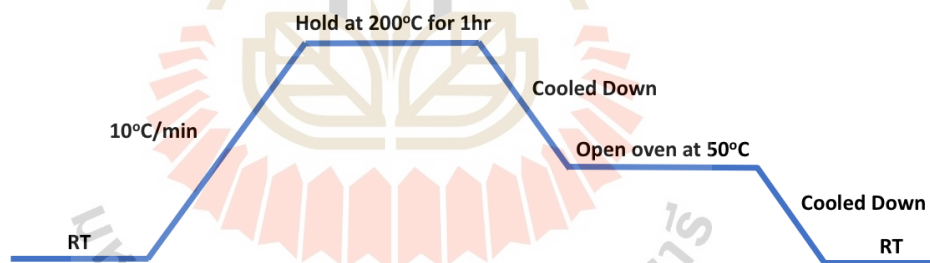


**Figure 33** experimental setup of ex-situ thermal-treated system.

### 3.2.2 Measurements of XPS

At the Synchrotron Light Research Institute's SUT-NANOTEC-SLRI collaborative research facility, XPS measurements were carried out using a PHI5000 Versa probe II (ULVAC-PHI, Japan) equipped with a hemispherical electron energy analyzer (SLRI). As an excitation source, a monochromatic Al K X-ray (1486.6 eV)

was employed. The XPS survey scan ranged from 0 to 1400 eV, with a pass energy of 117.40 eV and a 1.0 eV energy step. For probing interest elements, high resolution XPS spectra were obtained with a pass energy of 46.95 eV and energy step resolutions of 0.05 eV. PHI Multipack XPS software was used to analyze the XPS spectra. The C 1S peak at 284.8 eV was used to calibrate the binding energy of all XPS spectra. Peak deconvolution was achieved via Shirley background removal and Gaussian-Lorentzian line shape combinations.

### **3.2.3 Measurements of NEXAFS**

The NEXAFS experiment was performed at Beamline 3.2 Ua Synchrotron Light Research Institute (SLRI). Partially electron yield mode was used for the NEXAFS measurements (PEY). The DLC films' carbon K-edge spectra were obtained in the energy range 270-330 eV, with a 0.1 eV energy step. By aligning the  $\pi^*$  resonance of highly oriented pyrolytic graphite at peak 284.8 eV, the feature of carbon K-edge was calibrated (HOPG).

### **3.2.4 Measurements of Raman**

A Dispersive Raman spectrometer was used to capture Raman spectra (Sentara, Bruker). A laser with a wavelength of 512 nm, a power of 50 mW, and an aperture of 25x1000  $\mu\text{m}$  was used to make the measurements. The spectra were recorded with Raman shift resolutions of 0.5  $\text{cm}^{-1}$  in the range 50-2700  $\text{cm}^{-1}$ .

### 3.3 Results and Discussion

#### 3.3.1 XPS Result

To examine the chemical composition of the DLC film, XPS measurements were carefully carried out. The presence of carbon, silicon, and oxygen can be seen in the XPS survey spectrum of the DLC layer at room temperature (RT) in Figure 34(d). Figure 34 shows high-resolution XPS spectra of the C 1s, O 1s, and Si 2p peaks (a-c). The Si substrate is responsible for the presence of Si in the DLC spectrum. The Si 2p peak in Figure 34(g) may be divided into two primary peaks with binding energies of 99.4 and 101.7 eV, respectively, corresponding to Si-O and Si-C. (Arezzo et al., 1994; Takagaki et al., 1992). The presence of O signal is due to oxygen contamination in the Si substrate and DLC films during production. The presence of oxygen pollution in the DLC film has already been reported (Dos Santos, 2015). The O1s in Figure 34(f) fit into four main peaks with binding energies of 533.2, 530.5, 532.3, and 531.7 eV, suggesting the presence of Si-O-Si, H-Si-O, O=C, and O-C peaks, respectively (Paparazzo, 1987; Dos Santos, 2015). The high-resolution spectra of C 1s in Figure 34(e) can be deconvoluted into five separate Gaussian peaks, centered at binding energies of 283.4 eV, 286.4 eV, 287.7 eV, 285.1 eV, and 284.4 eV, respectively, assigning to C-Si, C-O, C=O, C- $sp^3$ , and C- $sp^2$  (Bozack, 1994; Ahmed et al., 2013; Bociaga et al., 2015; Marcondes et al., 2004). The FWHM of the deconvoluted  $sp^3$  and  $sp^2$  C 1s peaks is set at 0.58-0.6 eV, with an E of 0.7 eV, according to the C 1s fitting parameters. In Figure 35, all peak deconvolutions were presented once more. Table 1 shows the relative atomic concentrations of Carbon species determined from XPS spectra.

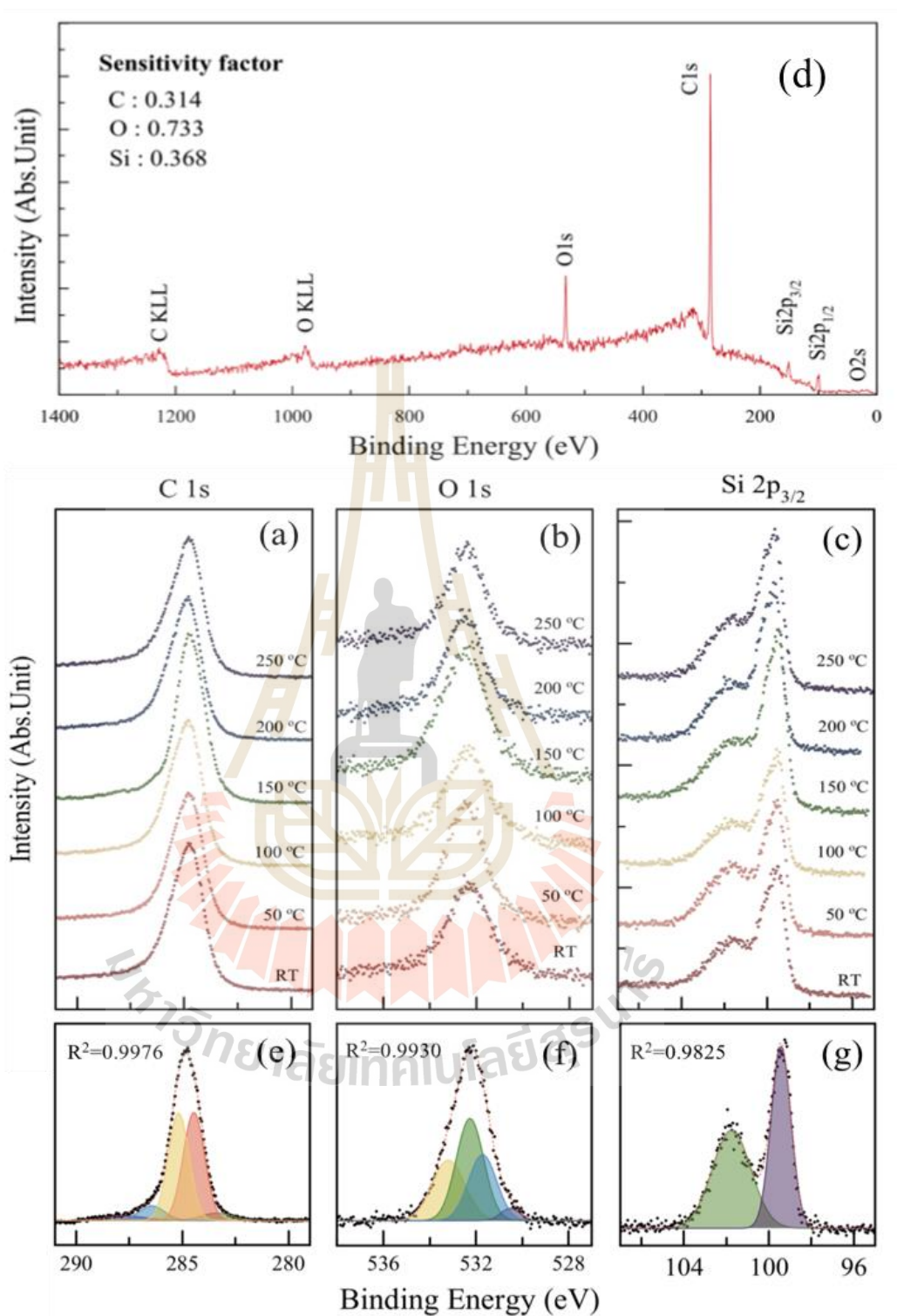


**Figure 34** High resolution XPS spectra of C 1s(a), O 1s(b), Si 2p(c) peaks, XPS survey spectra of the DLC film at RT(d), graph fitting of C 1s(e), O 1s(f), Si 2p(g).

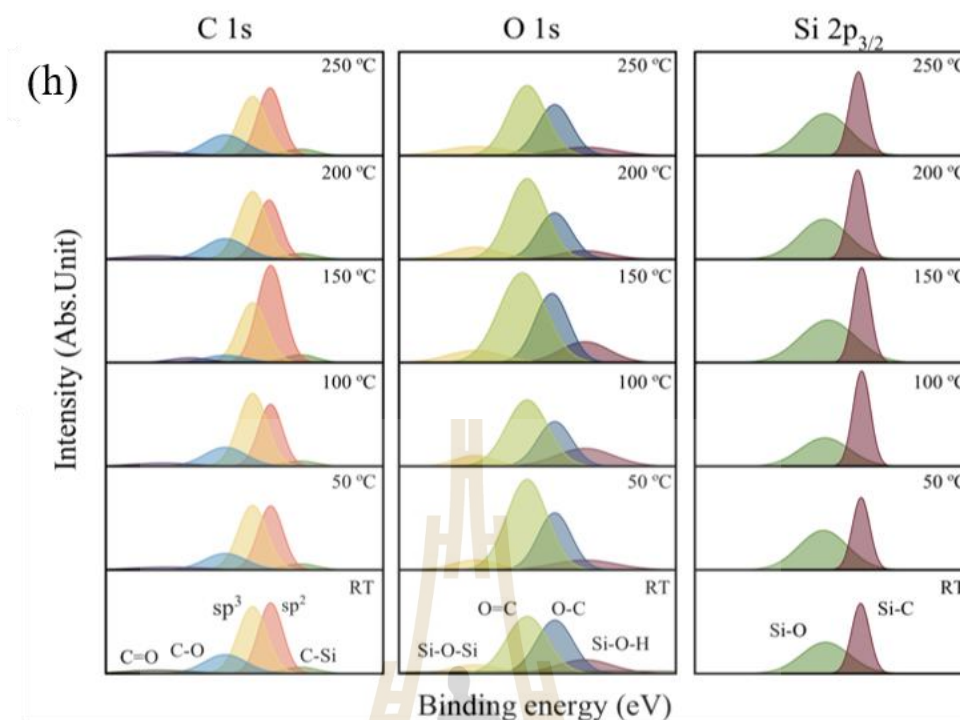


**Figure 35** All deconvolutions from spectra XPS of Thermal-treated DLC films.

### 3.3.2 NEXAFS Result

The carbon structure of the DLC films was studied in depth using NEXAFS studies. Figure 37 shows a stacked plot of carbon K-edge spectra from DLC films in the 270-330 eV region. The observed carbon K-edge spectra show the previously described DLC film characteristic. (Cody et al., 1998) The carbon K-edge spectra were fitted according to the literature (Singh et al., 2014; Watts et al., 2006) and compared to the carbon K-edge spectrum of HOPG to identify the chemical states and structure of carbon. The first observed peak and the shoulder peak at the energies of 284.8 and 286.7 eV indicate the transition state  $1s \rightarrow \pi^*$  (C=C) and  $1s \rightarrow \sigma^*$  (C-H), respectively. The results are in good agreement with the result of Raman spectroscopy that C-H is observed at approximately  $\sim 1200\text{-}1300\text{ cm}^{-1}$ . The transitions state of

$1s \rightarrow \pi^*$  and  $1s \rightarrow \sigma^*$  at the energies 288.5 and 303.1 eV shows the presence of (C=O) (Latham et al., 2017), confirming the oxygen contamination in DLC film. This result is in good agreement with XPS result. The observed peaks at the energies of 292.7 and 297.5 eV reveal the transitions state of  $1s \rightarrow \sigma^*$  (C=C) and  $1s \rightarrow \sigma^*$  (C-C), respectively. The  $sp^2$ -fractions of the DLC films calculated from the equation 4 (Jia et al., 2016; Osswald et al., 2006). Where the superscript " $\pi^*$ " is peak intensities of  $1s \rightarrow \pi^*$  C=C bonds, and the superscript "total" is the integration photon energy over range (280–320 eV). The subscripts "DLC" and "HOPG" refer to the peak area intensities in DLC films and HOPG (NT-MDT) as a reference, respectively. Table 1 shows the  $sp^3/sp^2$  ratios of DLC films, which are in good accord with the XPS data.

### 3.3.3 Raman Result

Raman spectroscopy was also used to investigate the carbon structure of the DLC films. At room temperature, the DLC films have a broad peak in the region of 50-2250  $\text{cm}^{-1}$  as shown in Figure 36(a). The Raman spectrum shows the D and G bands at  $\sim 1350 \text{ cm}^{-1}$  and  $\sim 1560 \text{ cm}^{-1}$  respectively, which are commonly seen in carbon structure (Robertson et al., 2002; RibeiroSoares et al., 2013; Ferrari and Robertson, 2000). D\*-band and G\*-band signals were also discovered at  $\sim 1100$ -1200 and  $\sim 1380$ -1420  $\text{cm}^{-1}$ , respectively.

These bands are caused by the aromatic ring's C=C stretching and C-H wagging modes, respectively (Wu et al., 2002; Francioso et al., 2005). The C-H bending (Francioso et al., 2005) and C-O stretching vibration (Xing et al., 2016) vibrations are reflected by the extra peaks at  $\sim 1200$ -1300 and  $\sim 1600$ -1800  $\text{cm}^{-1}$ , respectively. The Raman spectra of DLC films heated to various temperatures in Figure 36(b) show the

same feature as the DLC at room temperature. This means that their carbon structures are identical. Table 1 shows the  $I_D/I_G$  ratio of DLC films.

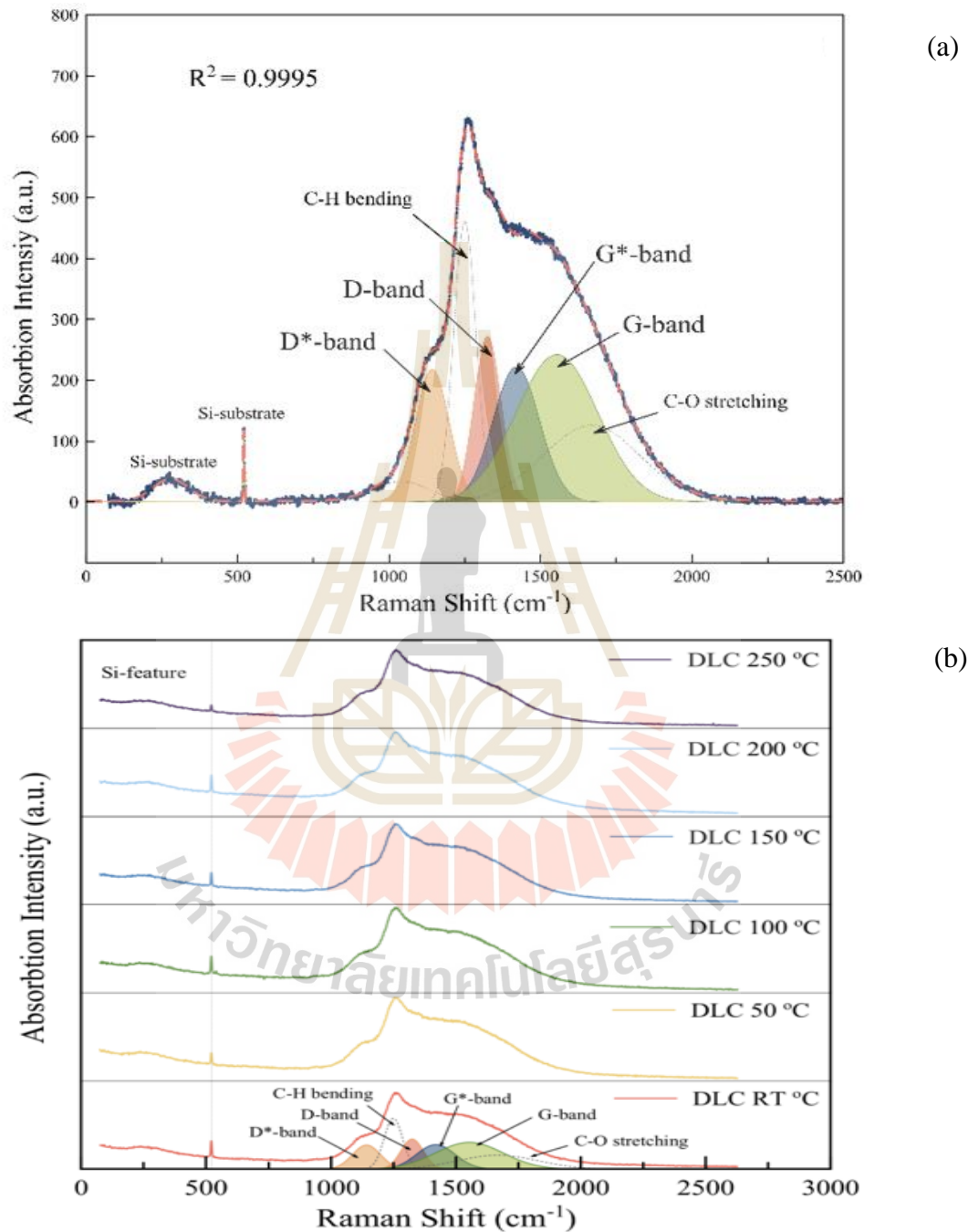


**Figure 36** Raman spectrum fitting of DLC film at RT(a) and, DLC films heated to difference five temperature (b).

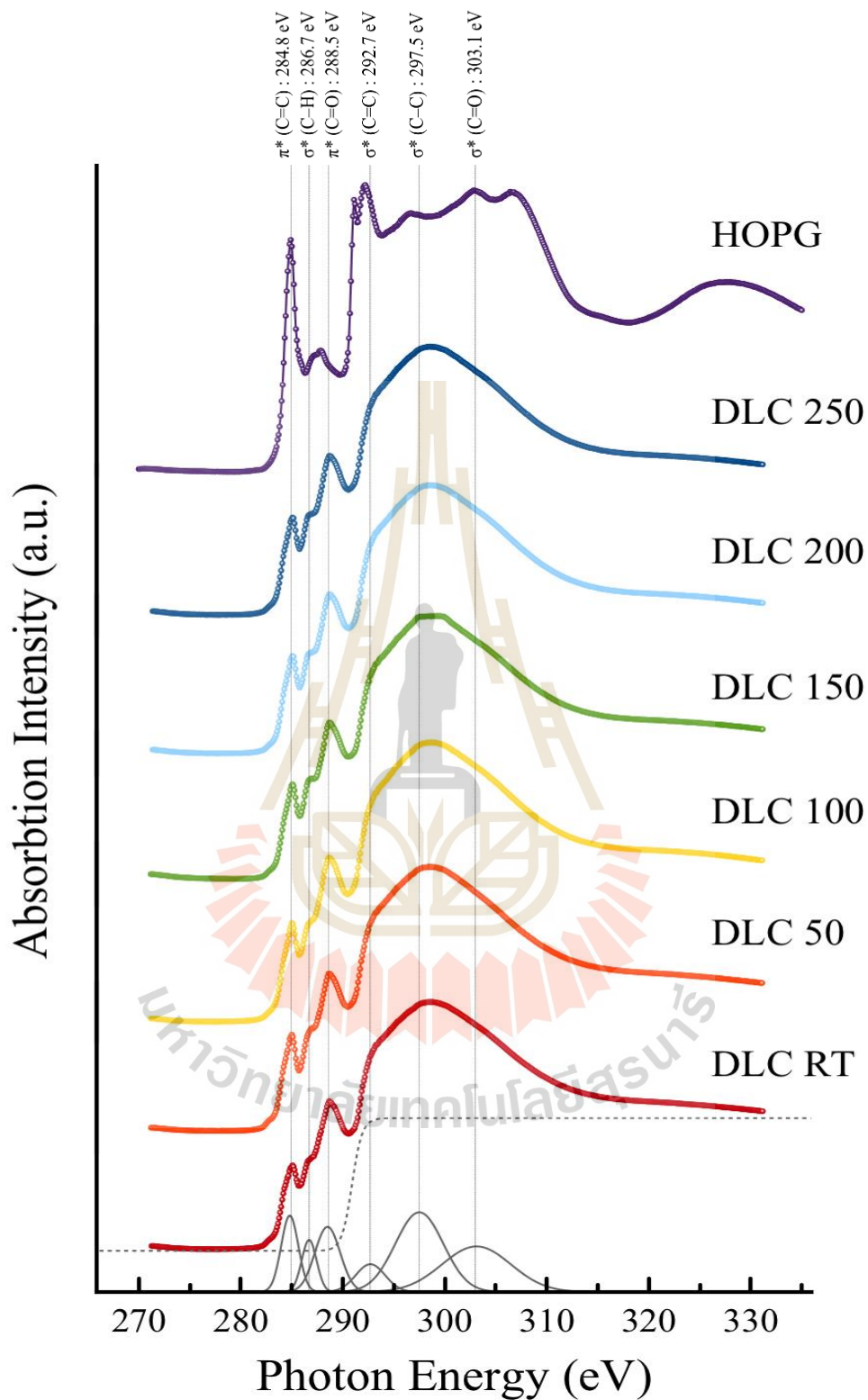


**Figure 37** NEXAFS carbon K-edge spectra of the DLC films and HOPG.

**Table 2** Characterized Results of Thermal-treat of DLC Films.

	HOPG	Thermal-treat of DLC films (°C)					
		RT	50	100	150	200	250
<b>X-ray absorption spectroscopy</b>							
C- $sp^3$ area, %	-	34.89	41.10	41.66	34.16	37.42	32.38
C- $sp^2$ area, %	-	38.73	35.47	32.65	51.63	35.22	38.21
C-O area, %	-	17.60	15.09	17.39	6.05	18.35	19.87
C=O area, %	-	4.34	4.18	4.71	3.23	5.25	4.86
C-Si area, %	-	4.44	4.17	3.59	4.92	3.76	4.67
$sp^3/sp^2$	-	0.90	1.16	1.28	0.66	1.06	0.85
<b>NEXAFS</b>							
$sp^3$ -friction, %	4.46	50.47	51.97	48.89	51.73	49.23	50.59
$sp^2$ -friction, %	95.54	49.53	48.03	51.11	48.27	50.77	49.41
$sp^3/sp^2$	0.05	1.02	1.08	0.96	1.07	0.97	1.02
<b>Raman spectroscopy</b>							

### 3.4 Summarize of Thermal-treated DLC and characterized

The effect of thermal treatment between RT to 250°C on the carbon structure of the DLC films was studied by combining of NEXAFS, XPS, Raman spectroscopy. The  $sp^3/sp^2$  ratio of the DLC were analyzed by NEXAFS which is consistent with XPS. It is observed that heat treatment does not significantly change the chemical compositions and  $sp^3/sp^2$  ration of DLC films. These results indicate that the thermal treatment below the temperature of 250°C does not affect the carbon structure of DLC film. This result is also supported by Raman spectroscopy study. Therefore, the thermal treatment below the temperature of 250°C in the manufacturing industry does not affect to the quality of DLC films or coating.

## CHAPTER IV

### INFLUENCE OF POWER DEPENDENCE BY PECVD

#### 4.1 Concept of power dependence by PECVD

The process for mixing 2 main carbon fractions is an interested factor for controlling ratio of  $sp^3/sp^2$ . And the contamination is also considered for film qualitative. As previously described, several processes such as physical vapor deposition (PVD), chemical vapor deposition (CVD), and pulsed laser deposition can be employed to create DLC films (Lin et al., 2017; Nakao et al., 2017; Guo et al., 2017; Lu et al., 2018). Therefore, the carbon properties which is related to  $sp^3$  and  $sp^2$  fraction depend on choosing deposition process. For example, sputtering technique give high  $sp^2$ -fraction. While, the filtered cathodic vacuum arc (FCVA) can fabricate rich  $sp^3$ -fraction. Because it can create amorphous carbon films with rich  $sp^3$ -fractions, plasma enhanced chemical vapor deposition (PECVD) is a deposition technology that is particularly appealing for DLC film creation, especially for industrial applications (Lusk et al., 2008; Zhang et al., 2019). However, just a few studies on DLC films made using the PECVD approach have been published (Zhou et al., 2015). Furthermore, the impact of deposition variables including RF power, gas flow rate, gas type, chamber size, and deposition duration on the structure of DLC films is still unknown.

In this chapter, PECVD was used to produce DLC films on a titanium substrate. Titanium is commonly utilized in medical devices (Hauert et al., 2013). It's also

usually encountered as interlayers or doping elements in DLC films to minimize internal stress and improve adhesion (Wang et al. , 2020). X-ray photoelectron spectroscopy (XPS), Raman spectroscopy, and synchrotron-based near-edge X-ray absorption fine structure (NEXAFS) spectroscopy were used to analyze the chemical composition and structure of the deposited DLC sheets. Deposition factors such as RF power and CH<sub>4</sub> flow rate were also investigated for their effects on the structure of produced films.

## 4.2 Experimental setup

At room temperature, DLC films were formed on titanium substrates with an area of 10×10 mm<sup>2</sup> and a thickness of 3.0 mm. The studies were carried out on a PECVD system (Nano-Master, NPE-1000) with a 3.8×10<sup>4</sup> cm<sup>3</sup> of chamber size. Figure 38 shows a schematic design of the PECVD system used in this study. The vacuum chamber was evacuated prior to the deposition process to provide a background pressure of about 0.05 Pa. The titanium substrates were cleaned with argon plasma at a flow rate of 10 cm<sup>3</sup>/min for 10 minutes at a fixed RF power of 100±2 W.

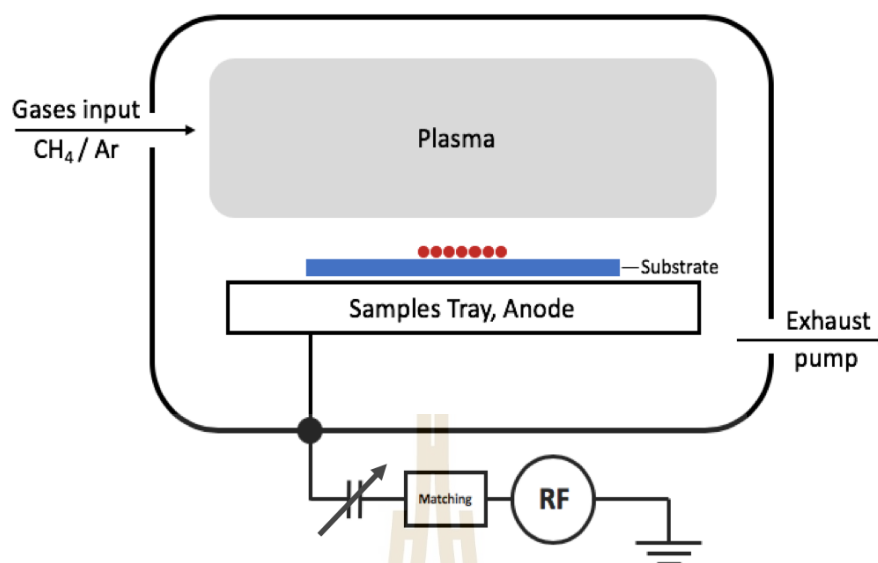


**Figure 38** Schematic diagram of PECVD system.

### 4.3 Deposition Conditions

RF powers of 60, 80, 100, 120, 140, and 160 W (5 W) were applied using an RF generator at 13.56 MHz to investigate the effect of RF power. The self-substrate bias was not used in this study. The flow rates of CH<sub>4</sub> and Ar gases (quality >99.9%) were kept at 5 (or 10) and 20 cm<sup>3</sup>/min, respectively. For all samples, the deposition time was 5 minutes. CH<sub>4</sub> was mixed with argon gas (flow rate fixed at 20 cm<sup>3</sup>/min) to investigate the effect of CH<sub>4</sub> flow rate. The flow rates of CH<sub>4</sub> gas were set at 5 and 10 cm<sup>3</sup>/min, respectively. Table 2 summarizes the deposition parameters.

**Table 3** The PECVD deposition parameters of DLC films.

Deposition parameters	Unit	Value
Chamber size	cm <sup>3</sup>	3.8×10 <sup>4</sup>
Base pressure	Pa	<0.05
Working pressure	Pa	3-4
Deposition time	min	5
Ar flow rate	(cm <sup>3</sup> /min)	20
CH <sub>4</sub> flow rate	(cm <sup>3</sup> /min)	5, 10
Power	<i>RF power (W)</i>	60-160

## 4.4 Film characterizations

### 4.4.1 XPS analysis

At the SUT-NANOTEC-SLRI collaborative research facility, Synchrotron Light Research Institute (SLRI), Thailand, XPS was performed using a PHI5000 Versa probe II (ULVAC-PHI, Japan) equipped with a hemispherical electron energy analyzer. The excitation source was an Al K  $\alpha$  X-ray gun (1486.6 eV). The survey scans were taken between 0 and 1400 eV, with a pass energy of 117.40 eV and a 1.0 eV energy step. High resolution XPS spectra were acquired with a pass energy of 46.95 eV and an energy step of 0.05 eV to probe the components of interest. The C 1s peak at 284.8 eV was used to calibrate the binding energy of all XPS spectra. Shirley background subtraction and Gaussian-Lorentzian were used as a subtract and function linear combinations, respectively.

### 4.4.2 Raman spectroscopy analysis

A dispersive Raman microscope (SENTERRA, Bruker) was used to perform Raman spectra with a green light laser source with a wavelength of 532 nm, a power of 25 mW, and a slit of 25x1000 microns. The vibration patterns were measured at a

resolution of 0.5  $\text{cm}^{-1}$  in the range of 50-2700  $\text{cm}^{-1}$ . By fitting the Raman spectra with two Gaussian peaks, the Raman parameters consisting of the D and G bands, as well as the  $I_D/I_G$  ratio of the films, were derived.

#### 4.4.3 NEXAFS analysis

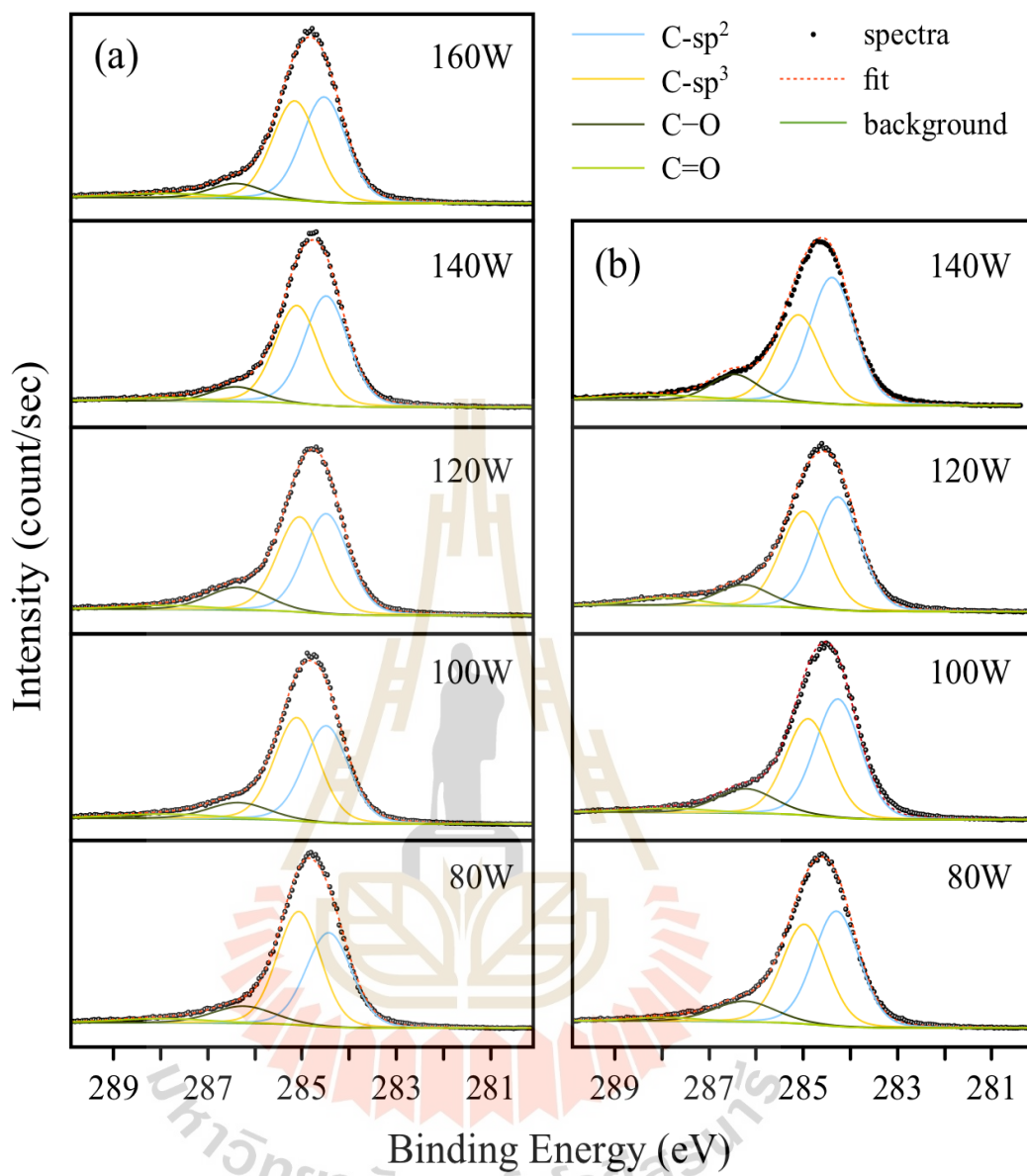
The NEXAFS experiment was carried out at the SLRI's Beamline 3.2Ua. Total electron yield (TEY) mode was used for the measurement. The storage ring released synchrotron radiation with an electron energy of 1.2 GeV. The DLC films' carbon *K*-edge spectra were collected in the energy range of 270-330 eV with a 0.1 eV energy step. The synchrotron ring's electron current was between 70 and 140 mA. By aligning the observed carbon *K*-edge spectra with the  $\pi^*$  resonance peak of highly orientated pyrolytic graphite (HOPG) at 284.8 eV, the spectra were calibrated.

### 4.5 Results and Discussion

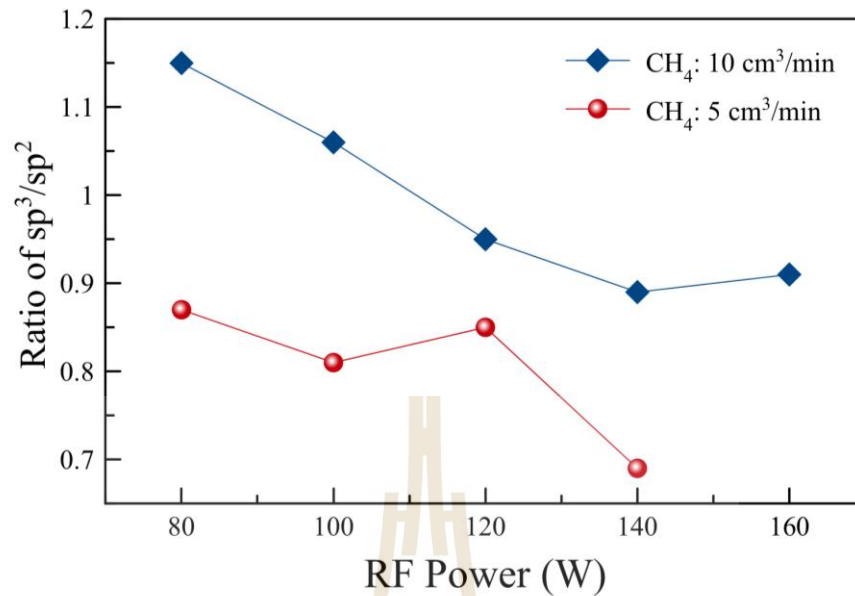
PECVD was used to successfully deposit amorphous carbon (*a*-C) films with 12 conditions on a titanium substrate. The films deposited with a  $\text{CH}_4$  flow rate of 5  $\text{cm}^3/\text{min}$  and RF power of 60 and 160 W were peeled off after deposition, whereas the film deposited with a flow rate of 10  $\text{cm}^3/\text{min}$  and RF power of 60 and 160 W was peeled off after Raman spectroscopic measurement. The films are steady black and glossy in all other conditions. As indicated in the supplemental information, the film thickness of all successfully deposited films was evaluated using a scanning electron microscopy (SEM) cross-section picture. Table 3 shows that the measured film thicknesses are about in the range of 80-250 nm.

The chemical composition and chemical bonding of the DLC film were investigated using XPS. Figure 39 shows high-resolution XPS C 1s spectra of

deposited films at various RF powers and CH<sub>4</sub> flow rates. At binding energies of 286.3, 287.9, 285.2, and 284.5 eV, all of the C 1s peaks can be fitted into four major peaks, which correspond to C-O, C=O, C-*sp*<sup>3</sup>, and C-*sp*<sup>2</sup>, respectively (Ahmed et al., 2013; Bozack et al, 1994; Bociaga et al., 2015). The occurrence of C-O and C= O bonds may be due to contamination from oxygen present in the chamber during deposition and subsequent air exposure. On the sample surface, a little amount of oxygen can be trapped. Previous studies have also noted the presence of oxygen in DLC films (Zhou et al., 2015; Lux et al., 2019). Table 3 shows the respective atomic concentrations of C-O, C= O, C-*sp*<sup>3</sup> and C-*sp*<sup>2</sup> bonds estimated from the XPS data. Figure 40 also shows plots of the computed *sp*<sup>3</sup>/*sp*<sup>2</sup> ratio vs RF power at CH<sub>4</sub> flow rates of 5 and 10 cm<sup>3</sup>/min. When the RF power is increased from 80 to 160W, the content of C-*sp*<sup>3</sup> marginally drops, according to the results of XPS examination. The *sp*<sup>3</sup>/*sp*<sup>2</sup> ratio of DLC films prepared with a CH<sub>4</sub> flow rate of 10 cm<sup>3</sup>/min is slightly greater than that of DLC films prepared with a flow rate of 5 cm<sup>3</sup>/min.



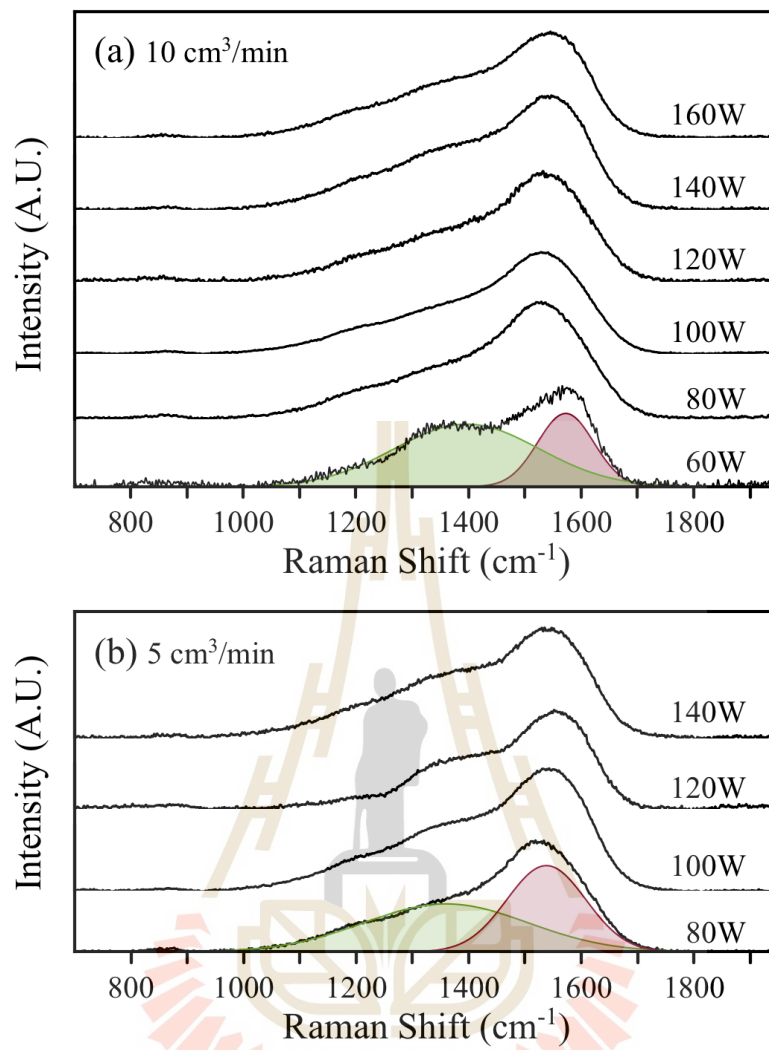
**Figure 39** High resolution XPS C 1s peaks of the DLC films prepared with different RF powers using CH<sub>4</sub> flow rates of (a) 10 cm<sup>3</sup>/min and (b) 5 cm<sup>3</sup>/min.



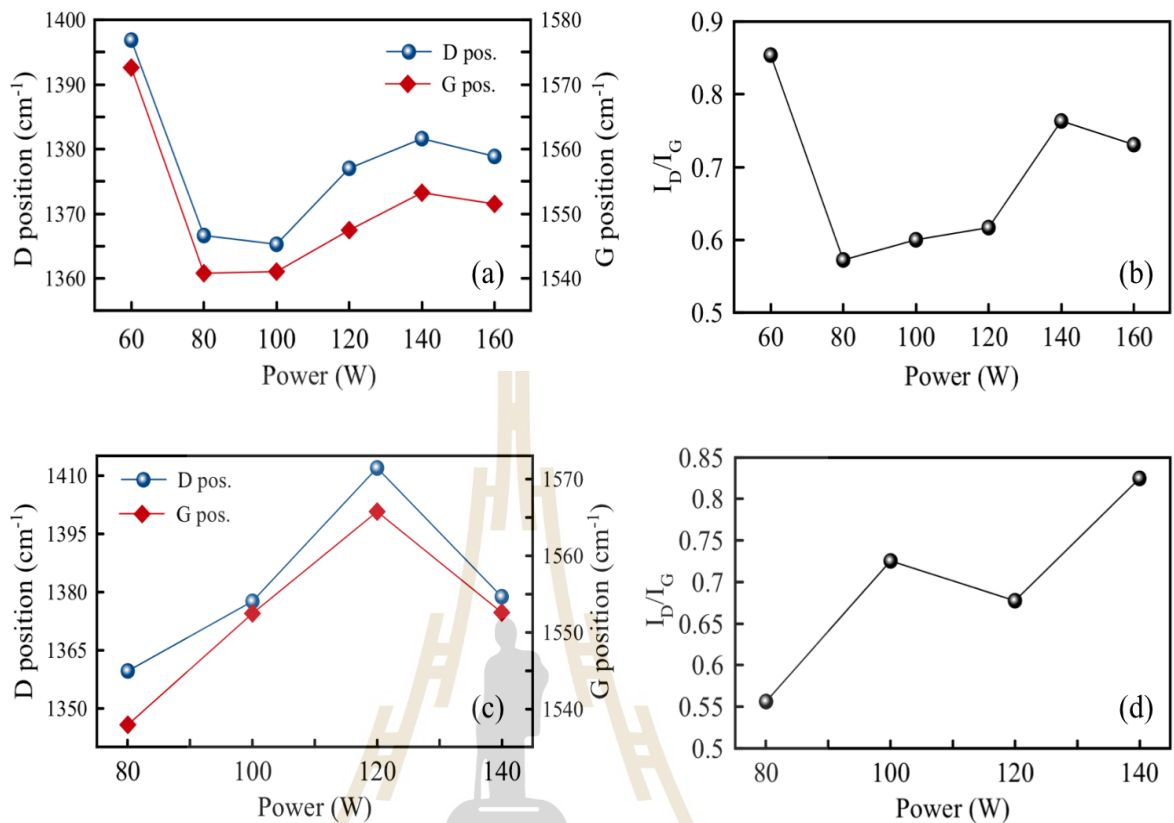
**Figure 40**  $sp^3/sp^2$  ratio of DLC films as a function of RF power using  $CH_4$  flow rate 10 (blue), and  $5 \text{ cm}^3/\text{min}$  (red).

Numerous studies have shown that Raman spectroscopy analysis may be utilized to measure the relative concentration of carbon bonds (Siegal M.P., 2000). The deposited films' Raman spectra in the region of  $700\text{-}1950 \text{ cm}^{-1}$  with various RF powers and  $CH_4$  flow rates are presented in Figure 41. After removing the background, all of the spectra can be fitted into two Gaussian peaks at  $\sim 1375$  and  $\sim 1560 \text{ cm}^{-1}$ , which correspond to disordered (D-band) and graphitic (G-band) structure, respectively. These two peaks are very common in carbon structures (Ferrari and Robertson, 2000). Table 3 shows the fitting results obtained from Raman spectra for all produced films. The Raman spectrum of the film deposited with RF power of  $60 \text{ W}$  and flow rate of  $10 \text{ cm}^3/\text{min}$  revealed a split peak like graphite feature and a shift in the G-band peak location toward wavenumber of  $\sim 1580 \text{ cm}^{-1}$ , indicating the production of graphite film as previously described (Ammar et al., 2015; Huang et

al., 2015). The films deposited with RF power ranging from 80 to 160 W show DLC structure with G-peak locations ranging from 1537.9-1565.8  $\text{cm}^{-1}$ , suggesting the production of DLC film (Robertson et al., 2002). When using an RF power of 80-160 W for deposition, the D and G peak positions change somewhat toward higher wavelengths as the RF power increases, as illustrated in Figure 42. The increase in disordered graphite structure in the film is shown by the shift of D-peak position toward higher wavelength (Ghadai et al., 2018). The structural expansion, which affects intermolecular distances and interaction strengths, is responsible for the shift of G-peak position toward higher wavenumber (Kim et al., 2004). The  $I_D/I_G$  ratio also increases as the RF power increases, showing that the degree of structural disorder in the films increases as well. This is because the density of the plasma cloud formed inside the chamber grows as the RF power increases. During deposition, hydrogen and oxygen inside the chamber cause additional disruption to the film. This is also supported by the XPS results, which show a rise in oxygen and  $sp^3$  concentration.



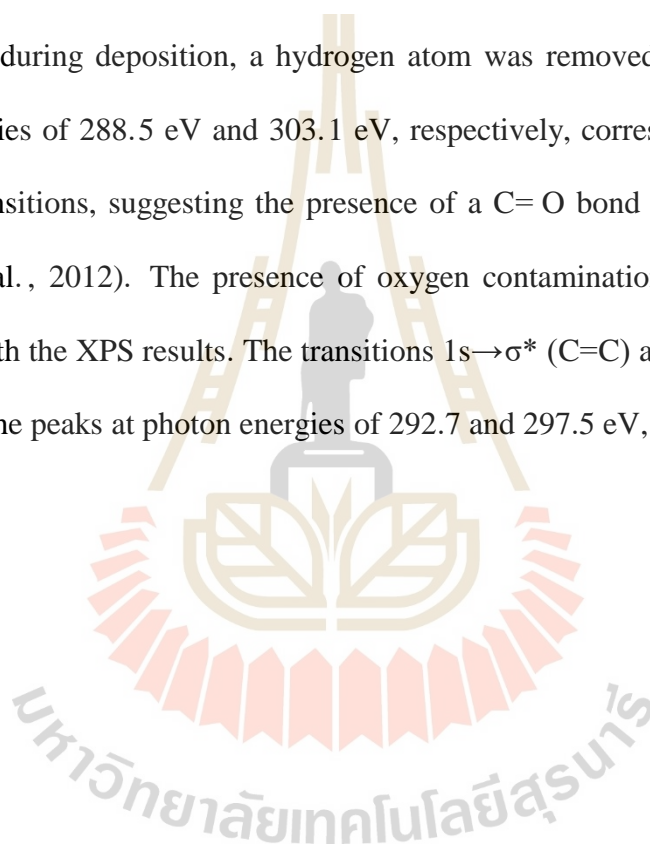
**Figure 41** Raman spectra of the DLC films prepared with different RF power using flow rates (a) 10 cm<sup>3</sup>/min and (b) 5 cm<sup>3</sup>/min.



**Figure 42** (a) Raman peaks position and (b) I<sub>D</sub>/I<sub>G</sub> at 10 cm<sup>3</sup>/min, (c) Raman peaks position and (d) I<sub>D</sub>/I<sub>G</sub> at 5 cm<sup>3</sup>/min, with difference RF power.

The electronic structure of the deposited DLC films was investigated using NEXAFS measurements. In the photon energy range of 270-330 eV, carbon K-edge spectra were collected. Athena packet version 0.9.26 was used to normalize these spectra. The produced DLC films' carbon K-edge NEXAFS spectra are displayed in Figure 43. As previously stated, all of the carbon K-edge spectra display the characteristics of DLC layer (Chunjaemsri et al., 2019; Cody et al., 1998). By comparing the carbon K-edge spectra to the carbon K-edge spectrum of HOPG reported in prior studies, six peaks were identified (Singh et al., 2014; Watts et al.,

2006). The electron state transition  $1s \rightarrow \pi^*$ , which corresponds to  $sp^2$  of the amorphous carbon structure, has a peak at photon energy of 284.8 eV. When the RF power is increased, the peak intensity rises, implying that the  $sp^2$  content in the DLC structure rises as well. Transition  $1s \rightarrow \sigma^*$ , C–H bond, is connected with the peaks at photon energy of 286.7. (Singh et al., 2014; Watts et al., 2006). As the RF power increases, the C–H peak intensity reduces slightly. As a result of the interaction with Ar gas in the chamber during deposition, a hydrogen atom was removed from  $CH_4$ . Peaks at photon energies of 288.5 eV and 303.1 eV, respectively, correspond to  $1s \rightarrow \pi^*$  and  $1s \rightarrow \sigma^*$  transitions, suggesting the presence of a C=O bond (Latham et al., 2017; Sedlmair et al., 2012). The presence of oxygen contamination in the DLC film is consistent with the XPS results. The transitions  $1s \rightarrow \sigma^*$  (C=C) and  $1s \rightarrow \sigma^*$  (C–C), are revealed by the peaks at photon energies of 292.7 and 297.5 eV, respectively.



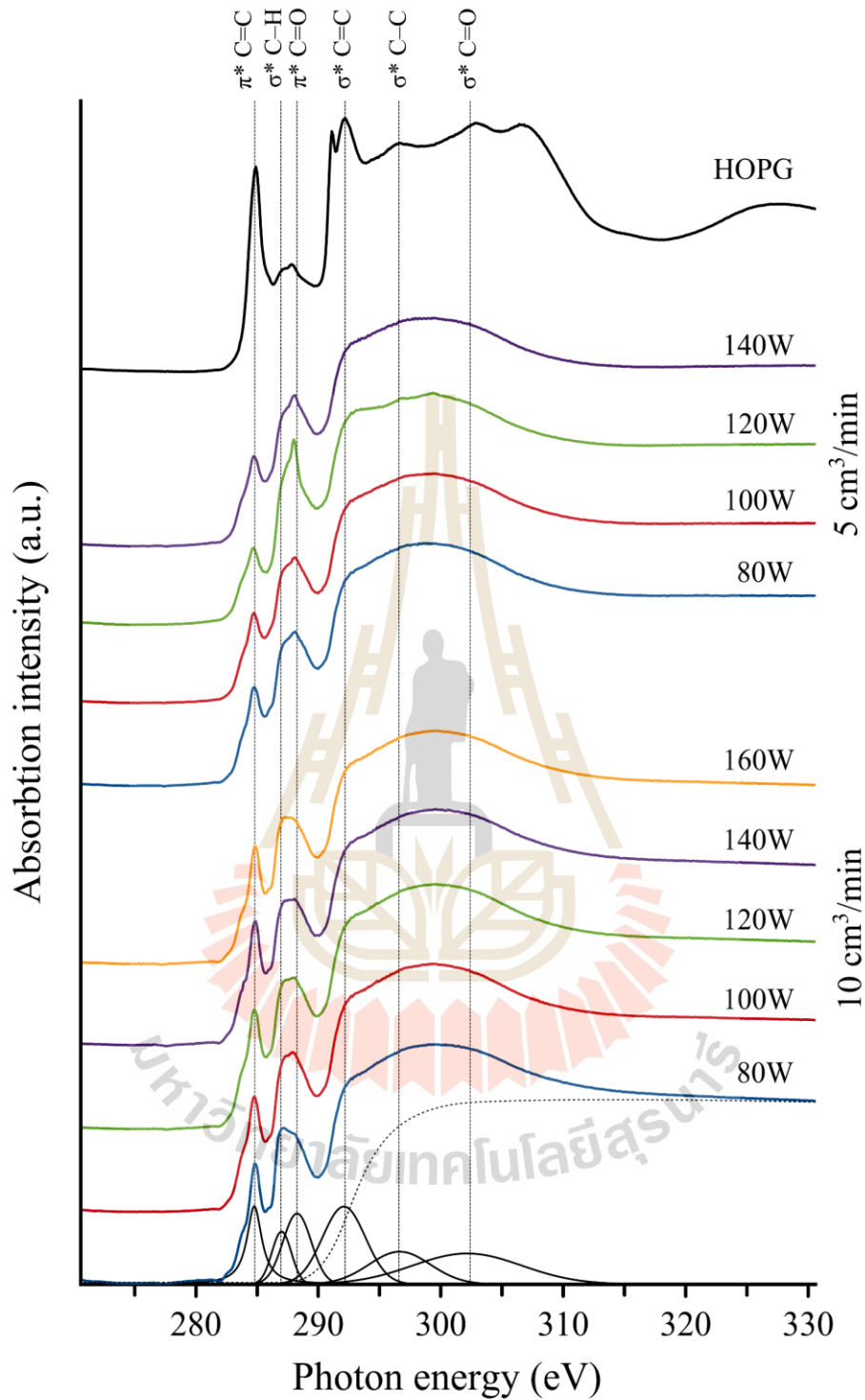


**Figure 43** Carbon *K*-edge NEXAFS spectra of the DLC films prepared with a different RF power using CH<sub>4</sub> flow rates of 5 cm<sup>3</sup>/min and 10 cm<sup>3</sup>/min, respectively.

**Table 4** Numerical characterized XPS and Raman results of DLC films for all preparation conditions.

CH <sub>4</sub> flow rate	10 cm <sup>3</sup> /min						5 cm <sup>3</sup> /min					
	60	80	100	120	140	160	60	80	100	120	140	160
<b>RF power (W)</b>												
<b>Films thickness (nm)</b>	-	117.7	140.5	151.9	179.5	244.9		83.2	142.0	129.1	169.6	-
<b>Chamber pressure</b>												
cleaning pressure, (Pascal)	2.47	2.43	2.42	2.35	2.42	2.71	2.44	2.57	2.55	2.63	2.27	2.56
working pressure, (Pascal)	3.57	3.27	3.31	3.31	3.54	3.84	3.50	3.50	3.47	3.44	2.90	3.46
<b>XPS</b>												
relative atomic concentration (%)												
C=O	-	3.45	4.31	3.14	2.31	4.35	-	2.32	3.14	4.38	4.92	-
C-O	-	10.17	9.64	13.04	7.03	7.50	-	11.48	12.72	10.38	11.19	-
C-C ( <i>sp</i> <sup>3</sup> -fraction)	-	46.21	44.32	40.85	42.80	42.01	-	40.00	37.78	39.26	34.27	-
C=C ( <i>sp</i> <sup>2</sup> -fraction)	-	40.17	41.73	42.97	47.86	46.14	-	46.20	46.36	45.98	49.62	-
<i>sp</i> <sup>3</sup> / <i>sp</i> <sup>2</sup> ratio	-	1.15	1.06	0.95	0.89	0.91	-	0.87	0.81	0.85	0.69	-
<b>Raman Spectroscopy</b>												
D-position, (cm <sup>-1</sup> )	1396.9	1366.7	1365.3	1377.0	1381.6	1378.9	-	1359.6	1377.6	1411.9	1378.8	-
G-position, (cm <sup>-1</sup> )	1572.6	1540.8	1541.1	1547.5	1553.3	1551.5	-	1537.9	1552.5	1565.8	1552.6	-
I <sub>D</sub> /I <sub>G</sub>	-	0.57	0.60	0.62	0.76	0.73	-	0.56	0.73	0.68	0.82	-

The SEM images of the DLC prepared by PECVD with different RF powers and CH<sub>4</sub> flow rate of and 10 cm<sup>3</sup>/min are shown in Figure 44. In the measurement, the probing head was set at 54° as shown in Figure 45. The thickness of DLC films was calculated by using law of right triangle as the following equation:

$$y = \frac{x}{\cos 54^\circ} \quad (7)$$

which  $y$  thickness of DLC films (nm)

$x$  range of SEM imaging (nm)

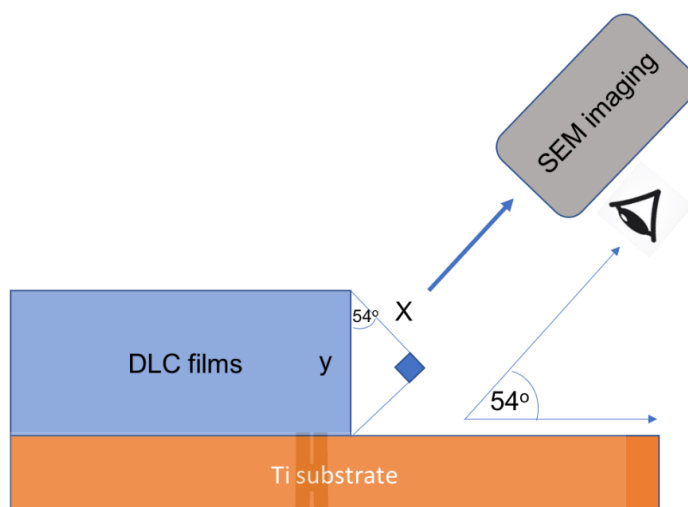


**Figure 44** SEM imaging diagram.

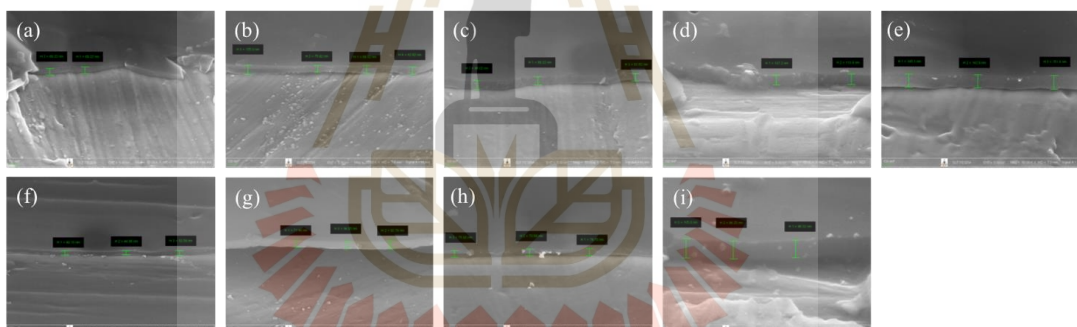


**Figure 45** SEM images of the DLC films deposited by PECVD at different RF powers using  $\text{CH}_4$  flow rates of (a-e) 10, and (f-h) 5  $\text{cm}^3/\text{min}$ .

#### 4.6 Summarize of RF power and gas flow rate with films properties

DLC films were successfully deposited on titanium substrates using the PECVD process in this chapter. XPS, Raman spectroscopy, and NEXAFS spectroscopy were used to investigate the effects of deposition circumstances, RF power, and  $\text{CH}_4$  gas flow rate on the chemical composition and structure of the films. When the RF power

is increased, the  $sp^3/sp^2$  ratio decreases, according to the XPS results. The  $sp^3/sp^2$  ratio tends to rise as the  $CH_4$  gas flow increases. The Raman spectroscopy results reveal that as the RF power increases, the degree of structural disorder in the films increases, whereas the NEXAFS results show that the hydrogen content decreases. These findings imply that the RF power and  $CH_4$  gas flow rate have a significant impact on the structure of DLC deposited using the PECVD process.

#### **4.7 Primary results of other interesting condition for PECVD**

There are the other interesting conditions for deposited DLC by using PECVD technique. In this part, time dependence and films polishing conditions was reported. However, deposition time is important factor for determining the significant properties of the amorphous carbon films. Moreover, substrate treatment is also important factor which control possibility of films forming. In this study, DLC was successfully deposited on titanium substrate. Time variation and substrate polishing were used in order to study prepared carbon films properties. Film characterization were successfully investigated by using Raman spectroscopy and X-ray photo electron spectroscopy (XPS) and synchrotron-based Near-edge X-ray absorption fine structure (NEXAFS). Time variation indicate increase in oxygen contamination with increasing time depositions. The results were confirmed by increasing of  $I_D/I_G$  and C-O area on Raman spectroscopy and XPS, respectively. Moreover, films polishing indicate easier of oxygen contamination and films peeling.

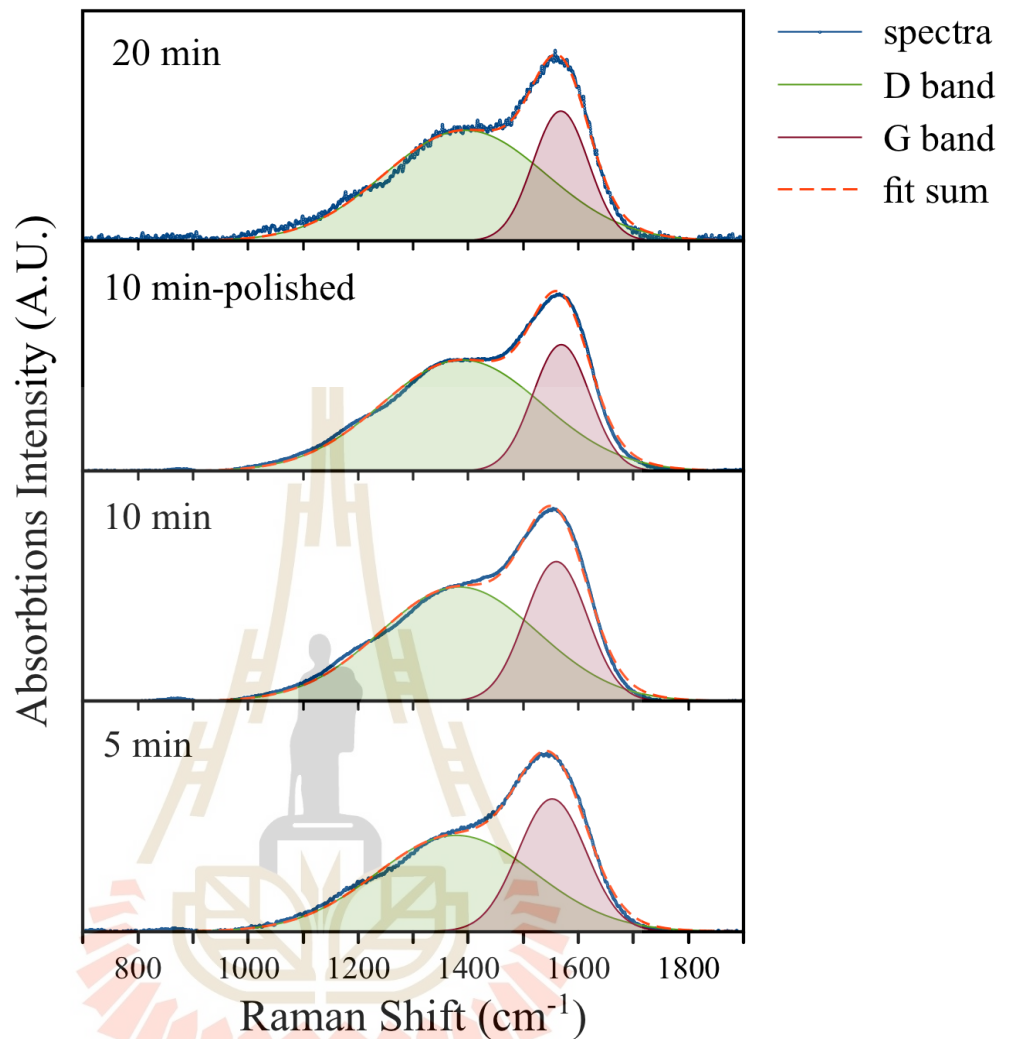


**Figure 46** Raman spectra of the DLC films prepared with different time and substrate-polished.

The Raman spectra was carried out from SLRI (Sentra, Bruker). Green light at wavelength 532 nm was used for studies behavior of  $sp^2$  vibrations. This this part, G-positions look slightly left shift which related to disturbed of structure. It also good agreement with  $I_D/I_G$  ratio which is reported in Table 4. The ratio shows same trend for amplitude and area fitting. While the film polishing related to significantly deference with non-polished at deposition time 10 min. The increasing in trend of

$I_D/I_G$  and G-positions indicated the disordering structure which probably occur from oxygen contaminated the depositions process. It highly possible demonstrate oxygen volume increasing in time and also films polishing.

**Table 5** Characterized of DLC films prepared with different time and substrate-polished.

Samples	G-positions ( $\text{cm}^{-1}$ )	$I_D/I_G$ (amp.)	$I_D/I_G$ (area)	$sp^3/sp^2$
DLC 5 min	$1552.5 \pm 0.1$	0.73	1.69	1.07
DLC 10 min	$1560.1 \pm 0.1$	0.82	2.06	0.77
DLC 10 min-polished	$1569.2 \pm 0.1$	0.88	2.46	0.69
DLC 20 min	$1568.2 \pm 0.1$	0.85	2.47	0.96

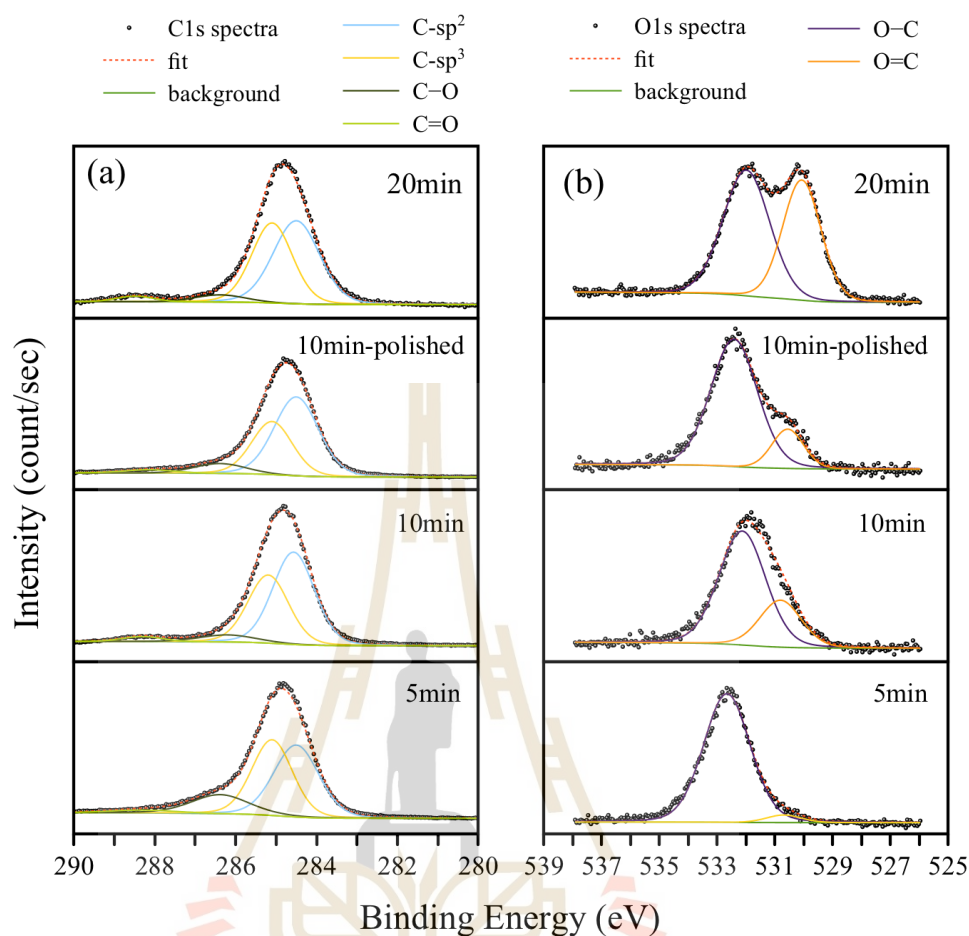


**Figure 47** XPS spectra of DLC films prepared with different time and substrate-polished.

The XPS results was successfully performed from BL-5.2, SLRI. Interpreting results begins with focus 2 high resolution regions, carbon and oxygen. The carbon spectra were fitted by 4 deconvoluted peaks which reported in Figure 47. Deconvoluted peak of C- $sp^2$  look slightly increase with times dependence. while C- $sp^3$  also related to decreasing in trend. The  $sp^3/sp^2$  calculated was reported in the Table 5. Also, the films polished give lower ratio of  $sp^3/sp^2$  which interested point for discussion. In the same, the increasing in oxygen O=C at photon energy 529-531 eV

were investigated by oxygen region, trends indicate to a good agreement which oxygen contaminated at carbon region at binding energy 288.5 eV. And the O-C of oxygen regions also look slightly decrease which increasing in deposition time.

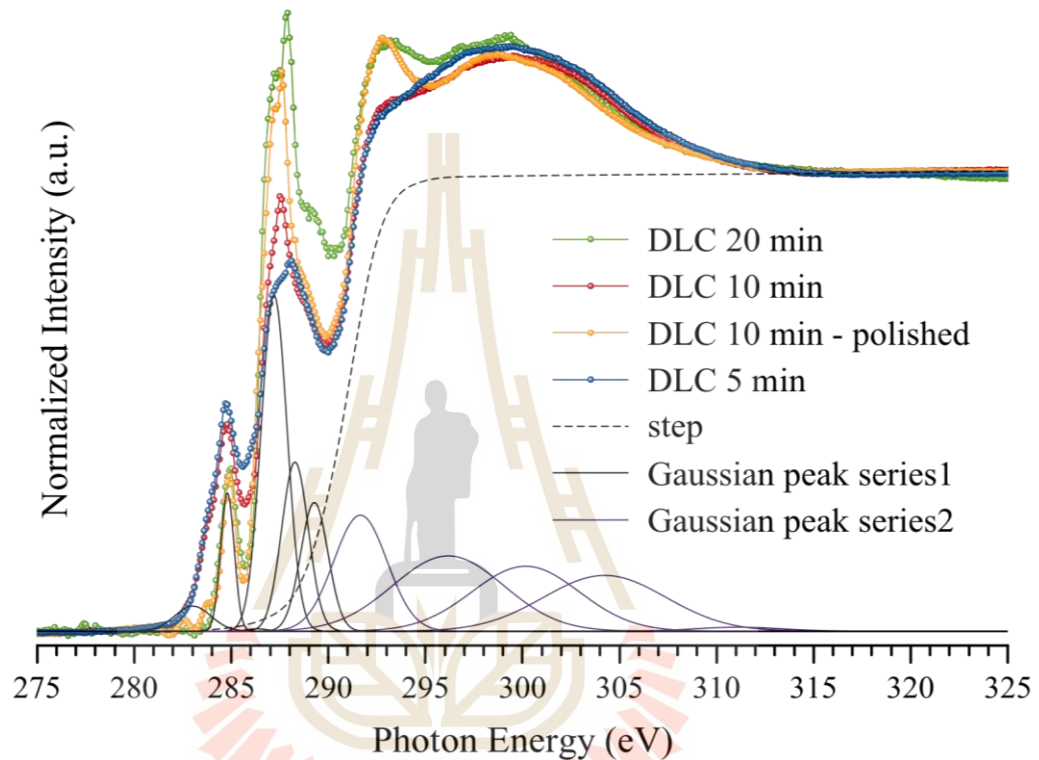


**Figure 48** NEXAFS spectra of DLC films prepared with different time and substrate-polished.

The NEXAFS spectra was successfully carries out from Bl.3.2Ua. the spectra were normalized by using Athena software. Deconvoluted peaks was also fitted for understanding the feature of spectra. In this case, the deconvoluted at photon energy was clearly deference which are indicated the hydrogen and oxygen contents in DLC films. Increasing of deposition time affect to increasing in oxygen content feature, it probably occurs from contamination in chamber. In the same, the substrate which

polished before deposition at 10 min, also give same trend of oxygen contaminated in Diamond-like carbon films. However, deconvoluted peak at photon energy 291.5 eV represent increasing in trend of C-C bonding, spectra related both increase with times substrate-polishing. This feature gives the interesting for deep details to study in future.



## CHAPTER V

### EFFECT OF ZN DOPED AND LOCAL STRUCTURE

#### 5.1 Zn-doped and introduction

Nowadays, the amorphous carbon has been deeply studied and applied my applications fields (Paul, 2017). The DLC structure was developed with doped-metal (M-DLC) and non-metal for improving the properties. For example, Si doped DLC (Si: DLC) causes low friction coefficient and high wear resistance against sliding (Liang et al. , 2017). Moreover, silver nanoparticle (AgNP) doped DLC coated synthetic silk tissue is used as antibacterial bandage, it is more effective for regeneration the human would (Schwarz et al., 2011; Juknius et al., 2016). Moreover, zinc was also chosen for studying in this work which is well known for antibacterial in biological application (Yonezawa et al. , 2020). Moreover, it also was used for solving osteoporosis problem in medical which improving calcium lose in bone of knee joint as the following reported (Yamaguchi, 2010). And carbon also is a material which is appropriate for bio-combativity (Thomson et al., 1991).

However, the previous researches hadn' t been widely studied in detail of deposition process. The most importance is less deeply studies behavior of zinc in amorphous carbon structure such as local environment, oxidation state, conductivity, electronic structure or zinc forming etc. (Wong et al., 2011; Tasdemir et al., 2014). These reasons lead to deeply studying in this research which base on synchrotron characterization techniques.

This work, Zn-doped DLC was fabricated by a reactive magnetron sputtering for introducing zinc in DLC films, while amorphous carbon was performed by using chemical vapor depositions technique (CVD). Variations of generated magnetron plasma was studied. In details of characterization, this work focused on analysis of local structure of Zn behavior inside DLC films. For classificatory carbon evolutions, disordering of films was studied by Raman spectroscopy. Also, near edge X-ray absorption fine structure (NEXAFS) were used for studying carbon bonding and electronic structure. Finally, zinc was investigated the local structure by X-ray absorption spectroscopy (XAS) which deeply study zinc behavior in DLC films.

## **5.2 Zn-doped DLC Experiment**

### **5.2.1 Zn-DLC film preparations**

In detail of depositions, silicon (100) was used as substrate which cleaned by ethanol and acetone in ultrasonic cleaner for 10 mins, respectively. As the reactive sputtering system, DC sputtering and DC pulse plasma CVD systems were combined. DC current for sputtering (PS) and DC pulse bias voltage for CVD (PC) were varied as parameters. The Ar and C<sub>2</sub>H<sub>2</sub> were used for cleaning process and deposition process at 20 cm<sup>3</sup>/min in flow rate, respectively. Working pressure was controlled at approximately 3 Pa. Depositions time is maintained at 60 min.

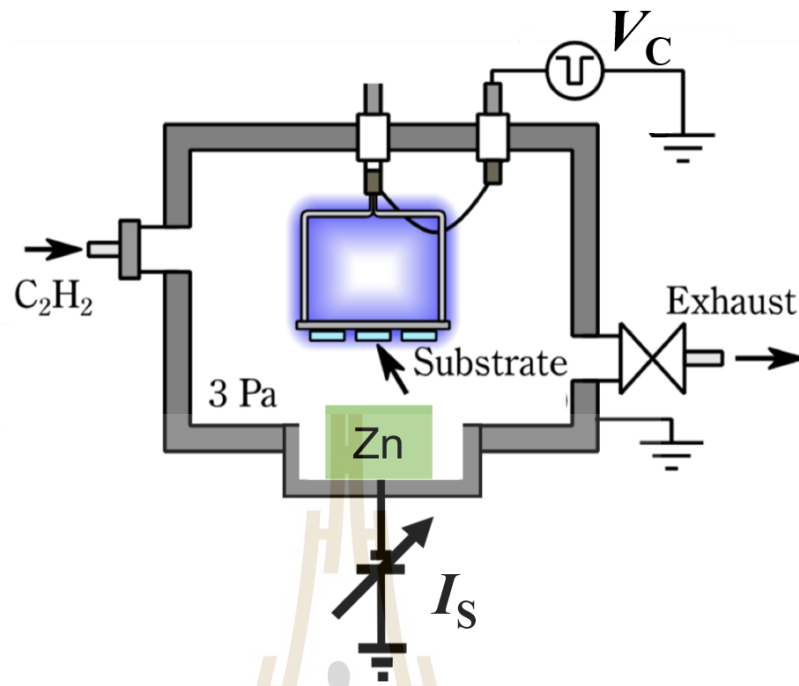


**Figure 49** Schematic diagram of CVD and sputtering system.

### 5.2.2 Zn-doped Deposition Conditions

The deposition system includes 2 techniques for depositions Zn-DLC films, the first is CVD technique which mainly used for depositions DLC, and the second is direct current (DC) sputtering for introduce Zn into the carbon structure.  $C_2H_2$  was used for depositions which (purity >99.9%) flow rate were kept at  $15 \text{ cm}^3/\text{min}$ . Pulse power supply ( $P_C$ ) was generate at 14.4 kHz.  $P_C$  voltage was controlled at 2.0 kV. Zn-target 4-inchs was used for introduce Zn in DLC films. Direct current ( $P_S$ ) were manually generated as current controlling, the current is 0.05, 0.1 and 0.2 A. The deposition time was 60 min for all samples.

**Table 6** The system deposition parameters of DLC films.

Deposition parameters	Unit	Value
Base pressure	Pa	<0.05
Working pressure	Pa	3
Deposition time	min	60
C <sub>2</sub> H <sub>2</sub> flow rate	(cm <sup>3</sup> /min)	15
CVD Pulsed bias voltage ( <i>V<sub>c</sub></i> )	kV	-2
DC sputtering current ( <i>I<sub>s</sub></i> )	<i>Current Ampere (A)</i>	0-0.2

### 5.3 Zn-DLC films characterizations

#### 5.3.1 Raman spectroscopy analysis

A dispersive Raman microscope (SENTERRA, Bruker) was used to perform Raman spectroscopy with a green light laser source with a wavelength of 532 nm, a power of 25 mW, and a slit of 25×1000 micron. The Raman spectra were recorded at a resolution of 0.5 cm<sup>-1</sup> in the range of 50-2700 cm<sup>-1</sup>. The parameters are the D and G bands, and the films I<sub>D</sub>/I<sub>G</sub> ratio was calculated by fitting the Raman spectra with two Gaussian peaks.

#### 5.3.2 Indentation hardness analysis

Hardness properties were investigated by indentations hardness technique at Tokyo Institute of Technology (TIT) which equipment is Elionix (ENT-1100a). Indenter shape is berkovich (Čech et al., 2016). It was controlled perpendicularly onto the coating applying a normal load of maximum for 3mN, under 0.1μm depth (less than 10% of thickness). Each sample was chosen for 16 points for loading-unloading cycles.

### **5.3.3 Laser microscopy**

Roughness morphology was successfully employed by using Laser microscopy technique. The thickness was also investigated.

### **5.3.4 X-ray Absorptions spectroscopy analysts**

Studying of Zn behavior was performed by 2 mains synchrotron-based spectroscopy techniques which are near edge X-ray absorption fine structure (NEXAFS) and X-ray absorption spectroscopy (XAS). The NEXAFS experiment was conducted at SLRI's Beamline 3.2Ua. Total electron yield (TEY) mode was used for the measurement. The storage ring released synchrotron radiation with an electron energy of 1.2 GeV. The DLC films' carbon K-edge spectra were collected in the energy range of 270-330 eV with a 0.1 eV energy step. The synchrotron ring's electron current was between 70-140 mA. By aligning the observed carbon K-edge spectra with the  $\pi^*$  resonance peak of highly orientated pyrolytic graphite (HOPG) at 284.8 eV, the spectra were calibrated. For investigating zinc local environment, behavior of zinc in DLC was performed by XAS at Bl-5.2, SLRI. The experiment was setup for Zn K-edge as FL-mode for thin films at edge energy 9659 eV. Zinc oxidation state was investigated by the X-ray absorption near edge structure (XANES) regions, and the neighboring atom of zinc was studied by qualitative of extended X-ray absorption fine structure (EXAFS) spectra.

### **5.3.5 Results and Discussion**

Amorphous carbon films with 4 conditions were successfully deposited on silicon substrate. Sample looks black and shiny without introducing zinc by sputtering. Increase in generated sputtering rate for introducing zinc inside DLC

structure indicate lower shiny properties and higher of dust on sample surface, however the plasma generated were stable during depositions.

Raman spectra in Figure 50 were shown mainly 2 deconvoluted peaks, it was well-known in  $I_D$  and  $I_G$  which stand for disordering band and graphite band, respectively (Filik., 2005). Increasing in generated sputtering rate affect to increasing in disordering structure of DLC films. Trend of amplitude position of  $I_D$  looks slightly right shift; it indicates Zn disruption which introduced in DLC structure. while the  $I_G$  band was decreased. The silicon feature hadn't been shown in these spectra as indicated to thick Zn-DLC films. Disordering of DLC was confirmed by  $I_D/I_G$  ratio as reported in Table 2.

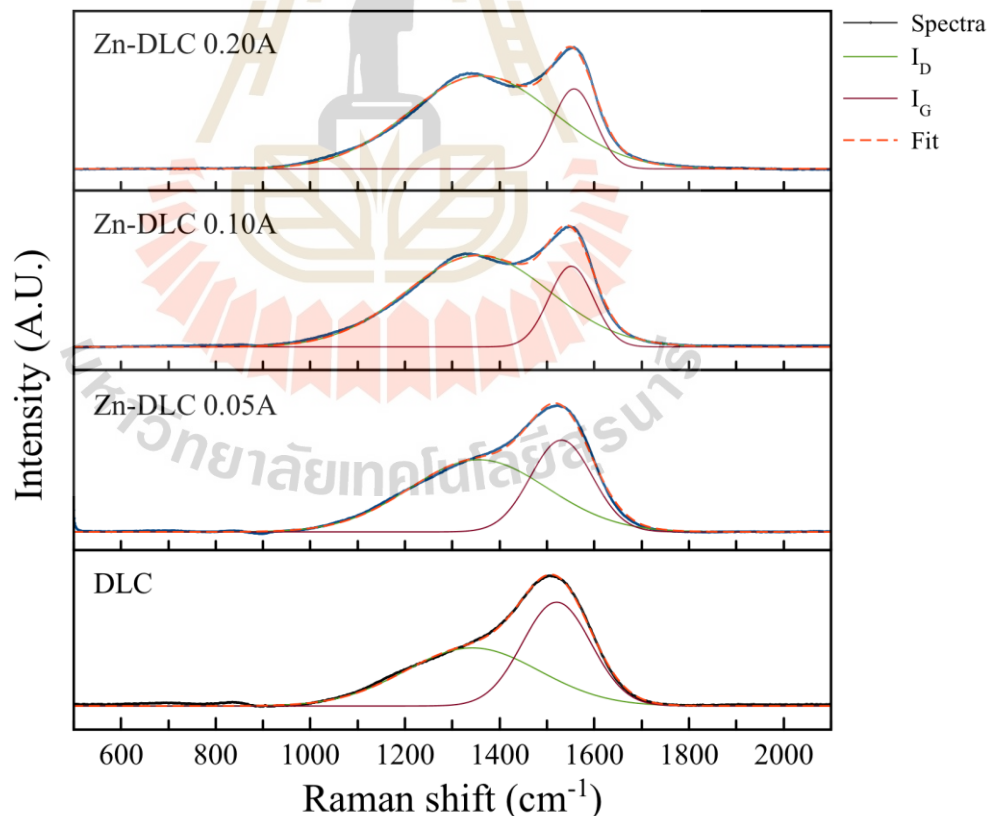


**Figure 50** Raman spectra of DLC films and Zn-DLC.

Amorphous carbon films also were studied the mechanical properties by indentation hardness test. Figure 4 shows load and un-load tip working of hardness properties. It was measured for 16 sampling positions as controlled at maximum load 3 mN. In detail, DLC depth is very homogenous, while increasing in sputtering current affect to non-homogenous of depth profiles. Zn-DLC 0.05A was showed slightly deference depth from DLC, while higher Zn-DLC at 0.1A indicate more values depth profile. It was shown most distributions depth values incase Zn-DLC 0.2A. Increase in higher rougher was increased with higher magnetron sputtering current, it was performed by using Laser microscopy (Figure 57) and AFM (Figure 60).

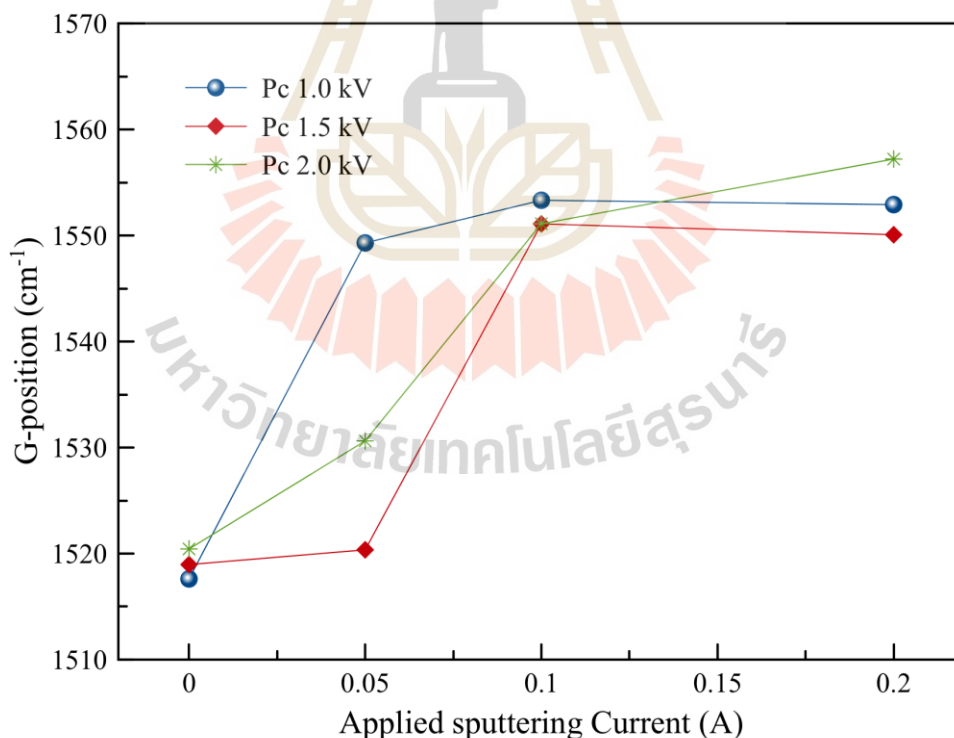


**Figure 51** G-positions of Raman spectra of DLC films and Zn-DLC.

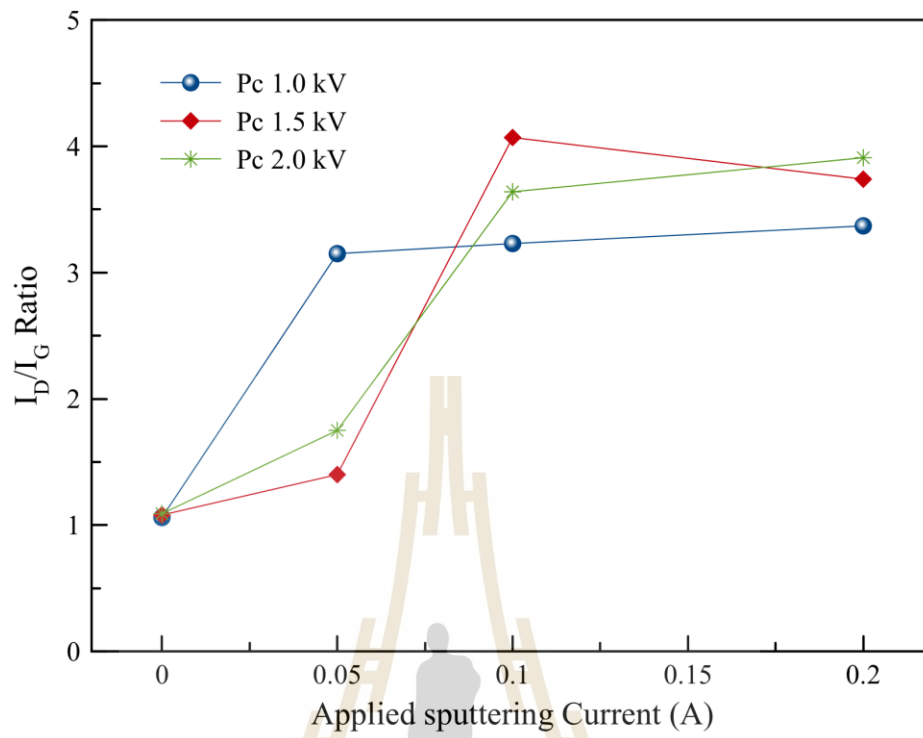


**Figure 51**  $I_D/I_G$  ratio of Raman spectra of DLC films and Zn-DLC.

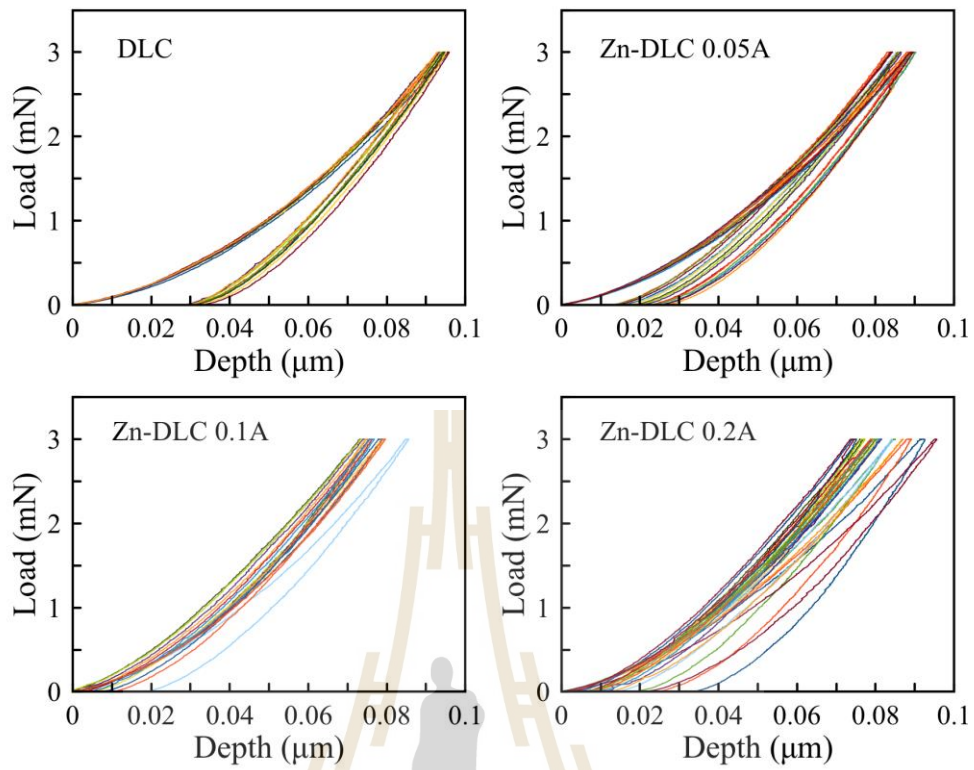


**Figure 53** Loading-unloading feature indentation hardness test of a) DLC, b) 0.05 Zn-DLC, c) 0.1Zn-DLC and d) 0.2Zn-DLC.

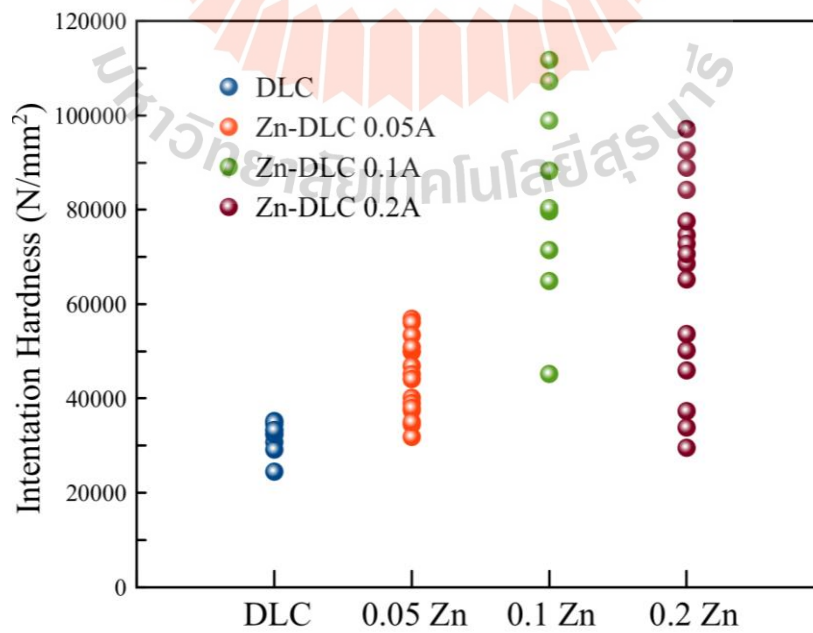


**Figure 54** Indentation hardness profile of DLC and Zn-DLC films.

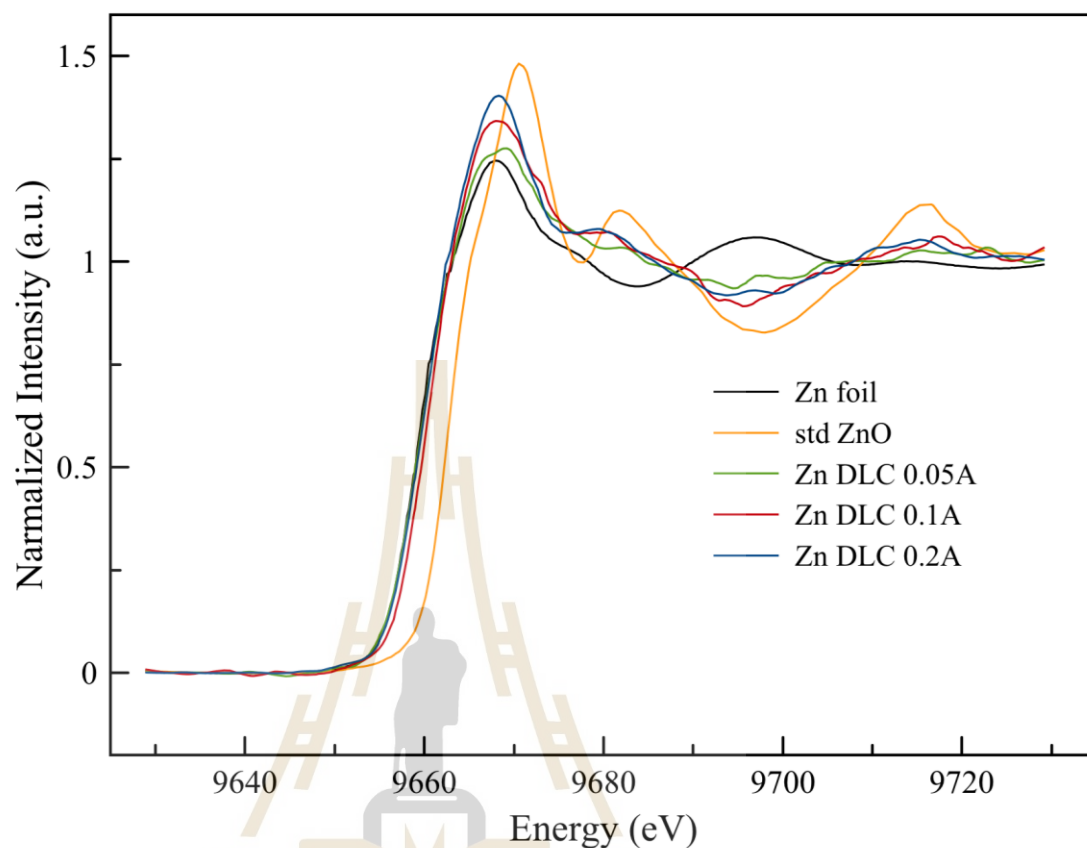


**Figure 55** Zn *K*-edge spectra of Zn doped DLC films.

For study Zn behavior, X-ray absorptions spectroscopy was used for investigation electronic excitations of Zn in DLC structure. Fluorescence mode was performed by fixing sample holder position at 45 degree for incident synchrotron light source. Zn *K*-edge spectra were successfully calibrated at the edge energy 9659 eV by standard Zn-foil from BL-5.2. XANES spectra were investigated in range 9630–9730 eV. The feature of Zn spectra was also considered with standard ZnO at edge energy 9669 eV. In Figure 55, the normalized Zn *K*-edge XANES spectra was performed. Edge energy of all spectra represent to zinc oxidation state which is very close to standard Zn foil. While, the oscillation feature of all samples is similar to the feature

of ZnO, they indicate the similarity of oxygen environment which is found in ZnO local structure. Increasing in generated zinc plasma affect higher white-line intensity which indicate increasing in oxygen vacancy. However, the zinc surrounding was made sure by EXAFS spectrum as reported in Figure 56. Zn-DLC 0.2A is proxy which highest zinc content. Its  $k$ -space spectrum was converted to  $R$ -space by Fourier transformations during wavenumber range 3-9  $\text{\AA}^{-1}$ .  $R$ -space spectrum was shown 3 main intensity regions. First shell intensity in range 1-2  $\text{\AA}$ , indicate possibility of mixing of oxygen and carbon regions. While, zinc behave majority metallic state in oxygen and carbon environment as neighboring atoms. It indicates non-bonding of zinc core-shell atom. The second peak as amplitude 2.67  $\text{\AA}$ , represent to zinc atom intensity as following reported (Liu et al. , 2019). However, the peak positions between first shell of Zn foil and second-shell of ZnO, indicated agreement of mixing of their structures. The lowest intensity in the third-shell also indicate possibility of secondary for oxygen shell and carbon environments.

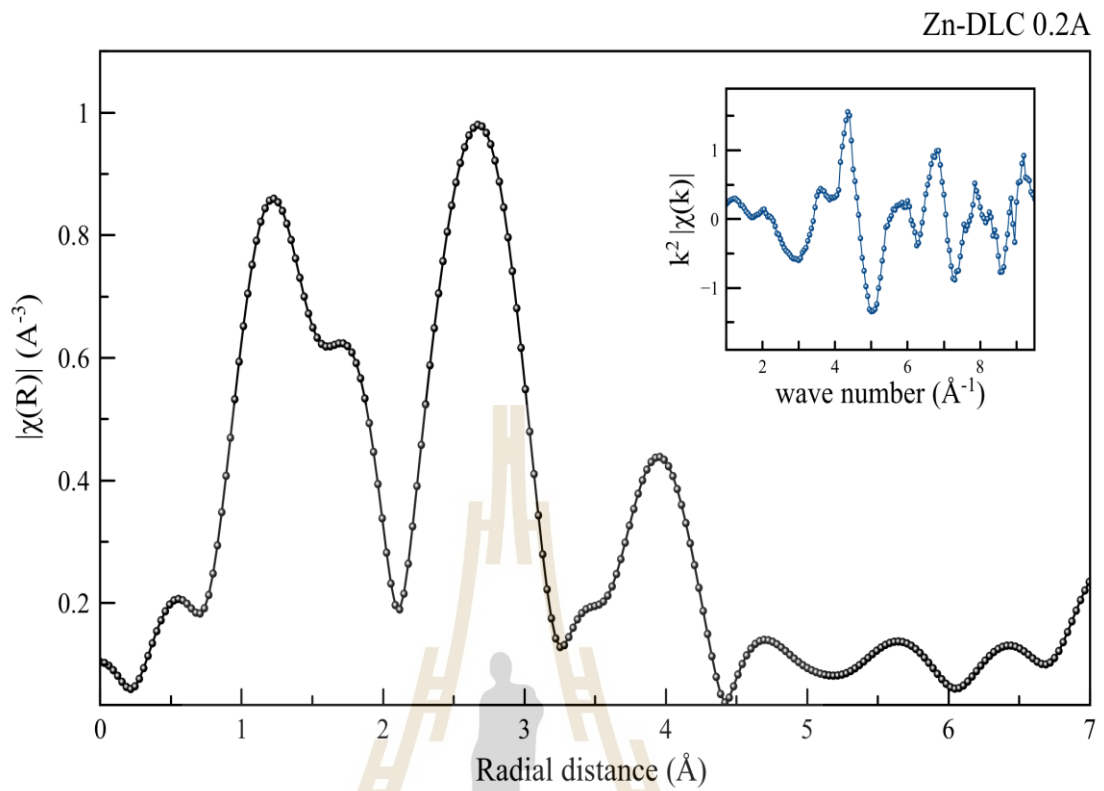


**Figure 56** Fourier transformation of  $k^2$ -weighted spectra of EXAFS Zn *K*-edge.

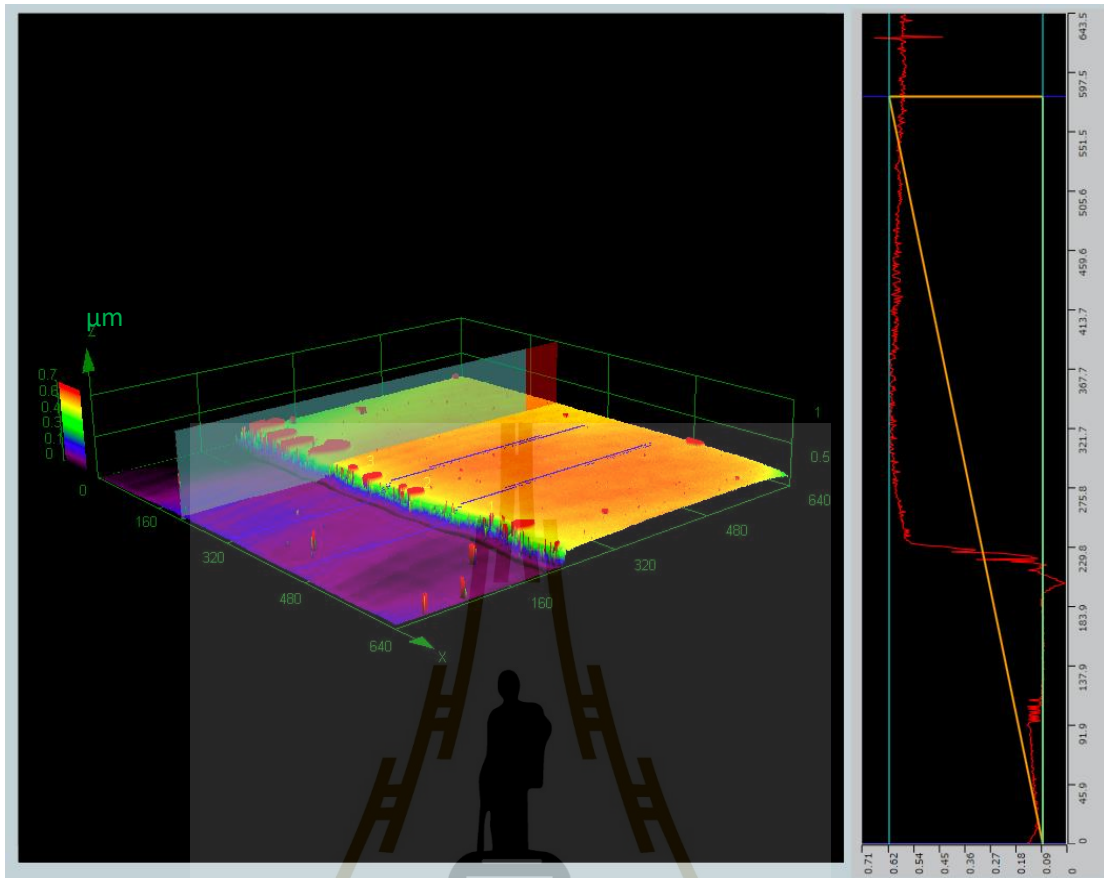


**Figure 57** Laser microscopy measuring by using step profiler for studying thickness.

Laser microscopy was also used to investigate the thickness of Zn-DLC films as reported in Figure 57. The reference plane represents the reference height surface. It was clearly seen by the reference color. The higher profile is related to film deposition, while the lower profile indicates the substrate covered by copper tape. In the results, the film thickness was successfully measured, which reports around  $1 \mu\text{m}$ . The trend of thickness slightly increases when the sputtering rate was higher. Thickness values were reported in Table 6.

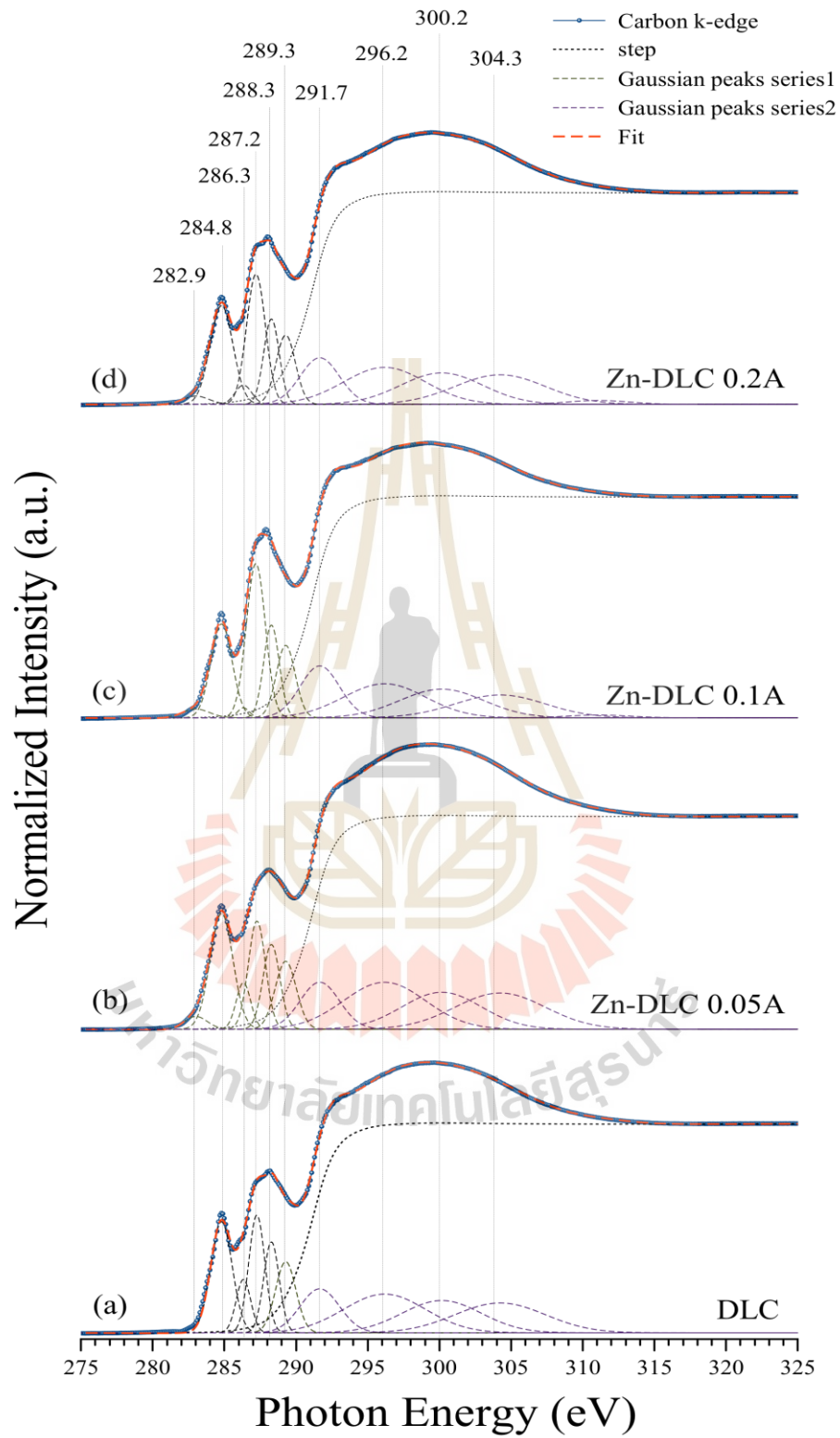


**Figure 58** Carbon K-edge of DLC and Zn-DLC spectra.

In Figure 58, the carbon *K*-edge of DLC spectra was performed. It exhibits the feature of DLC spectra as previously reported (Chunjaemsri et al., 2020; Rittihonget al., 2020). Arctan function was used as the background subtract. The spectra were normalized by using artemis software. The deconvolute peak of spectra in carbon region was summarized in Table 6.

**Table 7** Deconvoluted peaks of DLC filing in NEAXFS spectra.

Photon Energy (eV)	Electron excitation	Ref.
282.9		Carbine form
284.8	$1s \rightarrow \pi^*$	C=C
286.3	$1s \rightarrow \sigma^*$	C=C <sub>furan</sub>
287.2	$1s \rightarrow \sigma^*$	C-H
288.3	$1s \rightarrow \pi^*$	C=O
289.3	$1s \rightarrow \pi^*$	C≡C, C-OH
291.7	$1s \rightarrow \sigma^*$	C-C
296.2	$1s \rightarrow \sigma^*$	C=C
300.2	$1s \rightarrow \sigma^*$	C=O
304.3	$1s \rightarrow \sigma^*$	C≡C

To identify deconvoluted peak, the spectra were fitted by gaussian peaks which classified for 2 series which refer to the following reported (Latham et al., 2017). The first gaussians group as lower 290 eV, represent mainly electron excitations from  $1s \rightarrow \pi^*$ . Low intensity of photon energy at 282.9 eV, represent to carbine forming (Adelhelm et al., 2008). It indicates weak interaction of zinc with DLC structure, while XAS data show clearly Zn content signal. The peak position at photon energy 284.8 eV represents  $1s \rightarrow \pi^*$  of C=C, it indicates similarity C-*sp*<sup>2</sup> content in DLC structure. The amplitude at 287.2 eV relates H content as transition  $1s \rightarrow \sigma^*$  of C-H (Zhou et al., 2017), it increases in increasing of generating plasma. Peak positions at

photon energies 288.3 eV and 289.3 eV represent to  $1s \rightarrow \pi^*$  of C=O and C-N, respectively. These two features indicate films contamination which occurred from relaxations at films surface (Heymann et al., 2011). The second group as higher 290 eV, majority represent electron excitations from  $1s \rightarrow \sigma^*$ . The peak position at 291.7 eV is related to electron transitions of  $1s \rightarrow \sigma^*$ , C=C. Its trending shows slightly increasing of C- $sp^2$  content. While, decreasing of the peak positions at 296.2 eV slightly also decrease in C- $sp^3$  which assume electron transitions of  $1s \rightarrow \sigma^*$ , C-C. In deeply interpreting details, the overall values of deconvoluted peaks were reported in Table 7 and 8.

**Table 8** Summarized of the chemical characterization data of Zn-DLC films.

Samples	G-positions ( $\text{cm}^{-1}$ )	D-positions ( $\text{cm}^{-1}$ )	$I_D/I_G$	$sp^2/(sp^3+sp^2)$
DLC	$1520.4 \pm 0.1$	$1342.1 \pm 0.1$	$1.09 \pm 0.01$	0.273
Zn-DLC 0.05	$1530.6 \pm 0.1$	$1353.4 \pm 0.1$	$1.75 \pm 0.01$	0.258
Zn-DLC 0.10	$1551.1 \pm 0.1$	$1555.2 \pm 0.1$	$3.64 \pm 0.01$	0.224
Zn-DLC 0.20	$1557.2 \pm 0.1$	$1560.7 \pm 0.1$	$3.97 \pm 0.01$	0.237

**Table 9** Summarized of the physical characterization data of Zn-DLC films.

Samples	Hardness ( $\text{N/mm}^2$ )	Hardness variance ratio	Thickness ( $\mu\text{m}$ )	Roughness Ra (nm)
DLC	32,036	0.10	$0.98 \pm 0.01$	1.903
Zn-DLC 0.05	44,328	0.18	$1.10 \pm 0.01$	2.151
Zn-DLC 0.10	83,611	0.24	$1.29 \pm 0.01$	3.793
Zn-DLC 0.20	65,173	0.33	$1.31 \pm 0.01$	3.846

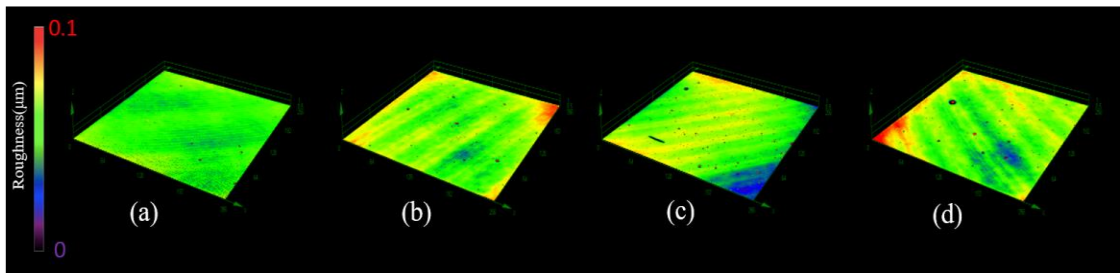


**Figure 59** Roughness profile of DLC and Zn-DLC films by Laser microscopy.

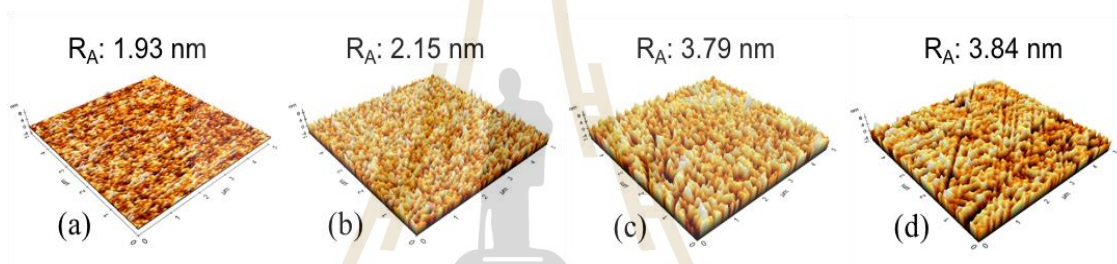


**Figure 60** Roughness profile of DLC and Zn-DLC films by AFM.

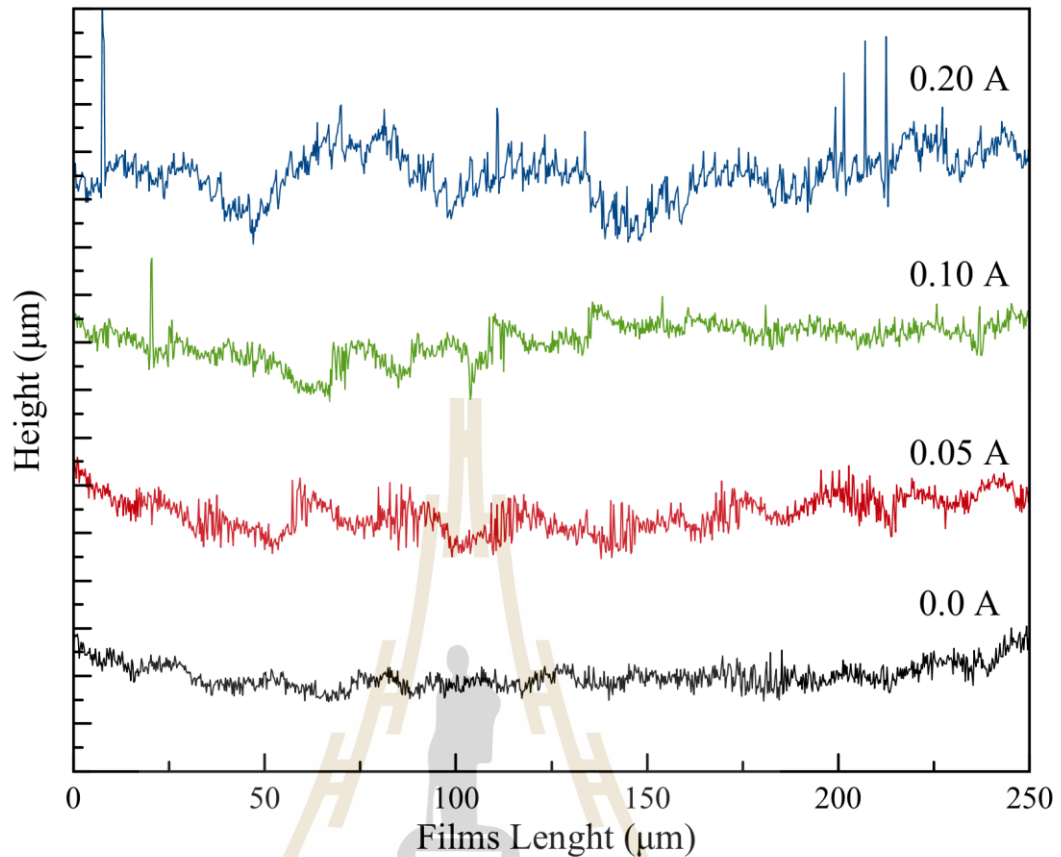


**Figure 61** 2D roughness profiles by Laser microscopy of DLC and Zn-DLC.

#### 5.4 Summarize of Zn-doped DLC

In this work, Zn doped DLC films were successfully deposited on Si substrate by combinations of CVD and DC sputtering techniques. The influences DC pulse sputtering was studied which higher Zn concentration increase in higher DC pulse generated. Loudness and depth profile distribution also increase in generating sputtering current performed by indentation hardness test. Disordering structure also increase in Zn introducing as report by Raman spectra. Zn oxidation state was successfully confirmed by XANES spectra. Moreover, local structure of Zn films was explained by EXAFS spectra as mostly live as zinc cluster and oxide form in DLC

structure. While, its local environment is suitable for bio-compatibility, these results promise the possibility utilization for driving Zn-DLC to biological applications.

## 5.5 Introduce of Ti-doped DLC and interesting

However, there are other interested doping elements which widely apply for industrial application. This section, Titanium (Ti) was primarily studied. It was well-known for improving frictions of DLC properties. It was also systematically characterized by using previously spectroscopy techniques.

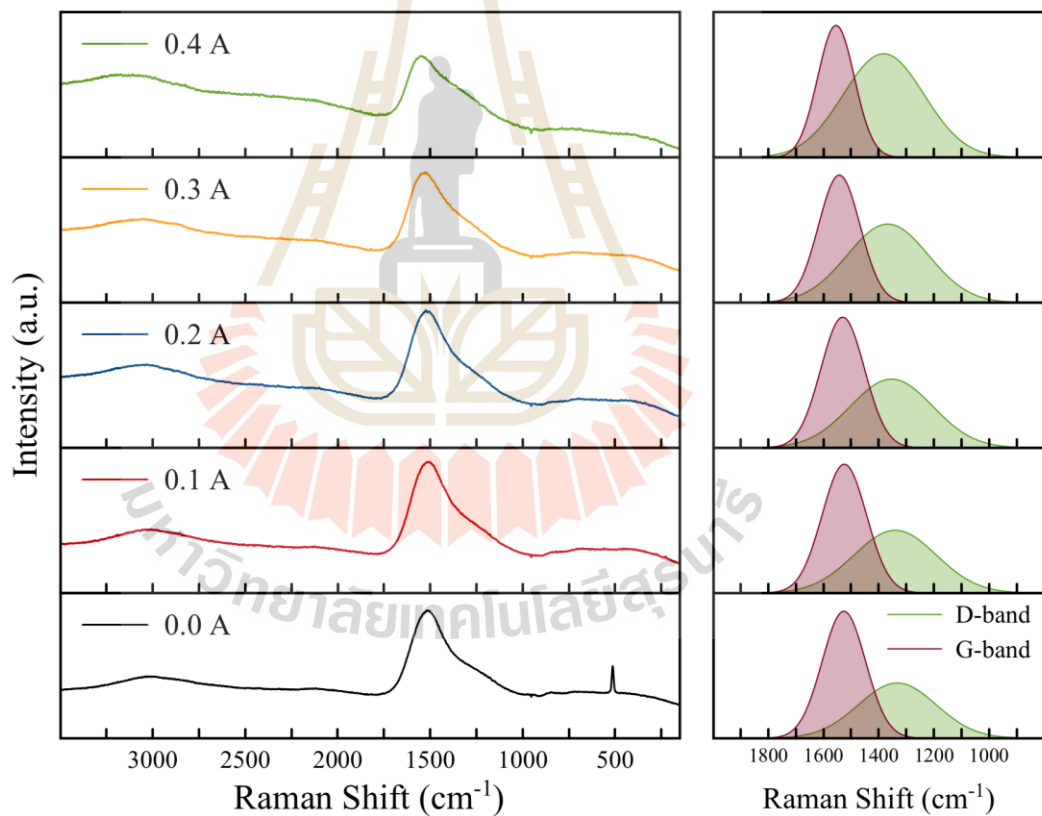


**Figure 62** Raman spectroscopy and fitting of Ti-DLC films.

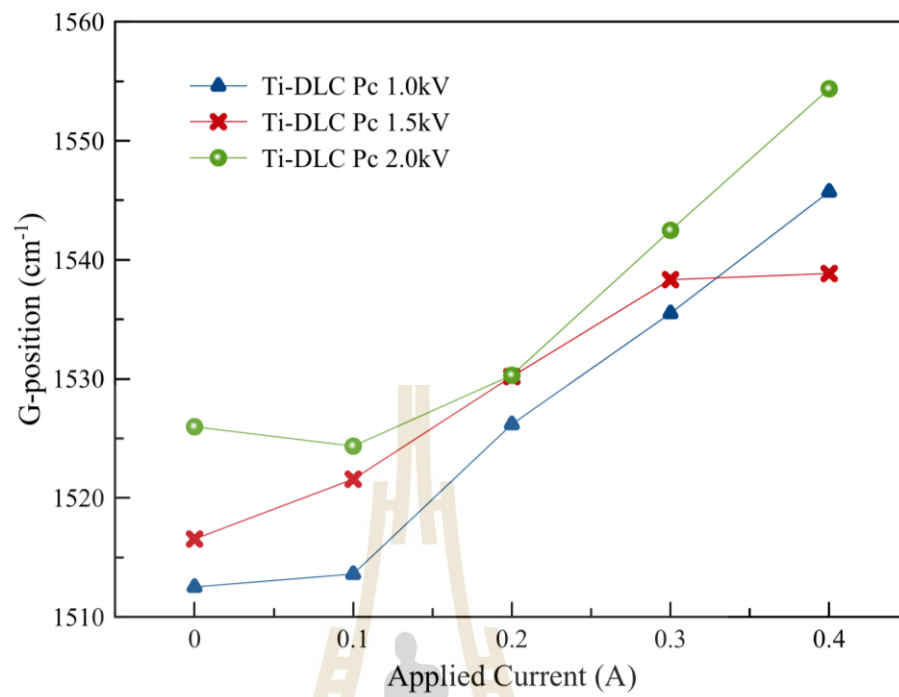


**Figure 63** G-positions of Raman spectroscopy of Ti-DLC films.

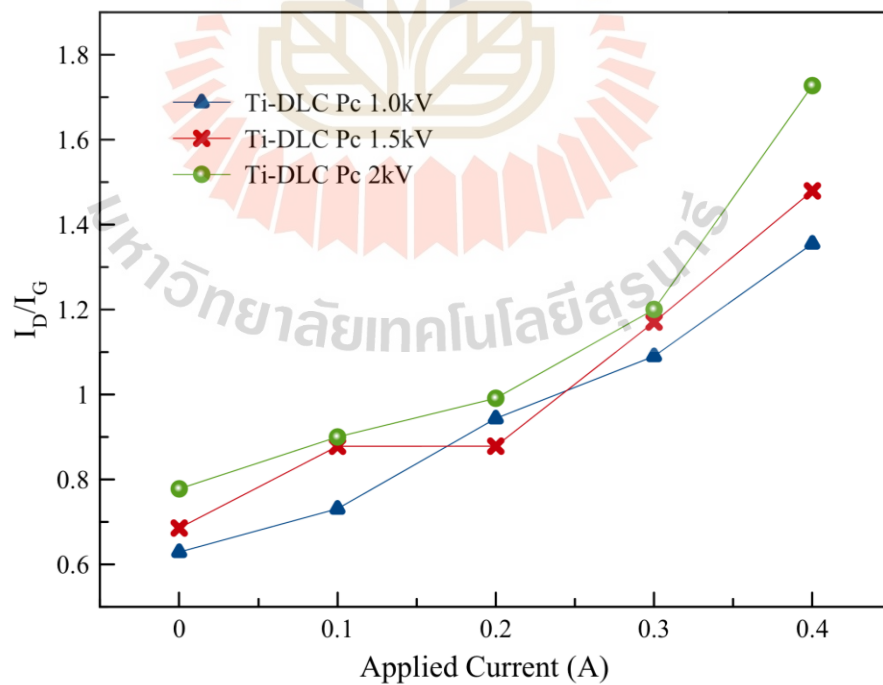


**Figure 64**  $I_D/I_G$  of Raman spectroscopy of Ti-DLC films.

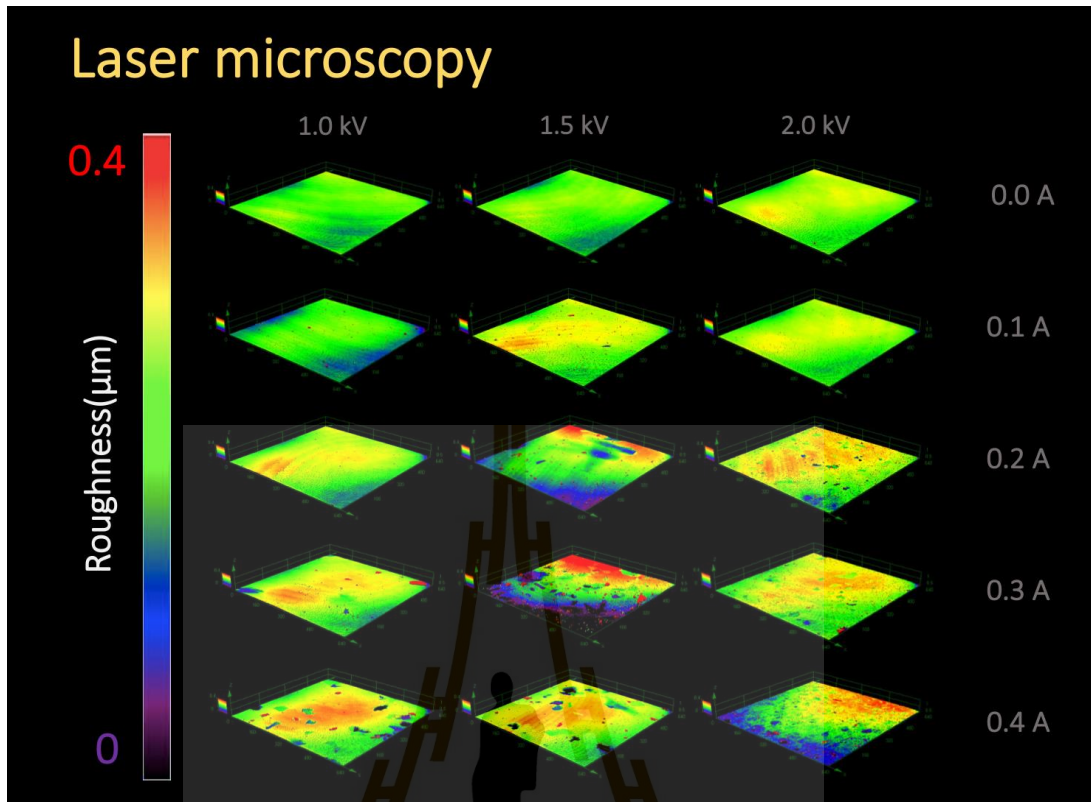


**Figure 65** Morphology profiles measured by Laser microscopy techniques of Ti-DLC.

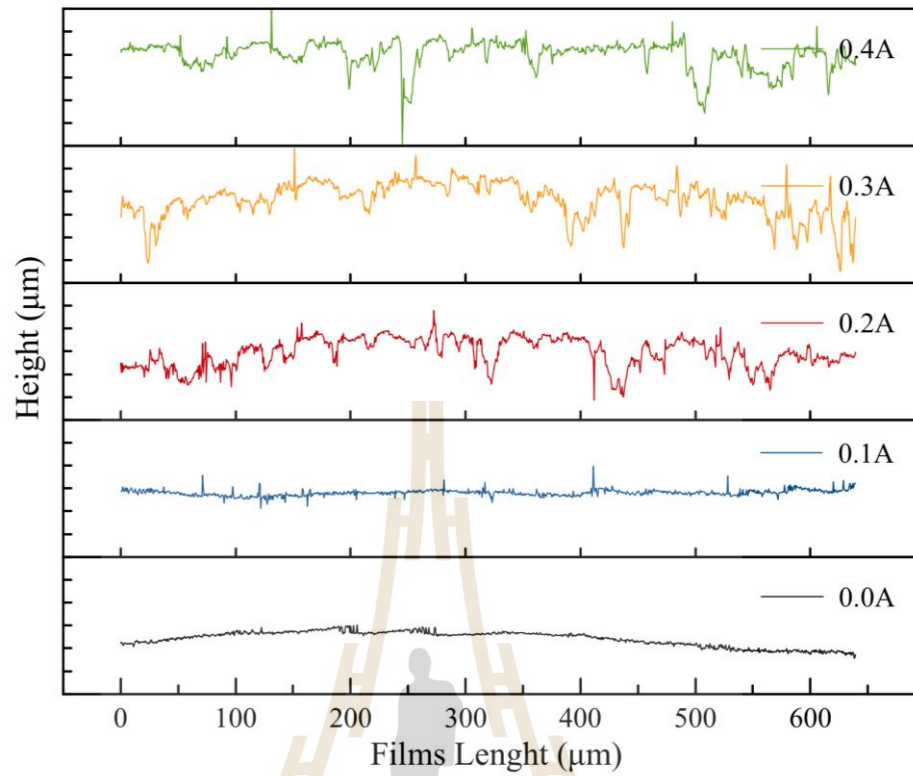


**Figure 66** 2D roughness profiles by Laser microscopy of Ti-DLC.



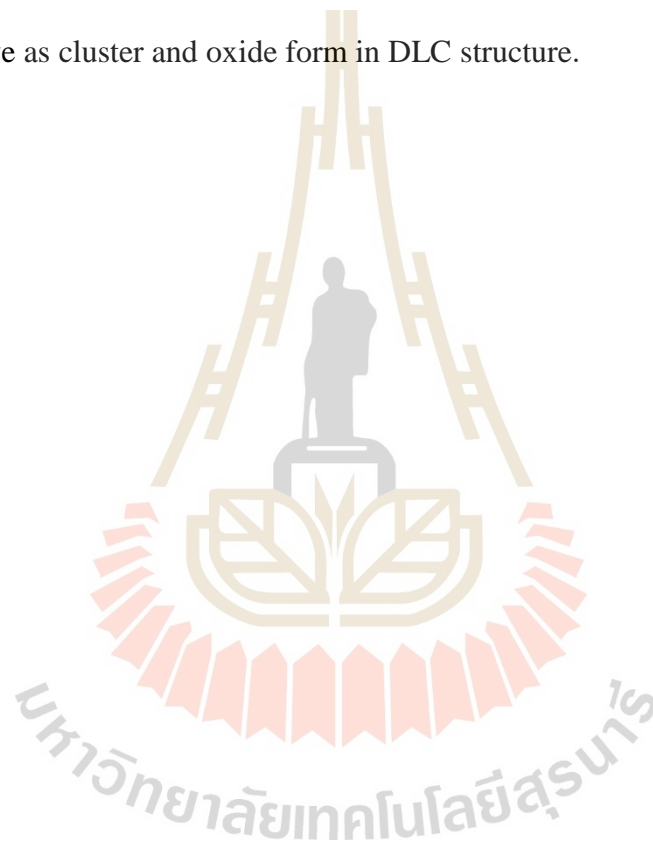
## CHAPTER VI

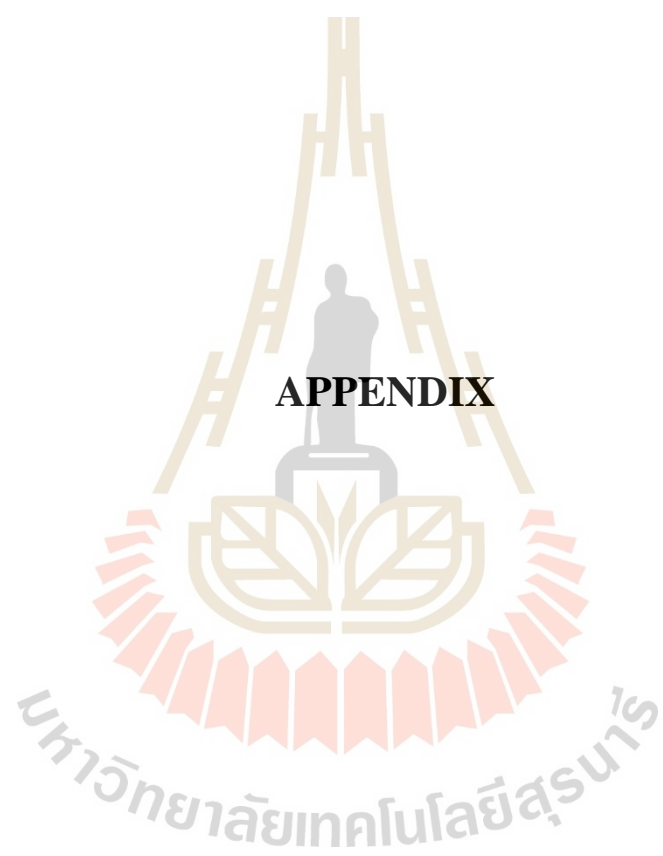
### CONCLUSION

In first, combination of NEXAFS, XPS, Raman spectroscopy were clearly used for the carbon thin films studying. The commercial films which prepared by FCA technique were studied based-on carbon composition. And, ex-situ thermal treatment of DLC films RT-250°C also were characterized. The significant change of  $sp^3/sp^2$  ratio of the DLC films were not observed. It related to good agreement with consistently trending from NEXAFS spectra. It was also supported by Raman spectroscopy study. These results indicate that the thermal treatment below the temperature of 250°C hardly affect to the carbon structure which it can be utilized for applications in the manufacturing of industry systems.

DLC films were prepared using the PECVD process in order to find a satisfactory deposited state. The chemical composition and structure of the films were investigated in relation to RF power and CH<sub>4</sub> gas flow rate. When the RF power was increased, the  $sp^3/sp^2$  ratio decreased. The  $sp^3/sp^2$  ratio tends to rise as the CH<sub>4</sub> gas flow increases. The Raman spectroscopy results reveal that as the RF power increases, the degree of structural disorder in the films increases, whereas the NEXAFS results show that the hydrogen concentration in the films reduces marginally. These findings imply that the RF power and CH<sub>4</sub> gas flow rate have a significant impact on the structure of DLC deposited using the PECVD process.

In this work, Zn doped DLC films were successfully deposited on Si substrate by combinations of CVD and DC sputtering techniques. The influences DC pulse sputtering was studied which higher Zn concentration increase in higher DC pulse generated. Loudness and depth profile distribution also increase in generating sputtering current. Disordering structure also increase in Zn introducing. XAS was successfully used for studying Zn behavior and its local structure on DLC films. Zn mostly behave as cluster and oxide form in DLC structure.





**APPENDIX**

## APPENDIX

Poster presentation at Materials Research Meeting (MRM-2019), Yokohama, Japan

*Materials Research Meeting 2019*  
December 10-14, 2019, Yokohama, Japan

### Synchrotron-based X-ray Absorptions Studies Diamond-like Carbon Films by Ar/CH<sub>4</sub> flow rates Dependence of PECVD Technique

\* Thanun Chunjaemsri<sup>1</sup>, Narong Chanlek<sup>2</sup>, Pinit Kidkhunthod<sup>2</sup>, Hideki Nakajima<sup>2</sup>, Sarayut Tunmee<sup>2</sup>, Rattikorn Yimmirun<sup>3</sup> and Saroj Rujirawat<sup>1</sup>

<sup>1</sup> School of Physics, Institute of Science, and NANOTEC-SUT COE on Advanced Functional Nanomaterials, Suranaree University of Technology, Nakhon Ratchasima, 30000, Thailand

<sup>2</sup> Synchrotron Light Research Institute (Public Organization), 111 University Avenue, Muang District, NakhonRatchasima 30000, Thailand

<sup>3</sup> School of Energy Science and Engineering, Vidyasirimedhi Institute of Science and Technology (VISTEC), Payupnai, Wangchan, Rayong 21210, Thailand

\* [thanunfunny@gmail.com](mailto:thanunfunny@gmail.com)

Keywords DLC films, NEXAFS, Raman spectroscopy, XPS, AFM

Diamond-like carbon (DLC) film properties are known to vary with important factors such as the ratio of sp<sup>3</sup> to sp<sup>2</sup> hybridization, film thickness, and contaminations. DLC coatings can improve tribological properties of the product such as hardness and friction as well as electrical resistivity etc.

Differences of film fabrications affect to a significant variation in DLC properties. Growing conditions are important factors to control significant properties of DLC include the sp<sup>2</sup>/sp<sup>3</sup> ratio, thickness of DLC film, and roughness. DLC thin films were prepared by using Plasma Enhanced Chemical Vapor Deposition (PECVD) on titanium substrate. Various of gases flow rate of Ar and CH<sub>4</sub> have been considered in the preparation of DLC films. The properties of prepared films were examined using X-ray photoelectron spectroscopy (XPS), Raman spectroscopy, atomic force microscopy (AFM) and synchrotron-based Near-edge X-ray absorption fine structure (NEXAFS). The results indicated an increase in both the ID/IG ratio and sp<sup>3</sup>/sp<sup>2</sup> ratio when increasing volume of CH<sub>4</sub> gases. The AFM results indicated that increasing of roughness of different prepared thin films. The behavior of transitions state of electron was investigated by NEXAFS representing to sp<sup>3</sup>/sp<sup>2</sup>. This is consistent with XPS results.

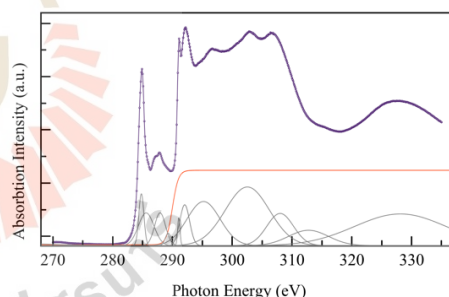


Figure NEXAFS Normalized of C K-edge Spectra

#### Reference

- 1) Li, L., Zhang, H., Zhang, Y., Chu, P. K., Tian, X., Xia, L., and Ma, X., 2002. Mater. Sci. Eng. B 94(1), 95-101.
- 2) Ferrari, A. C., Robertson, J., 2000. Phys. Rev. B. 61(20), 14095.
- 3) Osswald, S., Yushin, G., Mochalin, V., Kucheyev, S. O., and Gogotsi, Y., 2006. J. Am. Chem. Soc. 128(35), 11635-11642.
- 4) Dos Santos, F. C., Harb, S. V., Menu, M. J., Turq, V., Pulcinelli, S. H., Santilli, C. V., Hammer, P., 2015. RSC Adv. 5(129), 106754-106763.
- 5) Zhou, X., Tunmee, S., Suzuki, T., Phothongkam, P., Kanda, K., Komatsu, Saitoh, H. (2017). Relat. Mater. 73, 232-240.

Poster presentation at the 5<sup>th</sup> International Conference on Smart Materials and Nanotechnology (SmartMat@2020), Pattaya, Thailand.

*The 5th International Conference on Smart Materials and Nanotechnology  
(SmartMat@2020)  
1<sup>st</sup>-4<sup>th</sup> December 2020, Garden Cliff Resort & Spa Hotel, Pattaya, Thailand*



[www.smartmat-2020.com](http://www.smartmat-2020.com)

## **Influence of time-dependence and titanium substrate polishing-effect of Diamond-like carbon films by using PECVD.**

T. Chunjaemsri<sup>1,\*</sup>, N. Chanlek<sup>1,2</sup>, P. Kidkhunthod<sup>1,2</sup>, H. Nakajima<sup>2</sup>, S. Tunmee<sup>2</sup>,  
S. Rujirawat<sup>2</sup>, R. Yimnirun<sup>3</sup>, N. Ohtake<sup>4</sup>, and H. Akasaka<sup>4</sup>

<sup>1</sup>*Research Network NANOTEC-SUT on Advanced Nanomaterials and Characterization, School of Physics, Institute of Science, Suranaree University of Technology, Nakhon Ratchasima, Thailand*

<sup>2</sup>*Synchrotron Light Research Institute (Public Organization), Nakhon Ratchasima, Thailand*

<sup>3</sup>*Research Network of NANOTEC-VISTEC on Nanotechnology for Energy, and School of Energy Science and Engineering, Vidyasirimedhi Institute of Science and Technology, Wangchan, Rayong, Thailand*

<sup>4</sup>*Department of Mechanical Engineering Tokyo Institute of Technology, Tokyo, Japan*

*\*Email: Thanunfunny@gmail.com*

### **Abstract**

Diamond-like carbon (DLC) film is one of the interesting materials for coating to many applications. Previous studying, it was applied for high hardness, low wear, low electrical resistivity, and low friction coefficient etc. However, deposition time is important factor for determining the significant properties of the amorphous carbon films. Moreover, substrate treatment is also important factor which control possibility of films forming. In this study, DLC was successfully deposited on titanium substrate. Time variation and substrate polishing were used in order to study prepared carbon films properties. Films characterization were successfully investigated by using Raman spectroscopy and X-ray photo electron spectroscopy (XPS) and synchrotron-based Near-edge X-ray absorption fine structure (NEXAFS). Time variation indicate increase in oxygen contamination with increasing time depositions. The results were confirmed by increasing of  $I_D/I_G$  and C-O area on Raman spectroscopy and XPS, respectively. Moreover, films polishing indicate easier of oxygen contamination and films peeling.

**Keyword:** DLC, Raman spectroscopy, XPS, NEXAFS and PECVD

Poster presentation at the 17<sup>th</sup> International Conference on X-ray Absorption Fine Structure (XAFS 2018), Kraków, Poland.



## Synchrotron-based NEXAFS Analysis of Thermal-treated Diamond-Like Carbon Films

**Thanun Chunjaemsri<sup>1</sup>, Narong Chanlek<sup>2</sup>, Usa Sukkha<sup>3</sup>, Hideki Nakajima<sup>2</sup>, Saroj Rujirawat<sup>1,\*</sup>, Rattikorn Yimnirun<sup>4,5</sup> and Pinit Kidkhunthod<sup>2,\*</sup>**

<sup>1</sup>Research Network NANOTEC-SUT on Advanced Nanomaterials and Characterization, School of Physics, Institute of Science, Suranaree University of Technology, Nakhon Ratchasima, 30000, Thailand

<sup>2</sup>Synchrotron Light Research Institute (Public Organization), 111 University Avenue, Muang District, NakhonRatchasima 30000, Thailand

<sup>3</sup>Department of General Science and Liberal Arts, King Mongkut's Institute of Technology Ladkrabang, Prince of Chumphon Campus, Chumphon 86160, Thailand

<sup>4</sup>School of Energy Science and Engineering, Vidyasirimedhi Institute of Science and Technology (VISTEC), Wangchan, Rayong, 21210, Thailand

<sup>5</sup>Research Network of NANOTEC-VISTEC on Nanotechnology for Energy, Vidyasirimedhi Institute of Science and TECHNOLOGY (VISTEC), Wangchan, Rayong, 21210, Thailand

Recently, diamond-like carbon (DLC) has a great attention and has been widely used in many applications such as hard disk film, drill bit or hard coating materials etc. Different fabrications of DLC films affect to a significant variation in DLC film properties. Important factors controlling significant properties of DLC include the ratio of  $sp^2$  to  $sp^3$  hybridization, thickness of DLC films, contaminations, homogenous of film etc. In this work, the details of thermal-treated DLC analysis based on near-edge X-ray absorption fine structure (NEXAFS) of carbon composition structure such as C=C ( $1s \rightarrow \pi^*$ ,  $\sigma^*$ ) and C-C ( $1s \rightarrow \sigma^*$ ) were reported. Additionally, the Raman spectroscopy was included in this DLC study. The ratio of ID/IG was observed as clearly seen from the D-band and G-band peak positions at  $1350 \text{ cm}^{-1}$  and  $1560 \text{ cm}^{-1}$ , respectively. Moreover, X-ray photoelectron spectroscopy (XPS) technique confirmed the position of graphene at  $284.4 \text{ (} sp^2 \text{)} \text{ eV}$  and diamond position at  $285.1 \text{ (} sp^3 \text{)} \text{ eV}$ , which calculate the ratio of  $sp^2/sp^3$ , respectively.

**Keywords:** DLC films, NEXAFS, Raman spectroscopy, X-ray photoelectron spectroscopy

Online presentation in International Conference on New Diamond and Nano Carbons (NDNC 2020-2021), Kanazawa, Japan.



## Synchrotron-based investigations the local structure of Zn-doped Diamond-like carbon films.

T. Chunjaemsri<sup>1</sup>, N. Chanlek<sup>1,2</sup>, P. Kidkhunthod<sup>1,2</sup>, H. Nakajima<sup>2</sup>, S. Tunmee<sup>2</sup>, S. Rujirawat<sup>1</sup>, R. Yimnirun<sup>3</sup>, N. Ohtake<sup>4</sup>, and H. Akasaka<sup>4</sup>

<sup>1</sup> Research Network NANOTEC-SUT on Advanced Nanomaterials and Characterization, School of Physics, Institute of Science, Suranaree University of Technology, Nakhon Ratchasima, Thailand

<sup>2</sup> Synchrotron Light Research Institute (Public Organization), Nakhon Ratchasima, Thailand

<sup>3</sup> Research Network of NANOTEC-VISTEC on Nanotechnology for Energy, and School of Energy Science and Engineering, Vidyasirimedhi Institute of Science and Technology, Wangchan, Rayong, Thailand

<sup>4</sup> Department of Mechanical Engineering Tokyo Institute of Technology, Tokyo, Japan

[Thanunfunny@gmail.com](mailto:Thanunfunny@gmail.com)

### 1. Introduction

Diamond-like carbon (DLC) film is one of the interesting materials for coating to many applications. Previous studying, it was applied for high hardness, low wear, low electrical resistivity, and low friction coefficient etc. [1]. Zinc is well known for antibacterial in biological application [2]. Moreover, it also was used for solving osteoporosis problem in medical application which improving calcium lose in bone of knee joint. To combine these mechanical properties in DLC and antibacterial in Zn, Zn-doped DLC was studied by a reactive magnetron sputtering. This work focused to analysis of local structure of Zn behavior inside DLC films based on X-ray absorption technique (XAS) and Raman spectroscopy. Near edge X-ray absorption fine structure (NEXAFS) and X-ray photoelectron spectroscopy (XPS) were used as XAS for clarification of carbon evolutions, carbon bonding, and Zn contents.

### 2. Experimental method

In detail of depositions, silicon (100) was used as substrate which cleaned by ethanol and acetone in ultrasonic cleaner for 10 mins. As the reactive sputtering system, DC sputtering and DC pulse plasma CVD systems were combined. DC current for sputtering ( $P_s$ ) and DC pulse bias voltage for CVD ( $P_C$ ) were varied as parameters. The Ar and  $C_2H_2$  were used for cleaning process and deposition process at 20  $cm^3/min$  in flow rate, respectively. Working pressure was controlled at approximately 3 Pa. Depositions time is maintained at 60 min. Chemical composition in the film was investigated by glow-discharge optical emission spectroscopy (GD-OES). Raman spectroscopy was conducted to understand the  $sp^2$  hybridized carbon bonding condition. Ratio of  $sp^3/sp^2$  in carbon bonding system and Zn structure such as oxidations evolutions were investigated by NEXAFS and XPS.

### 3. Results and Discussion

The obtained films thickness were around of 0.6-1.3  $\mu m$ , and depended on the  $P_s$ . The Zn contents in the films increased from 2 to 8 at. %atom with increasing of the  $P_s$  as observed by GD-OES. To estimate the  $sp^2$  bonding network, Raman spectroscopy was conducted as shown in Figure 1. The ratio of  $I_D/I_G$  increased from 1.1 to 4.1 with increasing of the  $P_s$ . Raman spectra indicated disordering structure in  $sp^2$  carbon system in Zn-doped DLC films was increased with introduction of Zn.

### 4. Summary

Zn-doped DLC was deposited from the combined system of the DC magnetron sputtering with DC pulse bias voltage for CVD. Raman data suggested that doped Zn atoms limited to  $sp^2$  carbon clusters

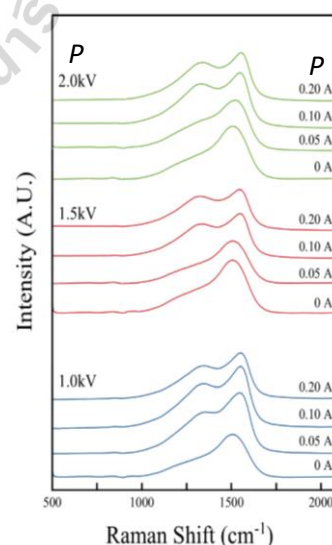


Figure Raman spectra of Zn-doped DLC films; varying  $P_s$  and  $P_C$  as deposition condition.

[1] Xiao et al., 2017, Journal of Materials Research, 32(7), 1231-1238.

[2] Hatada et al., 2019, Coatings, 9(2), 125.

Online presentation in the 21<sup>st</sup> International Union of Materials Research Societies-  
International Conference in Asia (IUMRS-ICA 2020), full online conference



The 21<sup>st</sup> International Union of Materials Research Societies – International Conference in Asia  
(IUMRS-ICA2020), 23-26 February 2021  
The Empress Convention Center, Chiang Mai, Thailand

## Power dependent local structure of HfO<sub>2</sub> films prepared by magnetron sputtering technique

T. Chunjaemsri<sup>a,\*</sup>, E. Chongsereechoen<sup>a,d</sup>, P. Thangdee<sup>a</sup>, N. Chanlek<sup>a,b</sup>, P. Kidkhunthod<sup>a,b</sup>,  
S. Rujirawat<sup>b</sup>, R. Yimnirun<sup>c</sup>, and P. Songsiriritthigul<sup>a,b</sup>

<sup>a</sup>Research Network NANOTEC-SUT on Advanced Nanomaterials and Characterization, School of Physics, Institute of Science, Suranaree University of Technology, Nakhon Ratchasima, Thailand

<sup>b</sup>Synchrotron Light Research Institute (Public Organization), Nakhon Ratchasima, Thailand

<sup>c</sup>Research Network of NANOTEC-VISTEC on Nanotechnology for Energy, and School of Energy Science and Engineering, Vidyasirimedhi Institute of Science and Technology, Wangchan, Rayong, Thailand

<sup>d</sup>Faculty of Science and Technology, Valaya Alongkorn Rajabhat University, Klong Luang, Pathum Thani, Thailand

\*Email: [Thanunfunny@gmail.com](mailto:Thanunfunny@gmail.com)

---

### Abstract

The advantages of HfO<sub>2</sub> film properties are well-known, for example high electrical insulation, high melting point and high dielectric constant. It was widely used for many applications such as optical coating, semiconductor device etc. However, deposition technique and parameter are not clearly studied. In this work, HfO<sub>2</sub> layer was deposited by using RF magnetron sputtering system. The variation of RF power which affects to films properties was systematically studied. In details, trending of films morphology from AFM results was reported that higher surface roughness of the deposited films with increasing sputtering power. XRD results were shown the diffraction patterns of HfO<sub>2</sub> films as majority in amorphous structure. Moreover, the vibrational modes of HfO<sub>2</sub> from Raman spectra indicate the possibility of films structure relating with XRD results. Moreover, hafnium oxidations state and local structure was deeply studied by synchrotron-based X-ray absorption spectroscopy (XAS) using Hf L3-edge of XANES and EXAFS analyses.

*Keywords: HfO<sub>2</sub> films, Raman spectroscopy, Local structure, XAS, AFM*

Poster presentation at ASIAN Conference on X-ray Absorption Spectroscopy (ACXAS 2019) Chiangmai, Thailand.



## Synchrotron-based X-ray Absorptions Studies Diamond-like Carbon Films by Ar/CH<sub>4</sub> flow rates Dependence of PECVD Technique

Thanun Chunjaemsri<sup>1,\*</sup>, Narong Chanlek<sup>2</sup>, Pinit Kidkhunthod<sup>2</sup>, Hideki Nakajima<sup>2</sup>, Rattikorn Yimmirun<sup>3</sup> and Saroj Rujirawat<sup>1</sup>

<sup>1</sup>*School of Physics, Institute of Science, and NANOTEC-SUT COE on Advanced Functional Nanomaterials, Suranaree University of Technology, Nakhon Ratchasima, 30000, Thailand*

<sup>2</sup>*Synchrotron Light Research Institute (Public Organization), 111 University Avenue, Muang District, NakhonRatchasima 30000, Thailand*

<sup>3</sup>*School of Energy Science and Engineering, Vidyasirimedhi Institute of Science and Technology (VISTEC), Payupnai, Wangchan, Rayong 21210, Thailand*

\*Corresponding Author: [thanunfunny@gmail.com](mailto:thanunfunny@gmail.com)

Symposia: Graphene, DLC, and Carbon-based materials

Differences of film fabrications affect to a significant variation in DLC properties. Growing conditions are important factors to control significant properties of DLC include the sp<sup>2</sup>/sp<sup>3</sup> ratio, thickness of DLC film, and roughness. DLC thin films were prepared by using Plasma Enhanced Chemical Vapor Deposition (PECVD) on titanium substrate. Various of gases flow rate of Ar and CH<sub>4</sub> have been considered in the preparation of DLC films. The properties of prepared films were examined using X-ray photoelectron spectroscopy (XPS), Raman spectroscopy, atomic force microscopy (AFM) and synchrotron-based Near-edge X-ray absorption fine structure (NEXAFS). The results indicated an increase in both the I<sub>D</sub>/I<sub>G</sub> ratio and sp<sup>3</sup>/sp<sup>2</sup> ratio when increasing volume of CH<sub>4</sub> gases. The AFM results indicated that increasing of roughness of different prepared thin films. The behavior of transitions state of electron was investigated by NEXAFS representing to sp<sup>3</sup>/sp<sup>2</sup>. This is consistent with XPS results.

**Keywords:** DLC films, NEXAFS, Raman spectroscopy, XPS, AFM

Poster presentation at the 14<sup>th</sup> International conference on materials chemistry (MC14), July 2019, Birmingham, United Kingdom

8-11 July 2019  
Birmingham, UK

**14<sup>th</sup> International conference  
on materials chemistry (MC14)**



## **Synchrotron-based x-ray absorptions studies of novel structure Ti-doped DLC films fabricated by dual-head of magnetron sputtering**

Thanun Chunjaemsri<sup>1</sup>, Narong Chanlek<sup>2</sup>, Saroj Rujirawat<sup>1</sup>, Hideki Nakajima<sup>2</sup>, Rattikorn Yimnirun<sup>3</sup> and Pinit Kidkhunthod<sup>2</sup>

<sup>1</sup>Suranaree University of Technology, Thailand,

<sup>2</sup>Synchrotron Light Research Institute, Thailand and <sup>3</sup>VISTEC Thailand

Differences of film fabrications affect to a significant variation in DLC properties. Growing conditions are important factors to control significant properties of DLC include the  $sp^2/sp^3$  ratio, thickness of DLC film, and roughness. Titanium doped DLC thin films (Ti-DLC) were prepared by using dual-head of magnetron sputtering on titanium substrate. Various flowing rate of argon gases and time variations were used. The properties of prepared films were examined using X-ray photoelectron spectroscopy (XPS), Raman spectroscopy, atomic force microscopy (AFM) and synchrotron-based Near-edge X-ray absorption fine structure (NEXAFS). The results indicated an increase in both the  $I_D/I_G$  ratio and  $sp^3/sp^2$  ratio when increasing volume of argon gases. AFM showed increasing of roughness of different prepared thin films. The behavior of transitions state of electron was investigated by NEXAFS representing to  $sp^3/sp^2$ . This is consistent with XPS results. Moreover, powerful technique of EXAFS showed the local structure of Ti-DLC films measured by fluorescence-mode where the disordered structure of thin films was clearly observed.

Keywords: Ti-DLC, NEXAFS, Raman spectroscopy, XPS, XAS

### **References**

1. Ferrari, A. C., & Robertson, J., 2000. Interpretation of Raman spectra of disordered and amorphous carbon. *Phys. Rev. B*, 61(20), 14095.
2. Schwarz, F. P., Hauser-Gerspach, I., Waltimo, T., & Stritzker, B. (2011). Antibacterial properties of silver containing diamond like carbon coatings produced by ion induced polymer densification. *Surface and Coatings Technology*, 205(20), 4850-4854.
3. Wu, Y., Zhou, S., Zhao, W., & Ouyang, L. (2018). Comparative corrosion resistance properties between (Cu, Ce)-DLC and Ti co-doped (Cu, Ce)/Ti-DLC films prepared via magnetron sputtering method. *Chemical Physics Letters*.
4. C Ji, L., Li, H., Zhao, F., Chen, J., & Zhou, H. (2008). Microstructure and mechanical properties of Mo/DLC nanocomposite films. *Diamond and Related Materials*, 17(11), 1949-1954.
5. Marciano, F. R., Lima-Oliveira, D. A., Da-Silva, N. S., Diniz, A. V., Corat, E. J., & Trava-Airoldi, V. J. (2009). Antibacterial activity of DLC films containing TiO<sub>2</sub> nanoparticles. *Journal of colloid and interface science*, 340(1), 87-92.
6. Amin, M. S., Randeniya, L. K., Bendavid, A., Martin, P. J., & Preston, E. W. (2012). Biomimetic apatite growth from simulated body fluid on various oxide containing DLC thin films. *Diamond and Related Materials*, 21, 42-49.



Contents lists available at ScienceDirect

## Radiation Physics and Chemistry

journal homepage: [www.elsevier.com/locate/radphyschem](http://www.elsevier.com/locate/radphyschem)

## Synchrotron-based NEXAFS analysis of thermal-treated diamond-like carbon films



Thanun Chunjaemsri<sup>a</sup>, Narong Chanlek<sup>a,b</sup>, Usa Sukkha<sup>c</sup>, Hideki Nakajima<sup>b</sup>, Saroj Rujirawat<sup>a</sup>, Rattikorn Yimnirun<sup>d</sup>, Pinit Kidkhunthod<sup>a,b,\*</sup>

<sup>a</sup> Research Network NANOTEC-SUT on Advanced Nanomaterials and Characterization, School of Physics, Institute of Science, Suranaree University of Technology, Nakhon Ratchasima, Thailand

<sup>b</sup> Synchrotron Light Research Institute (Public Organization), Nakhon Ratchasima, Thailand

<sup>c</sup> Department of General Science and Liberal Arts, King Mongkui's Institute of Technology Ladkrabang, Prince of Chumphon Campus, Chumphon, Thailand

<sup>d</sup> Research Network of NANOTEC-VISTEC on Nanotechnology for Energy, School of Energy Science and Engineering, Vidyasirimedhi Institute of Science and Technology, Wangchan, Rayong, Thailand

## ARTICLE INFO

## Keywords:

DLC films  
NEXAFS  
Raman spectroscopy  
X-ray photoelectron spectroscopy

## ABSTRACT

Diamond-like carbon (DLC) film properties are known to vary with important factors such as the ratio of  $sp^3$  to  $sp^2$  hybridization, film thickness, and contaminations. In this work, the carbon bonding contents in DLC thin films, thermal-treated with various temperatures between room temperature to 250 °C, were studied by near-edge X-ray absorption fine structure (NEXAFS), X-ray photoelectron spectroscopy (XPS), and Raman spectroscopy. From NEXAFS measurements, the  $sp^3/sp^2$  ratios of DLC films were found to be unaffected by the thermal treatments. The results indicate that thermal treatment below 250 °C does not affect the carbon bonding contents in DLC thin film.

## 1. Introduction

Recently, diamond-like carbon (DLC) has attracted great attention owing to its outstanding properties suitable for many applications such as hard disk protective film, wear protection, and food processing. DLC coatings can improve tribological properties of the product such as hardness and friction as well as electrical resistivity. The properties of DLC films are strongly related to its structure, especially the ratio of  $sp^3$  to  $sp^2$  hybridizations of carbon bonds (Li et al., 2002). DLC films can be classified using ternary phase diagram of amorphous carbons (Ferrari and Robertson, 2000). DLC film with high  $sp^3/sp^2$  ratio exhibits high hardness and is widely used in protective coating industry. Many spectroscopic techniques such as X-ray photoelectron spectroscopy (XPS), Fourier transform infrared spectroscopy (FTIR), Raman spectroscopy, and nuclear magnetic resonance (NMR) have been utilized to characterize the carbon structure of DLC films (Zhou et al., 2017). XPS can provide information about chemical compositions and  $sp^3/sp^2$  ratio of the DLC films. Since, the  $sp^3/sp^2$  ratio from XPS is estimated from the C1s peak, it is therefore strongly dependent on fitting procedure (Dos Santos et al., 2015). Raman spectroscopy can give information about the graphite and disorder structure of DLC films, using D-band and G-

band of the Raman spectrum. The ratio of D-band and G-band intensities,  $I_D/I_G$ , is correlated to the  $sp^3/sp^2$  ratio (Ferrari and Robertson, 2000). Recently, near edge X-ray absorption fine structure (NEXAFS) has been used to study the structure of DLC films (Osswald et al., 2006). NEXAFS is a powerful technique which can determine specific bonds of carbon (e.g., C=C, C-C, and C-O bonds) and also  $sp^3/sp^2$  ratio of DLC films (Latham et al., 2017; Hemraj-Benny et al., 2006). In some industrial applications, heat treatment is usually applied to the DLC coated materials during the production process. The heat treatment with too high temperature may alter the carbon bonding content in DLC resulting in nondurable films. Therefore, it is of interest to know if the DLC film carbon bonding content is affected by thermal treatment.

In this work, synchrotron-based NEXAFS is used to study thermal-treated DLC films prepared by filtered cathodic arc (FCA). The ratio of  $sp^3/sp^2$  is used to evaluate the change of DLC film carbon bonding content after temperature treatment. XPS and Raman spectroscopy are also performed to compare with NEXAFS.

\* Corresponding author. Research Network NANOTEC-SUT on Advanced Nanomaterials and Characterization, School of Physics, Institute of Science, Suranaree University of Technology, Nakhon Ratchasima, Thailand  
E-mail address: [pinit@slri.or.th](mailto:pinit@slri.or.th) (P. Kidkhunthod).

<https://doi.org/10.1016/j.radphyschem.2019.04.021>

Received 26 September 2018; Received in revised form 7 April 2019; Accepted 12 April 2019

Available online 13 April 2019

0969-806X/ © 2019 Elsevier Ltd. All rights reserved.

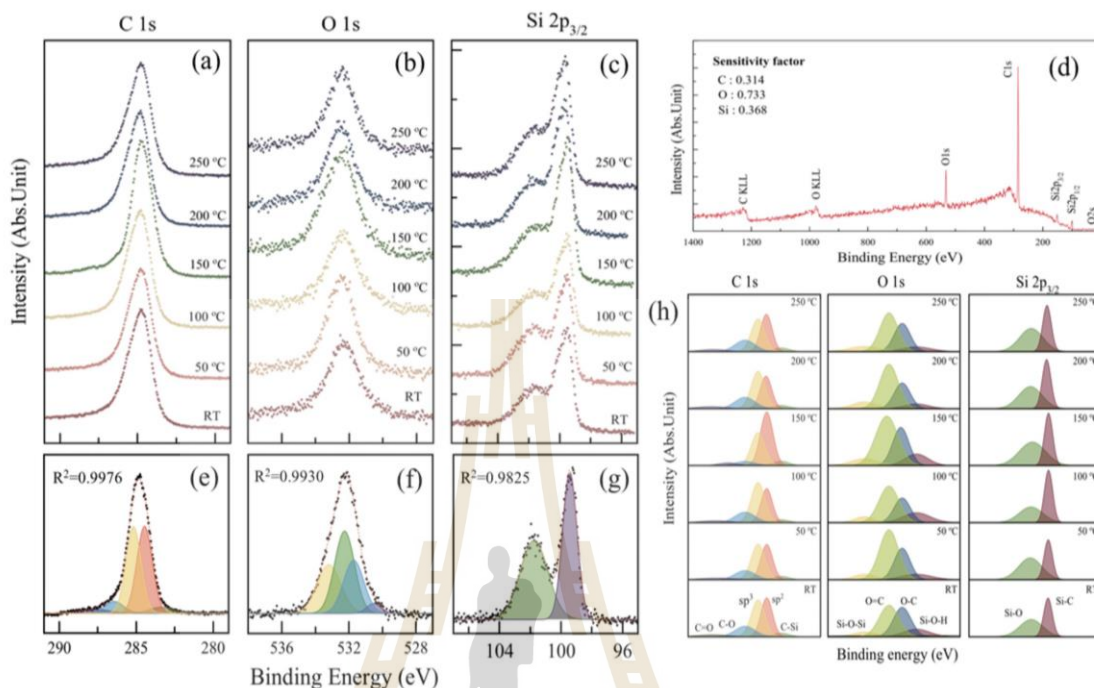


Fig. 1. High resolution XPS spectra of (a) C1s, (b) O1s, (c) Si2p peaks. (d) XPS survey spectra of the DLC film at RT. Graph fitting of (e) C1s, (f) O1, (g) Si2p, and (h) all peaks deconvolutions.

Table 1  
Characterized results of DLC films.

	HOPG	RT	Thermal-treated DLC films (°C)				
			50	100	150	200	250
<b>XPS</b>							
C-sp <sup>3</sup> area, %	–	34.89	41.10	41.66	34.16	37.42	32.38
C-sp <sup>2</sup> area, %	–	38.73	35.47	32.65	51.63	35.22	38.21
C-O area, %	–	17.60	15.09	17.39	6.05	18.35	19.87
C=O area, %	–	4.34	4.18	4.71	3.23	5.25	4.86
C-Si area, %	–	4.44	4.17	3.59	4.92	3.76	4.67
sp <sup>3</sup> /sp <sup>2</sup>	–	0.90	1.16	1.28	0.66	1.06	0.85
<b>NEXAFS</b>							
sp <sup>3</sup> -fraction, %	4.46	50.47	51.97	48.89	51.73	49.23	50.59
sp <sup>2</sup> -fraction, %	95.54	49.53	48.03	51.11	48.27	50.77	49.41
sp <sup>3</sup> /sp <sup>2</sup>	0.05	1.02	1.08	0.96	1.07	0.97	1.02
<b>Raman Spectroscopy</b>							
D-band area, %	–	27.11	25.52	20.72	29.50	33.76	27.48
G-band area, %	–	72.89	74.48	79.28	70.50	66.24	72.52
I <sub>D</sub> /I <sub>G</sub>	–	0.37	0.34	0.26	0.42	0.51	0.38

## 2. Experiment and characterizations

### 2.1. DLC films preparation and heat treatment

DLC thin films were deposited by filtered cathodic arc (FCA) on cleaned Si(100) substrates without removing of oxide from silicon surface. The thickness of DLC films, deposited in same batch, was estimated to be 30 Å approximately. To study the effect of heat treatment, five samples were heated in air from room temperature to 50, 100, 150, 200, and 250 °C using a temperature ramping rate of 10 °C/min. Each sample was hold at corresponding temperature for 1 h and then cooled down to room temperature using the cooling rate of 5 °C/min.

### 2.2. XPS measurements

XPS measurements were performed using a PHI5000 Versa probe II (ULVAC-PHI, Japan) equipped with a hemispherical electron energy analyzer at the SUT-NANOTEC-SLRI joint research facility, Synchrotron Light Research Institute (SLRI). A monochromatic Al K $\alpha$  X-ray gun (1486.6 eV) was used as the excitation source. The XPS survey scans were collected from 0 to 1400 eV with pass energy 117.40 eV and energy step 1.0 eV. High resolutions XPS spectra were collected with pass energy 46.95 eV and energy step 0.05 eV for probing elements of interested. The XPS spectra were analyzed by PHI Multipak XPS software. The binding energy of all XPS spectra were calibrated with the C1s peak at 284.8 eV. The Shirley background subtraction and combinations of Gaussian-Lorentzian line shape were applied for peak deconvolution.

### 2.3. NEXAFS measurements

The NEXAFS experiment was carried out at Beamline 3.2Ua Synchrotron Light Research Institute (SLRI), Thailand. The NEXAFS measurement were performed by partial electron yield mode (PEY). The carbon K-edge spectra of the DLC films were collected in an energy range of 270–330 eV with energy step 0.1 eV. The position of carbon K-edge was calibrated by aligning the  $\pi^*$  resonance peak of highly oriented graphite (HOPG) to 284.8 eV pyrolytic.

### 2.4. Raman measurements

Raman spectra were collected by a wavelength dispersive Raman microscope (SENTERRA, Bruker) using 512 nm laser excitation, 50 mW power, and 25  $\mu\text{m}$   $\times$  1000  $\mu\text{m}$  slit. The spectra were measured in 50–2700  $\text{cm}^{-1}$  range with Raman shift 0.5  $\text{cm}^{-1}$  resolution.

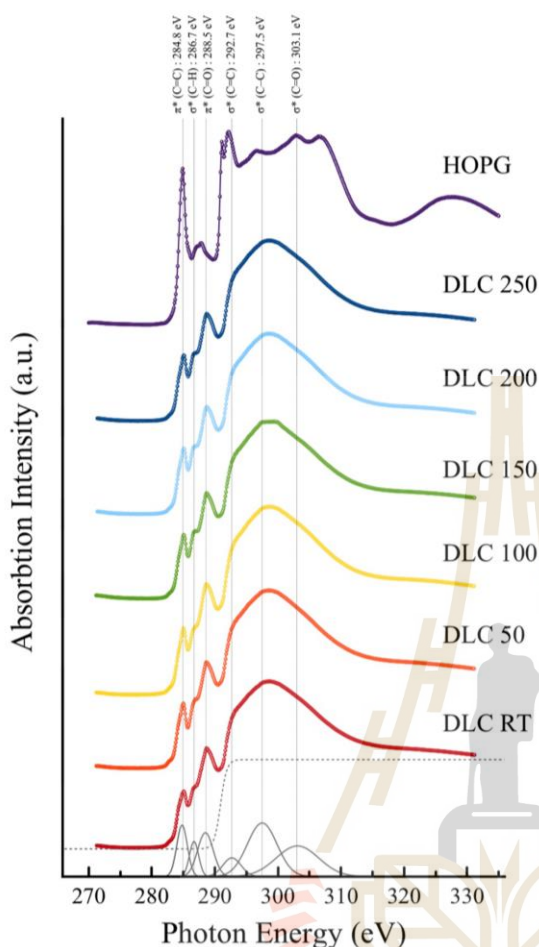


Fig. 2. NEXAFS carbon K-edge spectra of the DLC thermal treated films and HOPG.

### 3. Results and discussion

#### 3.1. XPS result

XPS measurement were carefully perform to analyze chemical composition of the DLC film. The XPS survey spectrum of the DLC film at room temperature (RT) in Fig. 1(d) shows the presence of carbon, silicon and oxygen. High resolutions XPS spectra of the C1s, O1s, Si2p peaks are shown in Fig. 1(a–c). The Si peaks in the survey spectrum are from the Si substrate. The Si2p peak in Fig. 1(g) can be fitted into two main peaks at the binding energies of 99.4 eV and 101.7 eV corresponding to Si–O and Si–C, respectively (Arezzo et al., 1994; Takagaki et al., 1992). The O peaks are attributed to oxide from the Si substrate and oxygen contaminations in the DLC films during preparation. The observed oxygen contaminations in the DLC film has been report previously (Dos Santos et al., 2015). The O1s in Fig. 1(f) can be fitted into four main peaks at the binding energies of 533.2 eV, 530.5 eV, 532.3 eV, and 531.7 eV indicating the presence of Si–O–Si, H–Si–O, O=C and O–C peaks, respectively (Paparazzo, 1987; Dos Santos et al., 2015). High resolutions spectrum of C1s in Fig. 1(e) can be deconvoluted into five different Gaussian peaks, centered at the binding energies of 283.4 eV, 286.4 eV, 287.7 eV, 285.1 eV, and 284.4 eV attributing to C–Si, C–O, C=O, C-sp<sup>3</sup> and C-sp<sup>2</sup>, respectively (Bozack, 1994; Ahmed et al., 2013; Bociaga et al., 2015; Marcondes et al., 2004). FWHM of the deconvoluted sp<sup>3</sup> and sp<sup>2</sup> C1s peaks are set at 0.58–0.6 eV with ΔE of 0.7 eV. All peak deconvolutions were shown in Fig. 1(h). The relative atomic concentrations of carbon species calculated from the XPS spectra are reported in Table 1.

#### 3.2. NEXAFS result

The NEXAFS measurements were employed to study the carbon bonding structure of the DLC films in detail. The stacked plot of carbon K-edge spectra in range 270–330 eV of the DLC films is shown in Fig. 2. The observed carbon K-edge spectra exhibit features of DLC film as reported previously (Cody et al., 1998). To identify the chemical states and structure of carbon, the carbon K-edge spectra were fitted following the literature (Singh et al., 2014; Watts et al., 2006), and compared with the carbon K-edge spectrum of HOPG. The first observed peak and the shoulder peak at the energies of 284.8 eV and 286.7 eV indicate the transitions 1s→π\* (C=C) and 1s→σ\*(C–H), respectively. The transitions 1s→π\* and 1s→σ\* at the energies 288.5 eV and 303.1 eV show the presence of (C=O) (Latham et al., 2017), confirming the oxygen

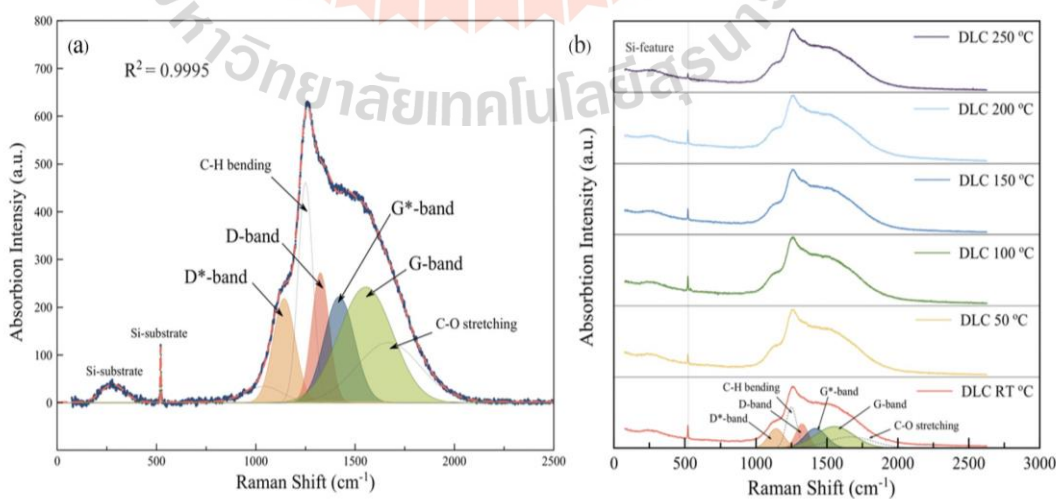


Fig. 3. Fitting of Raman spectra from (a) DLC film at RT and, (b) thermal treated DLC films.

contamination in DLC film. This result is in good agreement with XPS result. The observed peaks at the energies of 292.7 eV and 297.5 eV reveal the transitions  $1s \rightarrow \sigma^*$  (C=C) and  $1s \rightarrow \sigma^*$  (C-C), respectively. The  $sp^2$  fractions of the DLC films were calculated from the following equation (Jia et al., 2016; Osswald et al., 2006).

$$f_{sp^2} = \frac{I_{DLC}^{\pi^*} / I_{DLC}^{total}}{I_{HOPG}^{\pi^*} / I_{HOPG}^{total}} \quad (1)$$

where the superscript " $\pi^*$ " denotes the peak  $1s \rightarrow \pi^*$  C=C bonds, and the superscript "total" represents the integration photon energy over range 280–320 eV. The subscripts "DLC" and "HOPG" represents the peaks within DLC films and the reference HOPG, respectively. The ratio of  $sp^3/sp^2$  of DLC films are found to be 0.97–1.08 as reported in Table 1. From NEXAFS data, it is observed that heat treatment does not significantly change the chemical compositions and  $sp^3/sp^2$  ratio of DLC films.

### 3.3. Raman result

In addition, Raman spectroscopy was also employed. Fig. 3(a) shows a wide broad peak DLC Raman spectrum in the range of 50–2250  $cm^{-1}$  from RT film. The Raman spectrum reveals the D-band and G-band at  $\sim 1350 cm^{-1}$  and  $\sim 1560 cm^{-1}$ , respectively, which are typically observed in carbon structure (Ferrari and Robertson, 2000; Robertson, 2002; Ribeiro-Soares et al., 2013). In addition, D\* band and G\* band were detected at  $\sim 1100-1200 cm^{-1}$  and  $\sim 1380-1420 cm^{-1}$ , respectively. These bands can be assigned to C=C stretching and C-H wagging modes in aromatic ring, respectively (Wu et al., 2002; Francioso et al., 2005). The additional peaks at  $\sim 1200-1300 cm^{-1}$  and  $\sim 1600-1800 cm^{-1}$  represents C-H bending (Francioso et al., 2005) and C-O stretching vibration (Xing et al., 2016) respectively. The Raman spectra of the thermal treated DLC films at different temperatures exhibit similar features as shown in Fig. 3(b). This implies that the carbon bonding contents of those films are similar.

## 4. Conclusion

The effect of thermal treatment between RT to 250 °C on the carbon bonding contents of the DLC films was studied by NEXAFS, XPS, Raman spectroscopy. From NEXAFS data, significant change of  $sp^3/sp^2$  ratio from DLC films with different thermal treatments were not observed. This implies that the thermal treatment below 250 °C does not affect the carbon bonding content of DLC film. The result is applicable to the development of suitable thermal treatment process for DLC thin film for the industry.

## Acknowledgments

The authors would like to acknowledge the NANOTEC, NSTDA, Ministry of Science and Technology, Thailand, through its program of Research Network NANOTEC for partial financial support and the Synchrotron Light Research Institute (Public Organization), Thailand for XPS and NEXAFS experiments at BL-5.3 and BL-3.2Ua. T.

Chunjaemsri would like to acknowledge DPST program for Ph.D. scholarship.

## References

- Ahmed, M.H., Byrne, J.A., McLaughlin, J., Ahmed, W., 2013. Study of human serum albumin adsorption and conformational change on DLC and silicon doped DLC using XPS and FTIR spectroscopy. *J. Biomaterials Nanobiotechnol.* 4 (02), 194.
- Arezzo, F., Severini, E., Zacchetti, N., 1994. An XPS study of diamond films grown on differently pretreated silicon substrates. *Surf. Interface Anal.* 22 (1-12), 218–223.
- Bociaga, D., Komorowski, P., Batory, D., Szymanski, W., Olejnik, A., Jastrzebski, K., Jakubowski, W., 2015. Silver-doped nanocomposite carbon coatings (Ag-DLC) for biomedical applications-physicochemical and biological evaluation. *Appl. Surf. Sci.* 355, 388–397.
- Bozack, M.J., 1994. Single crystal 6H-SiC (0001) by XPS. *Surf. Sci. Spectra* 3 (1), 82–85.
- Cody, G.D., Ade, H., Wirick, S., Mitchell, G.D., Davis, A., 1998. Determination of chemical-structural changes in vitrinite accompanying luminescence alteration using C-NEXAFS analysis. *Org. Geochem.* 28 (7-8), 441–455.
- Dos Santos, F.C., Harb, S.V., Memu, M.J., Turq, V., Pulcinelli, S.H., Santilli, C.V., Hammer, P., 2015. On the structure of high performance anticorrosive PMMA-siloxane-silica hybrid coatings. *RSC Adv.* 5 (129), 106754–106763.
- Ferrari, A.C., Robertson, J., 2000. Interpretation of Raman spectra of disordered and amorphous carbon. *Phys. Rev. B* 61 (20), 14095.
- Francioso, O., Sánchez-Cortés, S., Corrado, G., Gioacchini, P., Ciavatta, C., 2005. Characterization of soil organic carbon in long-term amendment trials. *Spectrosc. Lett.* 38 (3), 283–291.
- Hemraj-Benny, T., Banerjee, S., Sambasivan, S., Balasubramanian, M., Fischer, D.A., Eres, G., Misewich, J.A., 2006. Near-edge X-ray absorption fine structure spectroscopy as a tool for investigating nanomaterials. *Small* 2 (1), 26–35.
- Jia, L., Sugiura, H., Kondo, H., Takeda, K., Ishikawa, K., Oda, O., Hori, M., 2016. Effect of gas residence time on near-edge X-ray absorption fine structures of hydrogenated amorphous carbon films grown by plasma-enhanced chemical vapor deposition. *Jpn. J. Appl. Phys.* 55 (4), 040305.
- Latham, K.G., Simone, M.I., Dose, W.M., Allen, J.A., Donne, S.W., 2017. Synchrotron based NEXAFS study on nitrogen doped hydrothermal carbon: insights into surface functionalities and formation mechanisms. *Carbon* 114, 566–578.
- Li, L., Zhang, H., Zhang, Y., Chu, P.K., Tian, X., Xia, L., Ma, X., 2002. Structural analysis of arc deposited diamond-like carbon films by Raman and X-ray photoelectron spectroscopy. *Mater. Sci. Eng. B* 94 (1), 95–101.
- Marcondes, A.R., Ueda, M., Kostov, K.G., Beloto, A.F., Leite, N.F., Gomes, G.F., Lepienski, C.M., 2004. Improvements of ultra-high molecular weight polyethylene mechanical properties by nitrogen plasma immersion ion implantation. *Braz. J. Phys.* 34 (4B), 1667–1672.
- Osswald, S., Yushin, G., Mochalin, V., Kucheyev, S.O., Gogotsi, Y., 2006. Control of  $sp^2/sp^3$  carbon ratio and surface chemistry of nanodiamond powders by selective oxidation in air. *J. Am. Chem. Soc.* 128 (35), 11635–11642.
- Paparazzo, E., 1987. XPS and auger spectroscopy studies on mixtures of the oxides  $SiO_2$ ,  $Al_2O_3$ ,  $Fe_2O_3$  and  $Cr_2O_3$ . *Electron Spectrosc. Relat. Phenom.* 43 (2), 97–112.
- Ribeiro-Soares, J., Cançado, L.G., Falcão, N.P.S., Martins Ferreira, E.H., Achete, C.A., Jorio, A., 2013. The use of Raman spectroscopy to characterize the carbon materials found in Amazonian anthrosoils. *Raman Spectrosc.* 44 (2), 283–289.
- Robertson, J., 2002. Diamond-like amorphous carbon. *Mater. Sci. Eng.* 37 (4-6), 129–281.
- Singh, B., Fang, Y., Cowie, B.C., Thomsen, L., 2014. NEXAFS and XPS characterisation of carbon functional groups of fresh and aged biochars. *Org. Geochem.* 77, 1–10.
- Takagaki, T., Igari, Y., Takaoka, T., Kusunoki, I., 1992. XPS study of the reaction of the Si (100) surface with a C<sub>2</sub>H<sub>4</sub> beam. *Appl. Surf. Sci.* 92, 287–290.
- Watts, B., Thomsen, L., Dastoor, P.C., 2006. Methods in carbon K-edge NEXAFS: experiment and analysis. *J. Electron. Spectrosc. Relat.* 151 (2), 105–120.
- Wu, Y.H., Hsu, C.M., Chia, C.T., Lin, I.N., Cheng, C.L., 2002. Field emission and Raman spectroscopy studies of atomic hydrogen etching on boron and nitrogen doped DLC films. *Diamond Relat. Mater.* 11 (3-6), 804–808.
- Xing, Z., Du, C., Zeng, Y., Ma, F., Zhou, J., 2016. Characterizing typical farmland soils in China using Raman spectroscopy. *Geoderma* 268, 147–155.
- Zhou, X., Tunmee, S., Suzuki, T., Phothongkam, P., Kanda, K., Komatsu, K., et al., 2017. Quantitative NEXAFS and solid-state NMR studies of  $sp^3/(sp^2+sp^3)$  ratio in the hydrogenated DLC films. *Diam. Relat. Mater.* 73, 232–240.



## Influence of RF power and CH<sub>4</sub> flow rate on properties of diamond-like carbon films deposited by PECVD technique

Thanun Chunjamsri <sup>a</sup>, Ekachai Chongserecharoen <sup>a, d</sup>, Narong Chanlek <sup>a, b</sup>, Pinit Kidkhunthod <sup>a, b</sup>, Hideki Nakajima <sup>b</sup>, Sarayut Tunmee <sup>b</sup>, Rattikorn Yimnirun <sup>c</sup>, Saroj Rujirawat <sup>a, b</sup>

<sup>a</sup> Research Network NANOTEC-SUT on Advanced Nanomaterials and Characterization, School of Physics, Institute of Science, Suranaree University of Technology, Nakhon Ratchasima, Thailand

<sup>b</sup> Synchrotron Light Research Institute (Public Organization), Nakhon Ratchasima, Thailand

<sup>c</sup> Research Network of NANOTEC-VISTEC on Nanotechnology for Energy and School of Energy Science and Engineering, Vidyasirimedhi Institute of Science and Technology, Wangchan, Rayong, Thailand

<sup>d</sup> Faculty of Science and Technology, Valaya Alongkorn Rajabhat University, Klong Luang, Pathumthani, Thailand

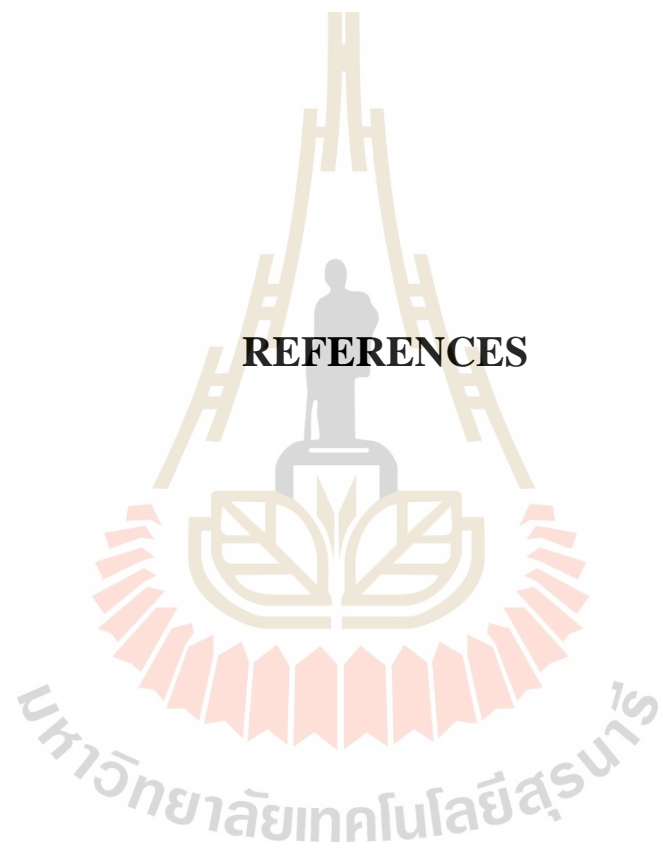
### Abstract

In this work, Diamond like carbon (DLC) films were deposited on titanium substrate by plasma enhanced chemical vapor deposition (PECVD) technique. The influences of RF power and CH<sub>4</sub> gas flow rate on the properties of the DLC films were studied using X-ray photoelectron spectroscopy (XPS), Raman spectroscopy and synchrotron-based near-edge X-ray absorption fine structure (NEXAFS) spectroscopy. The results show that the  $sp^3/sp^2$  ratio decreases, while the  $I_D/I_G$  increases when RF power increases. The  $sp^3/sp^2$  ratio increases with CH<sub>4</sub> flow rate.

### Keywords

PECVD; DLC films; NEXAFS; Raman spectroscopy; XPS

## REFERENCES



## REFERENCES

- Adelhelm, C., Balden, M., Kost, F., Herrmann, A., and Lindig, S. (2008). Thermal induced structural changes of aC and aC: Ti films analyzed by NEXAFS and XPS. **Journal of Physics: Conference Series**. 100(6): 062033. IOP Publishing.
- Ahmed, M. H., Byrne, J. A., McLaughlin, J., Ahmed, W., (2013). Study of human serum albumin adsorption and conformational change on DLC and silicon doped DLC using XPS and FTIR spectroscopy. **Journal of Biomate. Nanobiotech**. 4(2): 194.
- Aisenberg, S., and Chabot, R. (1971). Ion - beam deposition of thin films of diamondlike carbon. **Journal of Applied Physics**. 42(7): 2953-2958.
- Allison, L. E. (1960). Wet-combustion apparatus and procedure for organic and inorganic carbon in soil. **Soil Science Society of America Journal**. 24(1): 36-40.
- Ammar, M. R., Galy, N., Rouzaud, J. N., Toulhoat, N., Vaudey, C. E., Simon, P., Moncoffre, N. (2015). Characterizing various types of defects in nuclear graphite using Raman scattering: heat treatment, ion irradiation and polishing. **Carbon**. 95: 364-373.
- Arezzo, F., Severini, E., and Zacchetti, N. (1994). An XPS study of diamond films grown on differently pretreated silicon substrates. **Surface and Interface Analysis**. 22(1-12): 218-223.
- Azóroff, L. V. (1963). Theory of extended fine structure of x-ray absorption edges. **Reviews of Modern Physics**. 35(4): 1012.

- Bewilogua, K., Hofmann, D. (2014). History of diamond-like carbon films—from first experiments to worldwide applications. **Surface and Coatings Technology**. 242: 214-225.
- Blackburn, J. L., Ferguson, A. J., Cho, C., and Grunlan, J. C. (2018). Carbon - nanotube -based thermoelectric materials and devices. **Advanced Materials**. 30(11): 1704386.
- Bociaga, D., Komorowski, P., Batory, D., Szymanski, W., Olejnik, A., Jastrzebski, K., and Jakubowski, W. (2015). Silver-doped nanocomposite carbon coatings (Ag-DLC) for biomedical applications – physiochemical and biological evaluation. **Applied Surface Science**. 355: 388-397.
- Bozack, M. J. (1994). Single Crystal 6H-SiC 0001 by XPS. **Surface Science Spectra**. 3(1): 82-85.
- Bryce, D. L., and Sward, G. D. (2006). Solid - state NMR spectroscopy of the quadrupolar halogens: chlorine- 35/ 37, bromine- 79/ 81, and iodine- 127. **Magnetic Resonance in Chemistry**. 44(4): 409-450.
- Catena, A., Agnello, S., Cannas, M., Gelardi, F. M., Wehner, S., and Fischer, C. B. (2017). Evolution of the sp<sup>2</sup> content and revealed multilayer growth of amorphous hydrogenated carbon (aC : H) films on selected thermoplastic materials. **Carbon**. 117: 351-359.
- Čech, J., Haušild, P., Kovářik, O., and Materna, A. (2016). Examination of Berkovich indenter tip bluntness. **Materials and Design**. 109: 347-353.
- Chung, S. C., Lin, A. S., Chang, J. R., and Shih, H. C. (2000). EXAFS study of atmospheric corrosion products on zinc at the initial stage. **Corrosion Science**. 42(9): 1599-1610.

- Chunjaemsri, T., Chanlek, N., Sukkha, U., Nakajima, H., Rujirawat, S., Yimnirun, R., and Kidkhunthod, P. (2020). Synchrotron-based NEXAFS analysis of thermal-treated diamond-like carbon films. **Radiation Physics and Chemistry**. 175: 108271.
- Chunjaemsri, T., Chongserecharoen, E., Chanlek, N., Kidkhunthod, P., Nakajima, H., Tunmee, S., and Rujirawat, S. (2020). Influence of RF power and CH<sub>4</sub> flow rate on properties of diamond-like carbon films deposited by PECVD technique. **Radiation Physics and Chemistry**. 176: 109073.
- Cody, G. D., Ade, H., Wirick, S., Mitchell, G. D., and Davis, A. (1998). Determination of chemical-structural changes in vitrinite accompanying luminescence alteration using C-NEXAFS analysis. *Org. Geochem.* 28(7-8): 441-455.
- Dhandapani, V. S., Kang, K. M., Seo, K. J., Kim, C. L., and Kim, D. E. (2019). Enhancement of tribological properties of DLC by incorporation of amorphous titanium using magnetron sputtering process. **Ceramics International**. 45(9): 11971-11981.
- Dos Santos, F. C., Harb, S. V., Menu, M. J., Turq, V., Pulcinelli, S. H., Santilli, C. V., Hammer, P. (2015). On the structure of high performance anticorrosive PMMA–siloxane–silica hybrid coatings. **RSC Advances**. 5(129): 106754-106763.
- Dwivedi, N., Kumar, S., Malik, H. K., Rauthan, C. M. S., and Panwar, O. S. (2011). Correlation of sp<sup>3</sup> and sp<sup>2</sup> fraction of carbon with electrical, optical and nano-mechanical properties of argon-diluted diamond-like carbon films. **Applied Surface Science**. 257(15): 6804-6810.

- Elzwawi, S., Kim, H. S., Heinhold, R., Lynam, M., Turner, G., Partridge, J. G., and Allen, M. W. (2012). Device quality ZnO grown using a filtered cathodic vacuum arc. **Physica B: Condensed Matter**. 407(15): 2903-2906.
- Ferrari, A. C., and Robertson, J. (2000). Interpretation of Raman spectra of disordered and amorphous carbon. **Physical Review Research**. B. 61(20): 14095.
- Fiaschi, G., Rota, A., Ballestrazzi, A., Marchetto, D., Vezzalini, E., and Valeri, S. (2019). A chemical, mechanical, and tribological analysis of DLC coatings deposited by magnetron sputtering. **Lubricants**. 7(4): 38.
- Filik, J. (2005). Raman spectroscopy: a simple, non-destructive way to characterise diamond and diamond-like materials. **Spectroscopy Europe**. 17(5): 10.
- Francioso, O., Sánchez-Cortés, S., Corrado, G., Gioacchini, P., and Ciavatta, C., (2005). Characterization of Soil Organic Carbon in Long-Term Amendment Trials, *Spectrosc. Lett.* 38(3): 283-291.
- Ghadai, R. K., Das, S., Kumar, D., Mondal, S. C., and Swain, B. P. (2018). Correlation between structural and mechanical properties of silicon doped DLC thin films. **Diamond and Related Materials**. 82: 25-32.
- Graham, B. L., Brusasco, V., Burgos, F., Cooper, B. G., Jensen, R., Kendrick, A., and Wanger, J. (2017). 2017 ERS/ ATS standards for single-breath carbon monoxide uptake in the lung. **European Respiratory Journal**. 49(1).
- Guo, T., Kong, C., Li, X., Guo, P., Wang, Z., and Wang, A. (2017). Microstructure and mechanical properties of Ti/ Al co-doped DLC films: Dependence on sputtering current, source gas, and substrate bias. **Applied Surface Science**. 410: 51-59.

- Guo, T., Kong, C., Li, X., Guo, P., Wang, Z., and Wang, A. (2017). Microstructure and mechanical properties of Ti/ Al co-doped DLC films: Dependence on sputtering current, source gas, and substrate bias. **Applied Surface Science**. 410: 51-59.
- Hähner, G. (2006). Near edge X-ray absorption fine structure spectroscopy as a tool to probe electronic and structural properties of thin organic films and liquids. **Chemical Society Reviews**. 35(12): 1244-1255.
- Hatada, R., Flege, S., Ensinger, W., Hesse, S., Tanabe, S., Nishimura, Y., Baba, K., (2020). Preparation of Aniline-based nitrogen-containing diamond-like carbon films with low electrical resistivity. **Coatings**. 10(1): 54.
- Hauert, R., Thorwarth, K., and Thorwarth, G. (2013). An overview on diamond-like carbon coatings in medical applications. **Surface and Coatings Technology**. 233, 119-130.
- He, M., and Yeo, C. (2018). Evaluation of thermal degradation of DLC film using a novel Raman spectroscopy technique. **Coatings**. 8(4): 143.
- Hemraj-Benny, T., Banerjee, S., Sambasivan, S., Balasubramanian, M., Fischer, D. A., Eres, G., and Misewich, J. A. (2006). Near-edge X-ray absorption fine structure spectroscopy as a tool for investigating nanomaterials. **Small**. 2(1): 26-35.
- Heymann, K., Lehmann, J., Solomon, D., Schmidt, M. W., and Regier, T. (2011). C 1s K-edge near edge X-ray absorption fine structure (NEXAFS) spectroscopy for characterizing functional group chemistry of black carbon. **Organic Geochemistry**. 42(9): 1055-1064.

- Huang, K., Bi, K., Liang, C., Lin, S., Wang, W. J., Yang, T. Z., Liu, J., Zhang, R., Fan, D. Y., Wang, Y.G., and Lei, M.(2015). Graphite carbon-supported Mo<sub>2</sub>C nanocomposites by a single-step solid state reaction for electrochemical oxygen reduction. **Plos One Journal**. 10(9): e0138330.
- Jastrzębski, K., Jastrzębska, A., and Bociąga, A.(2017). A review of mechanical properties of diamond-like carbon coatings with various dopants as candidates for biomedical applications. **Acta Innovations**. (22): 40-57.
- Jia, L., Sugiura, H., Kondo, H., Takeda, K., Ishikawa, K., Oda, O., and Hori, M. (2016). Effect of gas residence time on near-edge X-ray absorption fine structures of hydrogenated amorphous carbon films grown by plasma-enhanced chemical vapor deposition. **Japanese Journal of Applied Physics**. 55(4): 040305.
- Khademhosseini, V., Dideban, D., Ahmadi, M., Ismail, R., and Heidari, H. (2018). Single electron transistor scheme based on multiple quantum dot islands: carbon nanotube and fullerene. **ECS Journal of Solid State Science and Technology**. 7(10): M145.
- Kidkhunthod, P. (2017). Structural studies of advanced functional materials by synchrotron-based x-ray absorption spectroscopy: BL5. 2 at SLRI, Thailand. *Advances in Natural Sciences: Nanoscience and Nanotechnology*. 8(3): 035007.
- Kikuma, J., Yoneyama, K., Nomura, M., Konishi, T., Hashimoto, T., Mitsumoto, R., and Seki, K. (1998). Surface analysis of CVD carbon using NEXAFS, XPS and TEM. **Journal of Electron Spectroscopy and Related Phenomena**. 88: 919-925.

- Kim, C., Park, S. H., Cho, J. I., Lee, D. Y., Park, T. J., Lee, W. J., and Yang, K. S. (2004). Raman spectroscopic evaluation of polyacrylonitrile- based carbon nanofibers prepared by electrospinning. **Journal of Raman Spectroscopy**. 35(11): 928-933.
- Kim, H. I., Lince, J. R., Eryilmaz, O. L., and Erdemir, A. (2006). Environmental effects on the friction of hydrogenated DLC films. **Tribology Letters**. 21(1). 51-56.
- Kot, M., Major, Ł., and Lackner, J. (2013). The tribological phenomena of a new type of TiN/aC: H multilayer coatings. **Materials and Design**. 51: 280-286.
- Lackner, J. M., Waldhauser, W., and Kahn, M. (2015). Study of Gas Permeation Through Thin ta-C: H Films. **Acta Physica Polonica A**. 127(4): 1236-1239.
- Latham, K. G., Dose, W. M., Allen, J. A., and Donne, S. W. (2018). Nitrogen doped heat treated and activated hydrothermal carbon: NEXAFS examination of the carbon surface at different temperatures. **Carbon**. 128: 179-190.
- Latham, K. G., Simone, M. I., Dose, W. M., Allen, J. A., and Donne, S. W. (2017). Synchrotron based NEXAFS study on nitrogen doped hydrothermal carbon: Insights into surface functionalities and formation mechanisms. **Carbon**. 114: 566-578.
- Li, C., Huang, L., and Yuan, J. (2020). Effect of sp<sup>3</sup> Content on Adhesion and Tribological Properties of Non-Hydrogenated DLC Films. **Materials**. 13(8): 1911.
- Li, L., Zhang, H., Zhang, Y., Chu, P. K., Tian, X., Xia, L. and Ma, X. (2002). Structural analysis of arc deposited diamond-like carbon films by Raman and

- X-ray photoelectron spectroscopy. **Materials Science and Engineering**. 94(1): 95-101.
- Lin, J., Zhang, X., Lee, P., and Wei, R. (2017). Thick diamond like carbon coatings deposited by deep oscillation magnetron sputtering. **Surface and Coatings Technology**. 315: 294-302.
- Liu, D., Wang, B., Li, H., Huang, S., Liu, M., Wang, J., and Zhao, Y. (2019). Distinguished Zn, Co-N<sub>x</sub>-C-S<sub>y</sub> active sites confined in dendritic carbon for highly efficient oxygen reduction reaction and flexible Zn-air batteries. **Nano Energy**. 58: 277-283.
- Lu, Y., Huang, G., Guo, Y., and Wang, S. (2018). Diamond-like carbon film with gradient germanium-doped buffer layer by pulsed laser deposition **Surface and Coatings Technology**. 337: 290-295.
- Lusk, D., Gore, M., Boardman, W., Casserly, T., Boinapally, K., Oppus, M., Upadhyaya, D., Tudhope, A., Gupta, M., Cao, Y. and Lapp, S. (2008). Thick DLC films deposited by PECVD on the internal surface of cylindrical substrates. **Diamond and Related Materials**. 17(7-10): 1613-1621.
- Lux, H., Edling, M., Lucci, M., Kitzmann, J., Villringer, C., Siemroth, P., and Schrader, S. (2019). The Role of Substrate Temperature and Magnetic Filtering for DLC by Cathodic Arc Evaporation. **Coatings**. 9(5): 345.
- Ma, T., Liu, Z., Wen, J., Gao, Y., Ren, X., Chen, H., and Ren, W. (2017). Tailoring the thermal and electrical transport properties of graphene films by grain size engineering. **Nature Communications**. 8(1): 1-9.
- Maeda, T., Endo, F., and Hotta, A. (2015). Highly functionalized polyethylene terephthalate for food packaging. In Poly (Ethylene Terephthalate) Based

- Blends. **Composites and Nanocomposites** (pp. 213-234). William Andrew Publishing.
- Mangolini, F., McClimon, J. B., Segersten, J., Hilbert, J., Heaney, P., Lukes, J. R., and Carpick, R. W. (2019). Silicon Oxide-Rich Diamond-Like Carbon: A Conformal, Ultrasoft Thin Film Material with High Thermo- Oxidative Stability. **Adv. Materials and Interfaces**. 6(2): 1801416.
- Marcondes, A. R., Ueda, M., Kostov, K. G., Beloto, A. F., Leite, N. F., Gomes, G. F., and Lepienski, C. M. (2004). Improvements of ultra-high molecular weight polyethylene mechanical properties by nitrogen plasma immersion ion implantation. **Brazilia Journal Physics**. 34(4B): 1667-1672.
- Maruno, H., and Nishimoto, A. (2018). Adhesion and durability of multi-interlayered diamond-like carbon films deposited on aluminum alloy. **Surface and Coatings Technology**. 354: 134-144.
- Mikamoto, K., Nishitani, T., Tsubaki, Y., Shirakura, A., and Suzuki, T. (2020). Improvement of durability and sliding properties of food packaging equipment by combined treatment of Diamond-like carbon coating and Fine particle bombarding. **Journal of Applied Packaging Research**. 12(1): 4.
- Milenov, T. I., Avramova, I. A., Dikovska, A., Karaivanova, D., Terziyska, P., Kolev, S. K., and Valcheva, E. P. (2021). Modification of graphene-like, hydrogenated amorphous, hydrogenated tetrahedral amorphous carbon and amorphous carbon thin films by UV-C light. **Surfaces and Interfaces**. 24: 101073.
- Nakao, S., Kimura, T., Suyama, T., and Azuma, K. (2017). Conductive diamond-like carbon films prepared by high power pulsed magnetron sputtering with bipolar

- type plasma based ion implantation system. **Diamond and Related Materials**. 77: 122-130.
- Newville, M. (2001). EXAFS analysis using FEFF and FEFFIT. **Journal of Synchrotron Radiation**. 8(2): 96-100.
- Ning, C. M., Cui, X. J., Shang, L. L., Zhang, Y. J., and Zhang, G. A. (2020). Structure and properties of different elements doped diamond-like carbon on micro-arc oxidation coated AZ31B Mg alloy. **Diamond and Related Materials**. 106: 107832.
- Nishimoto, A., Furuya, E., and Kousaka, K. (2020). Nitriding and DLC Coating of Aluminum Alloy Using High-Current Pressure-Gradient-Type Plasma Source. **International Journal of Metallurgy and Metal Physics**. 5(1): 1-10.
- Osswald, S., Yushin, G., Mochalin, V., Kucheyev, S. O., and Gogotsi, Y. (2006). Control of  $sp^2/sp^3$  carbon ratio and surface chemistry of nanodiamond powders by selective oxidation in air. **Journal of the American Chemical Society**. 128(35): 11635-11642.
- Pancielejko, M., Czyżniewski, A., Gilewicz, A., Zavaleyev, V., and Szymański, W. (2012). The cutting properties and wear of the knives with DLC and W-DLC coatings, deposited by PVD methods, applied for wood and wood-based materials machining. **Archives of Materials Science and Engineering**. 58(2): 235-244.
- Paparazzo, E. (1987). XPS and auger spectroscopy studies on mixtures of the oxides  $SiO_2$ ,  $Al_2O_3$ ,  $Fe_2O_3$  and  $Cr_2O_3$ . **Journal of Electron Spectroscopy and Related Phenomena**. 43(2): 97-112.

- Paul, R. (2017). Diamond-like-carbon coatings for advanced biomedical applications. **Global Journal of Nanomedicine**. 2(5): 555598.
- Popov, I. V., Görne, A. L., Tchougréeff, A. L., and Dronskowski, R. (2019). Relative stability of diamond and graphite as seen through bonds and hybridizations. **Physical Chemistry Chemical Physics**. 21(21): 10961-10969.
- Ren, Z., Qin, H., Dong, Y., Doll, G. L., and Ye, C. (2019). A boron-doped diamond like carbon coating with high hardness and low friction coefficient. **Wear**. 436: 203031.
- Ribeiro-Soares, J., Cançado, L. G., Falcão, N. P. S., Martins Ferreira, E. H., Achete, C. A., and Jorio, A. (2013). The use of Raman spectroscopy to characterize the carbon materials found in Amazonian anthrosoils. **Raman Spectrosc**. 44(2): 283-289.
- Rittihong, U., Akasaka, H., Euaruksakul, C., Tomidokoro, M., Kamonsuttipajit, N., Nakajima, H., and Tunmee, S. (2020). Synchrotron-based spectroscopic analysis of diamond-like carbon films from different source gases. **Radiation Physics and Chemistry**. 173: 108944.
- Robertson, J. (2002). Diamond-like amorphous carbon. **Materials Science and Engineering**. 37(4-6): 129-281.
- Rohrbeck, M., Fischer, C., Wehner, S., Meier, J., and Manz, W. (2014). DLC-coated pure bioplastic foil: Effect of various sterilization methods on the surface morphology. **Vakuum in Forschung und Praxis**. 26(2): 42-47.
- Schroeder, V., Savagatrup, S., He, M., Lin, S., and Swager, T. M. (2018). Carbon nanotube chemical sensors. **Chemical Reviews**. 119(1): 599-663.

- Sedlmair, J., Gleber, S. C., Peth, C., Mann, K., Niemeyer, J., and Thieme, J., (2012). Characterization of refractory organic substances by NEXAFS using a compact X-ray source. **Journal of Soils and Sediments**. 12(1): 24-34.
- Shimada, T., Xie, W., Miura, T., Yanase, T., and Nagahama, T. (2015). Colorful carbon nanopopcorns formed by plasma CVD of diamond-like carbon from CH<sub>4</sub> and co-deposited C<sub>60</sub> followed by reaction with water vapor. **Bulletin of the American Physical Society**. 60.
- Siegal, M. P., Tallant, D. R., Provencio, P. N., Overmyer, D. L., Simpson, R. L., and Martinez-Miranda, L. J. (2000). Ultrahard carbon nanocomposite films. **Applied Physics Letters**. 76(21): 3052-3054.
- Singh, B., Fang, Y., Cowie, B. C., and Thomsen, L. (2014). NEXAFS and XPS characterisation of carbon functional groups of fresh and aged biochars. **Organic Geochemistry**. 77: 1-10.
- Siow, K. S., Britcher, L., Kumar, S., and Griesser, H. J. (2018). XPS study of sulfur and phosphorus compounds with different oxidation states. **Sains Malaysiana**. 47(8): 1913-1922.
- Srisang, C., Asanithi, P., Siangchaew, K., Limsuwan, S., Pokaipisit, A., and Limsuwan, P. (2012). Raman spectroscopy of DLC/a-Si bilayer film prepared by pulsed filtered cathodic arc. **Journal Nanomater**. 2012: 131.
- Strmčnik, E., Majdič, F., and Kalin, M. (2019). Water-lubricated behaviour of AISI 440C stainless steel and a DLC coating for an orbital hydraulic motor application. **Tribology International**. 131: 128-136.

- Takagaki, T., Igari, Y., Takaoka, T., and Kusunoki, I. (1992). XPS study of the reaction of the Si (100) surface with a C<sub>2</sub>H<sub>4</sub> beam. **Applied Surface Science** 92: 287-290.
- Tasdemir, H. A., Tokoroyama, T., Kousaka, H., Umehara, N., and Mabuchi, Y. (2014). Influence of zinc dialkyldithiophosphate tribofilm formation on the tribological performance of self-mated diamond-like carbon contacts under boundary lubrication. **Thin Solid Films**. 562: 389-397.
- Thomson, L. A., Law, F. C., Rushton, N., and Franks, J. (1991). Biocompatibility of diamond-like carbon coating. **Biomaterials**. 12(1): 37-40.
- Tyagi, A., Walia, R. S., Murtaza, Q., Pandey, S. M., Tyagi, P. K., and Bajaj, B. (2019). A critical review of diamond like carbon coating for wear resistance applications. **International Journal of Refractory Metals and Hard Materials**. 78: 107-122.
- Wang, Y., Zhang, M., Wang, Y., Zhang, G., and Lu, Z. (2020). Influence of currents on tribological behavior of diamond-like carbon films. **Applied Physics**. 126(4): 1-11.
- Watts, B., Thomsen, L., and Dastoor, P. C. (2006). Methods in carbon K-edge NEXAFS: experiment and analysis. *J. Electron. Spectroscopy and Related Phenomena*. 151(2): 105-120.
- Weiss, Z., and Vlcek, P. (2017). Analysis of shallow depth profiles of titanium nitride and N-implanted titanium by GD-OES: the “hydrogen effect” after the discharge startup and a correction thereof. **Journal of Analytical Atomic Spectrometry**. 32(12): 2476-2484.

- Wong, H., Foong, Y. M., and Chua, D. H. C. (2011). Improving the conductivity of diamond-like carbon films with zinc doping and its material properties. **Applied Surface Science**. 257(22): 9616-9620.
- Wu, Y. H., Hsu, C. M., Chia, C. T., Lin, I. N., and Cheng, C. L. (2002). Field emission and Raman spectroscopy studies of atomic hydrogen etching on boron and nitrogen doped DLC films. *Diamond Relat. Materials*. 11(3-6): 804-808.
- Xing, Z., Du, C., Zeng, Y., Ma, F., and Zhou, J. (2016). Characterizing typical farmland soils in China using Raman spectroscopy. **Geoderma**. 268: 147-155.
- Yamaguchi, M. (2010). Role of nutritional zinc in the prevention of osteoporosis. *Molecular and cellular biochemistry*. **Molecular and Cellular Biochemistry**. 338(1-2): 241-254.
- Yonezawa, K., Kawaguchi, M., Kaneuji, A., Ichiseki, T., Iinuma, Y., Kawamura, K., and Kawahara, N. (2020). Evaluation of antibacterial and cytotoxic properties of a fluorinated diamond-like carbon coating for the development of antibacterial medical implants. **Antibiotics**. 9(8): 495.
- Yoshitake, T., Nishiyama, T., and Nagayama, K. (2000). Growth of DLC thin films in hydrogen atmosphere by pulsed laser ablation of a PMMA target. **Journal of Materials Science letters**. 19(6): 489-490.
- Zhang, W., Obitani, K., Hirai, Y., Tsuchiya, T., and Tabata, O. (2019). Fracture strength of silicon torsional mirror resonators fully coated with submicrometer-thick PECVD DLC film. **Sensor and Actuator, A: Physical Journal**. 286: 28-34.

- Zhou, K. , Ke, P. , Li, X. , Zou, Y. , and Wang, A. (2015). Microstructure and electrochemical properties of nitrogen-doped DLC films deposited by PECVD technique. **Applied Surface Science**. 329: 281-286.
- Zhou, X., Tunmee, S., Suzuki, T., Phothongkam, P., Kanda, K., Komatsu, K., and Saitoh, H. (2017). Quantitative NEXAFS and solid-state NMR studies of  $sp^3/(sp^2+ sp^3)$  ratio in the hydrogenated DLC films. **Diamond and Related Materials**. 73: 232-240.
- Zhou, X., Zheng, Y., Shimizu, T., Euaruksakul, C., Tunmee, S., Wang, T., and Tang, Y. (2020). Colorful Diamond - Like Carbon Films from Different Micro/Nanostructures. **Advanced Optical Materials**. 8(11): 1902064.



## **CURRICULUM VITAE**

**Name:** Thanun Chunjaemsri  
**Date of birth:** 23 July 1993  
**Place of birth:** Sakon Nakhon, Thailand

### **Education:**

2006-2012: Princess Chulabhorn's college Mukdahan school,  
Mukdahan, Thailand (Science High school)  
2012-2016: Department of Physics, Science, KhonKaen University,  
KhonKaen, Thailand (Bachelor of Science)  
2016-2021: School of Physics, Science, Suranaree University of  
technology, Nakhonratchasima, Thailand (Doctor of  
philosophy in Physics)

### **Academic experience:**

1. Ph.D. Research of Tokyo Institute of Technology, Tokyo, Japan
2. Beamline 5.2 assistance scientist in Synchrotron Light Research Institute  
(Public Organization)
3. Staff and team organizer in 5th International Conference on Smart Materials  
and Nanotechnology (SmartMat@2020), Pattaya, Thailand.